EXPERIMENTAL STUDY OF IONIC POLYMER TRANSDUCERS: CHARACTERIZATION OF TRANSIENT RESPONSE IN SENSING

by

Bilge Kocer Yumer

BS, Middle East Technical University, 2007

MS, Middle East Technical University, 2010

Submitted to the Graduate Faculty of

Swanson School of Engineering in partial fulfillment

of the requirements for the degree of

Doctor of Philosophy

University of Pittsburgh

2014

UNIVERSITY OF PITTSBURGH

SWANSON SCHOOL OF ENGINEERING

This dissertation was presented

by

Bilge Kocer Yumer

It was defended on

August 20, 2014

and approved by

William W. Clark, Ph.D., Professor, Department of Mechanical Engineering and Materials Science

William S. Slaughter, Ph.D., Associate Professor, Department of Mechanical Engineering and Materials Science

Jung-Kun Lee, Ph.D., Associate Professor, Department of Mechanical Engineering and Materials Science

Barbar J. Akle, Ph.D., Associate Professor, Department of Industrial and Mechanical Engineering, Lebanese American University

Lisa M. Weiland, Ph.D., Renerge, Inc

Dissertation Director: Qing-Ming Wang, Ph.D., Professor, Department of Mechanical Engineering and Materials Science

EXPERIMENTAL STUDY OF IONIC POLYMER TRANSDUCERS: CHARACTERIZATION OF TRANSIENT RESPONSE IN SENSING

Bilge Kocer Yumer, PhD

University of Pittsburgh, 2014

Ionic Polymer Transducers (IPTs) display a sensing behavior, whereby a current signal is generated, when they are deformed. IPTs also exhibit bending deformation when a voltage difference is applied across the surfaces of the transducer, thus displaying actuation. However, the mechanisms responsible for actuation and sensing differ; research to date has focused predominantly on actuation, while identification of the fundamental physical mechanism responsible for IPT sensing remains an open topic. Nevertheless, IPTs are promising in sensing, reliable, flexible, light, and cost effective. Even so, they are poorly understood, which has limited their optimization and subsequently their widespread application. As sensors they are most often studied in bending mode; however a measurable signal can be generated in any mode of mechanical deformation. This thesis offers the streaming potential hypothesis as the mechanistic model explaining IPT sensing on the basis that it is uniquely able to predict the existence of a transient sensing signal in any mode of deformation. To date, streaming potential models of IPT transient sensing response under bending and shear have been presented. These models, however, have lacked access to appropriate transient experimental studies for validation; moreover, there has been a complete absence of study of the final compressive sensing mode. This thesis offers a modeling methodology appropriate to compression, while also offering experimental studies enabling validation studies for all IPT sensing modes. The experimental studies introduce novel test rigs enabling step-deflection application in bending, shear,

compression modes and *in situ* measurement of the resulting transient IPT current. Finally, because the ultimate goal of defining the physical mechanism primarily responsible for sensing is to enable widespread use of these transducers, electrode architecture studies are offered as illustration of the potential to optimize IPT sensing via the streaming potential hypothesis.

TABLE OF CONTENTS

LIST OF TABLES

LIST OF FIGURES

NOMENCLATURE

S	membrane`s midsurface
ρ^{-},ρ^{+}	metal protrusion into polymer surface
m	bending moment
ε_0	vacuum permittivity
ε_r	dielectric constant
C	concentration
c_0	fixed ions` concentration
t	time
r	distance from the channel center
θ	rotation around x axis
ϕ	rotation around z axis
I_s	streaming channel current
$I_{ave\_channel}(t,\theta,\phi)$	average streaming chanel current wrt time and rotation angles
$I_{ave\_channel}$	average streaming chanel current wrt time
I_{IPT}	total IPT current
$r_{channel}$	nanochannel radius
$\rho(r)$	charge density wrt radius
ρ_e	charge density of unipolar solution

$v(r)$	flow velocity in a nanochannel wrt radius
$v(r,t)$	flow velocity in a nanochannel wrt radius and time
P	pressure
ΔP	pressure difference
ΔP	pressure difference wrt time
μ	viscosity of the diluent
$l_{channel}$	nanochannel length
l_{IPT}	IPT length
w_{IPT}	IPT width
t_{IPT}	IPT thickness
$t_{electrode}$	electrode thickness
δ	deflection
E	elastic modulus
η	damping constant
$N_{channels}$	total number of nanochannels
f_l	electrolyte volume fraction
f_p	metal particulate volume fraction
f_c	channel volume fraction
Φ	porosity if the electrode region
β	evolution ratio
Ψ	distribution of the electrical potential field
$\varepsilon(t)$	strain wrt time
$\sigma(t)$	stress wrt time

V	volume

ACKNOWLEDGEMENTS

I am very thankful to Dr. Lisa Weiland for the valuable guidance and technical support she has provided to me throughout this study. She was always a source of enthusiasm and encouragement for me when facing challenging problems, and I am glad she always believed in me. I would also like to thank to Dr. Qing-Ming Wang for being committee chair and my committee for their technical support and helpful advices that contributed to the successful completion of this work. I gratefully acknowledge multiple communications with Barbar Akle in the recreation of his DAP method for this study and also the NSF for funding under CMMI 0747123.

I am pleased to express my special thanks to my parents Şükran and Atila, and my sister Behiye for their support and endless love throughout my life. I also heartily thank to my husband, and colleague, Ersin, with my deepest appreciation for his understanding and encouragement.

Thanks to my former lab mates Dr. Ursula Thérèse Zangrilli and Dr. Fei Gao for their friendship and help during my PhD study. Lastly, I offer my thanks to all my friends who supported me in any respect during the completion of this dissertation.

1.0 INTRODUCTION

Ionic Polymer Transducers (IPTs) sometimes referred to as Ionic Polymer Metal Composites (IPMCs), are electroded, diluent infused ionomers displaying both sensing and actuation. These transducers are fabricated by sandwiching an ionic polymer between high surface area electrodes. The IPMC naming convention is descriptive of one commonly employed fabrication approach, where metals are employed in the electrode. However, non-metallic conductive media can also be envisioned. Thus, this work favors the naming convention IPT because it is descriptive of functionality.

The mechanisms responsible for IPT actuation and sensing may differ; research to date has focused predominantly on actuation, while identification of the dominant mechanism responsible for IPT sensing remains an open topic. Thus, the focus of this research is sensing.

The first experimental studies on perfluorinated ionomers as electromechanical transducers began in the 1990s. Since that time, a variety of IPT applications have been studied, such as vibration sensors **[1**], micro- or macro-grippers **[2**], energy harvesters [3], tactile sensors for biomedical applications **[4**], and assorted artificial muscles to mimic: a fish tail **[2**], a contractile slithering serpent **[2**], a jellyfish **[5**], [6], and a manta ray **[7**], While this list is not exhaustive, the fact that it is dominated by actuation rather than sensing applications is consistent with the relative states of understanding of these responses **[8**], **[9**].

1.1 MOTIVATION AND OBJECTIVES

In spite of the latest progressions in the research of IPT transduction, there is still a certain amount of controversy regarding sensing characteristics **[10**]. Even so, IPTs show superior sensitivity in charge sensing mode compared to other types of electromechanical transducers (e.g. piezoelectric polymers) **[11**], **[12**]. IPTs are convenient for low voltage applications since they can run under 5V producing high strains, larger than 9%, and they can sense small strain changes **[13**]. Moreover, they are flexible and light **[16**], amenable to underwater and biomechanical applications, as well as facilitating the usage as mechanical sensors. Also, the lightweight, and flexibility of IPTs may enable their use in wearable electronics, haptic systems and soft robotics. Among the smart materials considered for artificial muscle study in biomimetic, (*i.e.* shape memory polymers and metals, piezoelectric polymers and ceramics, electrically active polymeric gels), the best match with natural muscles is observed for electro-active polymers (EAPs) [17] which is the family of polymers of to which IPTs belong. Furthermore, IPTs display long-term stability especially when infused with a non-volatile ionic liquid **[12**]. They can be cut easily in any geometric shape and size from a bigger transducer or directly fabricated in a desired form. While IPTs in actuation have been limited to bending if they are cantilevered, they are able to sense any type of deformation; bending, shear, tension, and compression. Thus, there is a compelling case for reaching consensus on the dominant physical mechanisms responsible for sensing response. Of the postulated IPT sensing theories, the streaming potential hypothesis is uniquely competent to predict the existence of a sensing signal in any deformation mode, which is especially noteworthy in the case of shear **[18**]. Furthermore, it is amenable to experimentally observed variations in sensing as a function of electrode

morphology. If validated, this hypothesis is compelling in that it could be adapted into a design tool to optimize IPT sensing under varied circumstances.

To date, development of the streaming potential hypothesis has relied largely on adapting experimental reports from the literature, where those studies were designed for a variety of alternate purposes. In particular, though rarely reported, a step stimulation is required to appropriately assess the streaming potential analyses and correlation to the models. Most IPT sensing experiments to date have imposed dynamic stimulation **[4]**, **[19]**-**[23]** while relatively few reports have studied step displacement stimulation for electromechanical characterization in sensing **[24]**, **[25]**. This is likely attributed to the fact that the step-displacement experimental design is more challenging in general, and especially as it relates to repeatability (Consider for instance that consistency can be achieved in frequency domain experiments more easily since data from a much greater period of time are averaged in the analysis **[21]**.) However, despite the experimental challenges inherent to step displacement characterization, or perhaps because of them, step displacement tests have rarely been performed and yet they are uniquely valuable for unveiling the transient physical mechanisms responsible for IPT sensing, especially as it relates to evaluation of the streaming potential hypothesis.

All in all, the proposed effort focuses on design and implementation of IPT step displacement sensing experiments, where the results will be useful in a broader sense to fill the gap in IPT sensing research, but additionally in the development of the streaming potential hypothesis. Furthermore, and in keeping with the streaming potential ideology, experiments addressing variations in loading type and/or electrode architecture are considered. Thus, the first of two significant objectives of this research is to accomplish experimental design and implementation for transient response characterization of Ionic Polymer Transducers in all IPT

sensing modes. The second significant objective is to complete the modeling framework for the streaming potential hypothesis such that compression, the only remaining unexplored mode, is addressed. This work not only expands the performance database in a general sense but also specifically facilitates testing of the streaming potential hypothesis which is proposed here as the responsible mechanism for IPT sensing. **Contributions** of this research can be itemized as follows;

(i) presentation of a reliable experimental design of step input applications for IPT sensing characterization which are especially challenging for shear and compression modes;

(ii) expansion of the sensing performance database of IPTs in a general sense;

(iii) specific facilitation of the evaluation of streaming potential hypothesis as the IPT sensing mechanism;

(iv) particular investigation of the electrode architecture so as to determine optimum architecture leading to highest sensitivity; and

(v) expansion of the streaming potential hypothesis and implementation of its implications for sensing modes other than bending.

1.2 ORGANIZATION

This dissertation is organized as follows: Section 1.0 introduces the research topic, motivation and the objectives are introduced. Section 2.0 provides a literature review in experimental studies on the anatomy of an IPT, actuation and sensing transductions. Furthermore, modeling background is presented and streaming potential modeling is introduced.

In Section 3.0 the transducer fabrication process is explained in detail. Section 4.0, Section 5.0 , and Section 6.0 present the experimental characterization of IPTs in bending, shear, and compression, respectively. Experimental results are discussed and compared to the modeling estimations. Moreover, streaming potential modeling for compression is proposed in Section 6.0 . Finally, Section 7.0 concludes the report.

2.0 BACKGROUND AND LITERATURE REVIEW

An IPT bends when a voltage difference is applied across the surfaces of the transducer performing actuation behavior. They also produce a voltage difference between the surfaces when they are deformed, exhibiting sensing behavior. This situation is illustrated for an IPT in bending mode in Figure 2.1; a cantilevered IPT bends in response to a voltage actuation (V) while it generates a measurable current (i) with a tip deflection (δ).

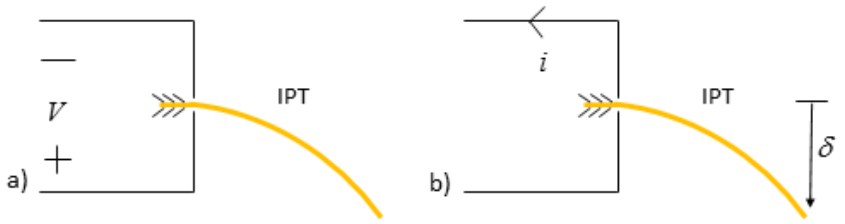

Figure 2.1. Ionic Polymer Transducers in Bending: a) Actuation, b) Sensing

However, the responses are not symmetric; an IPT needs to be excited with a ~2.5V step voltage across the IPT thickness in order to obtain a 10mm tip deflection, while it can generate only a few millivolts in response to the same tip displacement input **[24]**. Thus, it must be concluded that the physical mechanisms responsible for actuation and sensing differ. In this case,

the proposed theories in literature for actuation modeling may not be valid for sensing response estimation of the ionic polymer transducers.

2.1 IONIC POLYMER TRANSDUCER EXPERIMENTAL REPORTS

2.1.1 The Anatomy of an IPT

IPTs are composed of an electro-active ionomer, inserted between conductive electrode layers (Figure 2.2). The ionomer, which will be discussed in detail in Section 2.2, is typically Nafion, Flemion, or Aciplex. The base polymer is a flexible, thin film with thickness measured in micrometers and where the exact value changes based on the polymer type. Enabling to electro-active response is uptake of a diluent by the ionomer. Organic liquids, ionic liquids, and water constitute the most common diluents utilized in IPTs.

The electrode layer, whose thickness is variable but typically between 5μm and 50μm, plays an important role in transduction. Uniformity and depth of the electrode region are among the parameters that affect the transducer performance. For example, transducers having finer and more extensively distributed metal particulates in the electrode region [26], and the transducers having thicker electrode layers [13] exhibit better performance in actuation in terms of peak response since they have enhanced capacitance. Gold flakes, platinum or ruthenium dioxide particulates have been utilized in electrode layers. Furthermore, non-metallic conducting powders like single walled carbon nanotubes (SWNT) can also be employed in the electrode regions. Finally, the IPT outermost surfaces are typically thin gold layers, 50-100nm **[13]**, which are employed to increase surface conductivity.

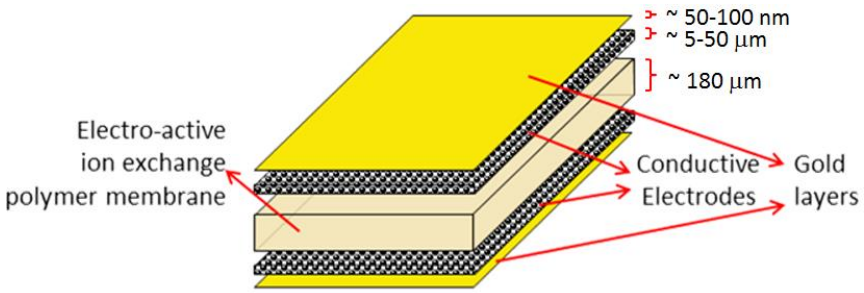

Figure 2.2. Schematic View of an IPT

The impregnation–reduction technique is a commonly used IPT fabrication method, which is an electroless chemical plating procedure. In the application of this method **[27]**-**[29]**, the membrane is first plunged into a metal salt solution, such as $PtNH_3Cl_2$, and then into $NaBH_4$ or $LiBH_4$ to enable metal population and reduction on the surfaces of the polymer membrane, respectively. Finally, a thin layer of gold is electroplated on both sides to increase the surface conductivity. If needed, ion exchanging is performed, for instance, by immersing the transducer into NaOH or LiOH solution. This method has widely been used as an IPT manufacturing technique **[29]** since its implementation started in the 1990s, which coincides with the beginning of experimental research in this field. The impregnation reduction approach remains in common use because it results in effective transduction, but it offers limited control over electrode architecture.

The Direct Assembly Process (DAP) **[30]**-**[31]** is a comparatively new fabrication technique, where an electrode solution is directly brushed or sprayed over the surfaces of the polymer membrane. The electrode solution is prepared by mixing and sonicating an electrically conductive powder such as platinum (Pt) or ruthenium dioxide (RuO_2) with the polymer solution

and diluent. The conductor–polymer mixture is applied onto the surfaces of the transducer in one of two ways; painting several layers of mixture on each side of the ion-exchange membrane by means of a brush/air spray, or painting several layers of mixture on a Teflon reinforced glass fabric, and then hot-pressing these decals on the polymer. Finally, a gold layer is melt-pressed on the outer surfaces of the transducer. Diluent uptake and ion exchange procedures can be accomplished after these steps where the fabrication method is called `Direct Assembly Process with Dry Membranes`, Figure 2.3. Alternatively, both the diluent uptake and the ion exchange process steps may be applied before electrode plating. IPT production with this technique is called `Direct Assembly Process with Solvated Membranes`, Figure 2.4. In this study, the `Direct Assembly Process with Solvated Membranes` technique is adopted to avoid swelling-induced cracks in the gold layer of the transducer which might be ensured via applying the steps requiring plunging before electrode plating and gold hot press. Although it is a relatively new fabrication process, the DAP is preferred for some applications since it is a flexible and fast method enabling increased control over electrode architecture [**32**].

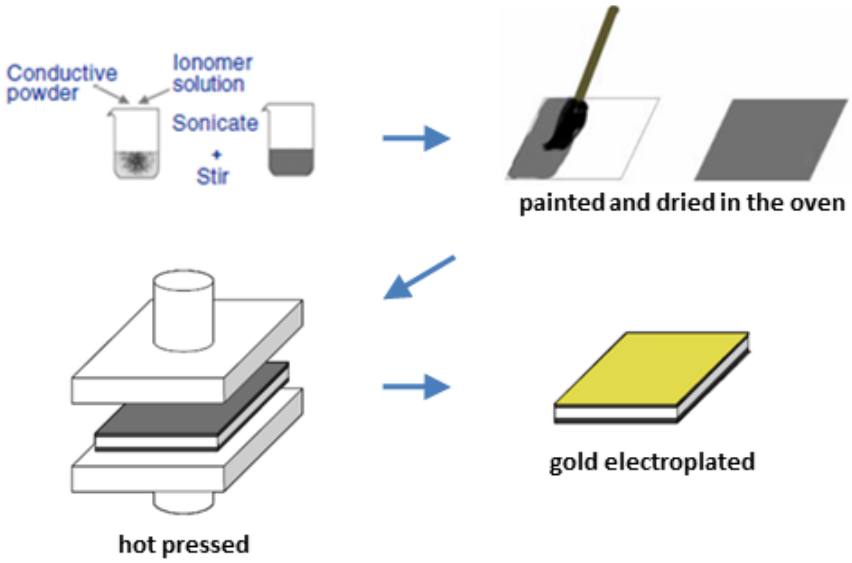

Figure 2.3. Schematic Illustration of Direct Assembly Process to Fabricate Dry Transducers [13]

The DAP not only allows the usage of any type of ionomer, diluent, and conducting powder (even non-metallic ones), but also makes the control of electrode composition and different thickness electrode application on the sides of the polymer possible. In this study, it is hypothesized that electrode architecture plays an important role in the evolution of IPT streaming potential derived sensing mechanism. Whether or not the DAP might result in enhanced sensitivity is not the goal here; the DAP was selected because it enables control over the fabrication of transducers in terms of electrode composition, which was also exercised to explore the implications of the streaming potential hypothesis.

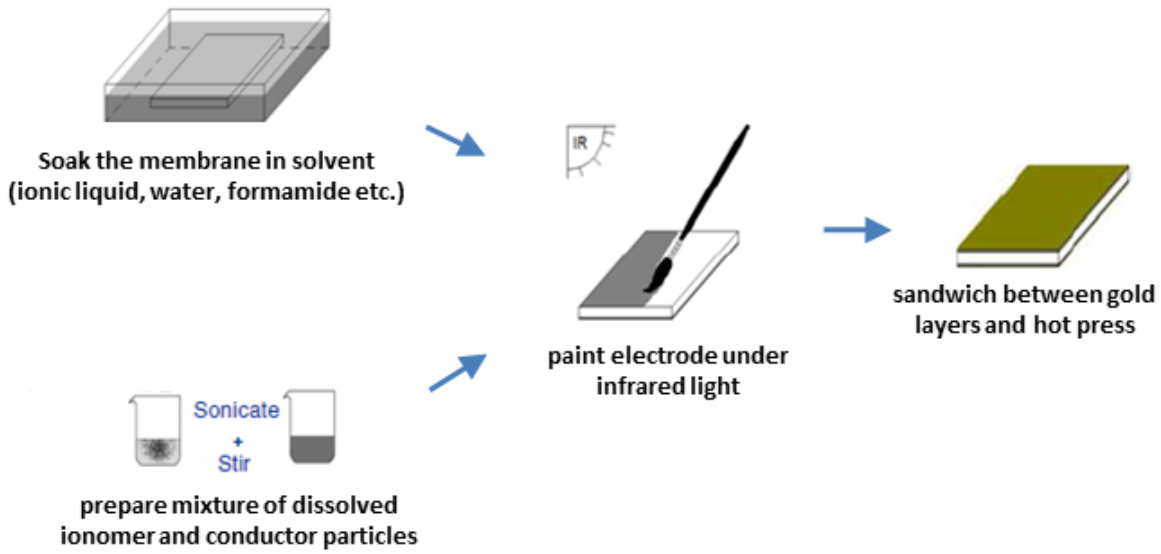

Figure 2.4. Schematic Illustration of Direct Assembly Process to Fabricate Solvated Transducers [13]

2.1.2 IPTs in Actuation

While this work focuses on IPT sensing, a brief review of IPT actuation warranted. A cantilevered IPT strip in the solvated state quickly bends towards the anode when a sudden small voltage (1V-3V) is applied across the thickness of the actuator [26], **[27]**. Alkali metal counter-ion incorporated, Nafion based transducers then slowly relax back towards the cathode although the electric potential is kept constant while relaxation occurs in the same direction (anode) for Flemion type IPT strips [33]. The magnitude in addition to speed of initial bending and back relaxation depend on the sort of the diluent and the cation type. In addition, IPTs can display an oscillatory bending motion when they are exposed to a sinusoidal electric potential.

It is widely accepted that when an electric field is applied across the faces of the transducer, free counter-ions are pulled towards the cathode along with diluent absorbed by the ionomer such as water molecules increasing cation density on one side of the membrane. Therefore, the surface of the IPT close to the cathode swells and expands which leads in IPT bending towards the anode. How bending occurs upon electric potential application is depicted in Figure 2.5.

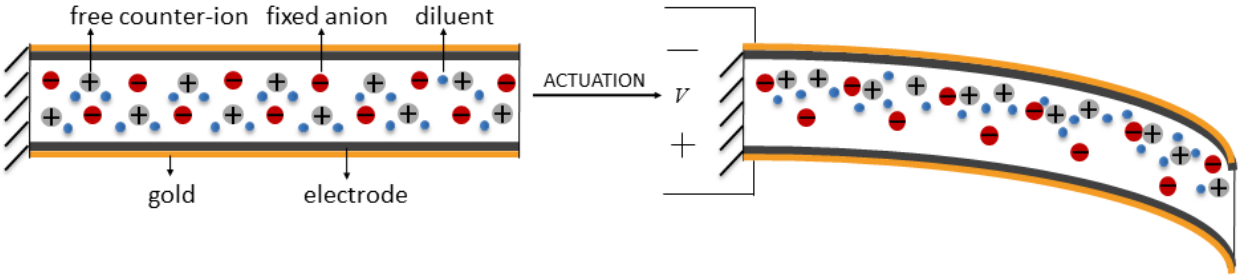

Figure 2.5. IPT Actuation: Free cations along with diluent move towards the cathode upon electric potential application causing IPT bending

The first observations of IPT actuation began with the report stating a quick bend of the perfluorosulfonic ion-exchange films in aqueous solution in response to sudden voltage stimulation slow enough to prevent electrolysis [34]. Similarly, Shahinpoor investigated electromechanic properties of ionic polymeric gels [35], [36]. Displacement and current responses of a platinum plated Nafion membrane were studied for various excitations in aqueous solution such as triangular voltage and step voltage **[27**], Figure 2.6. For example, for a periodic triangular stimulation, IPT bends in line with the stimulation pattern.

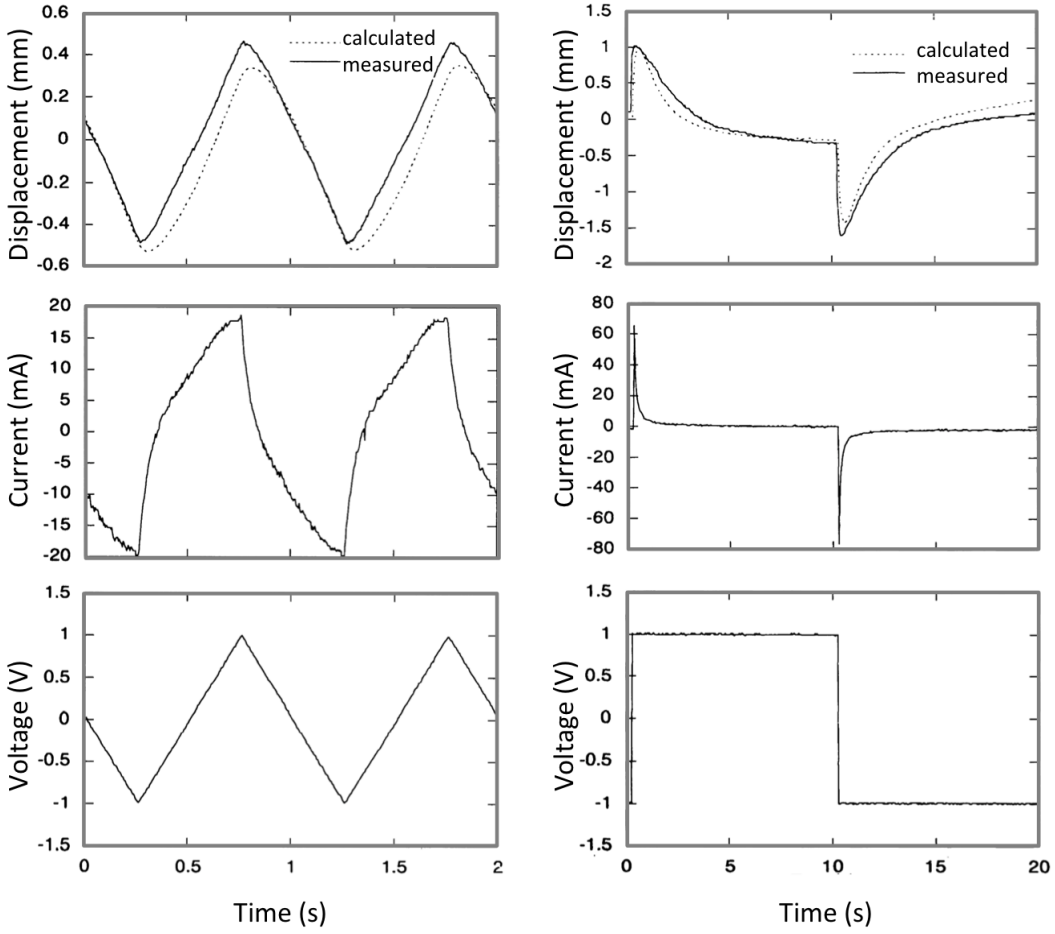

Figure 2.6. Displacement and Current Outputs of Ionic Polymer Actuators (plunged in a mixed solution of 0.1 M Na_2SO_4 and 10 mM H_2SO_4) in Response to Triangular and Step Voltages [27]

Ionic liquid based transducers fabricated employing the DAP were tested in actuation under dynamic loading and it was seen that they can operate in air for over 400,000 cycles with a negligible performance degradation in strain output [37], Figure 2.7. It is stated that, DAP based actuators can generate strains on the order of 10% in response to ±2 V, whereas the ones created by impregnation–reduction technique generate less than 1%.

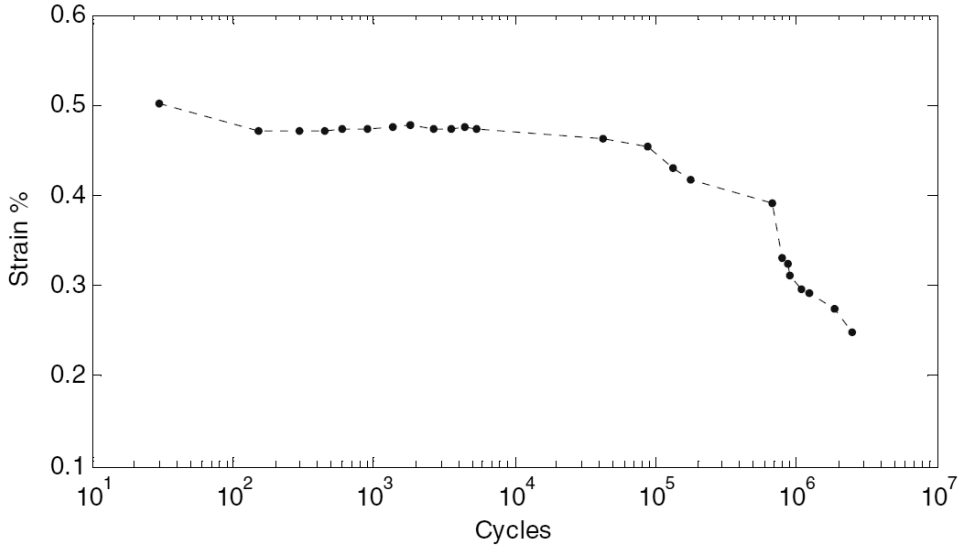

Figure 2.7. Reliability of the IPT Infused with an Ionic Liquid Diluent under Zero Humidity Condition [37]

Moreover, it was shown that actuator response is strongly correlated with conductive particulate percentage and percolation properties of the electrode. The optimum loading value to obtain maximum strain from the transducer was found out to be 42% and 30% by electrode volume for RuO_2 and SWNT particulates, respectively, Figure 2.8, [13]. Furthermore, extension of IPTs under voltage was investigated recently by Akle and Leo to explore extensional actuation behavior both experimentally and theoretically while the IPTs were fixed at the bottom **[14]**, **[15]**.

Thus, while this thesis argues that the fundamental physical mechanisms responsible for sensing differ from that of actuation, previous DAP based studies of IPT actuation indicate that both systems derive primary activity from electrode architecture.

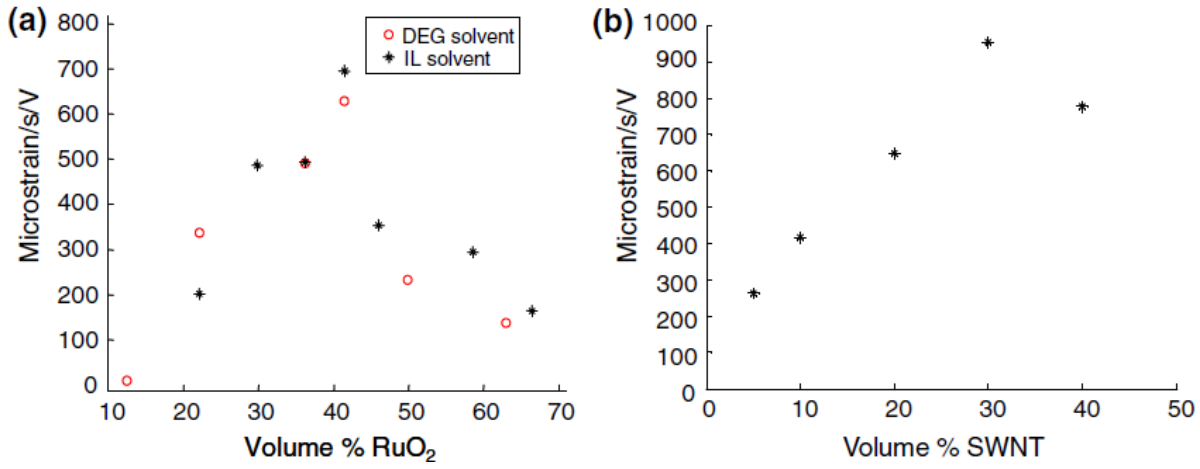

Figure 2.8. Strain Rate Output of the IPT as a Function of Conductive Media Volume % in the Electrode Region: a) RuO_2 b) SWNT [13] Copyright 2007 Springer

2.1.3 IPTs in Sensing

While quite a few reports have been published about IPT actuation, the number of studies issued on sensing transduction is much smaller **[10]**. The current state of IPT mechanoelectrical understanding has been derived predominantly from IPT bending mode actuation. And yet, IPTs produce a measurable current (a few microamperes) when they are deformed in any mode, shown schematically in Figure 2.9.

IPT sensing experiments began with a report by Sadeghipour et al. [38], where platinized circular Nafion membranes were tested under different pressure ratios; the produced voltage was found to be highly sensitive to the pressure ratio and to the presence of oxygen. Shahinpoor et al. **[24]** later reported a linear relationship between the voltage output and an imposed quasi-static tip displacement of an ion-exchanged transducer. Newbury and Leo **[39]** have since stated that the short circuit current is proportional to the transducer tip velocity, Figure 2.10. Similarly, Farinholt **[25]** indicates that current discharge due to a step change in displacement is

approximately proportional to velocity when the displacement has reached an approximately constant value.

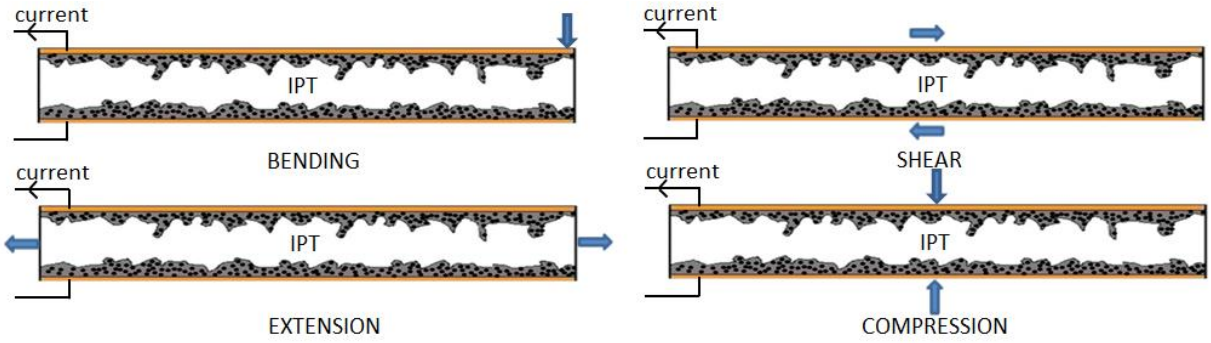

Figure 2.9. Schematic Showing IPT Deformation Modes

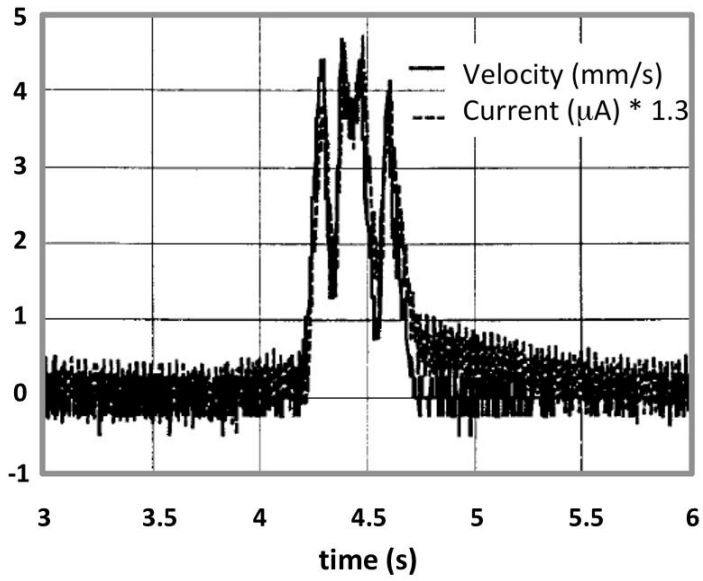

Figure 2.10. Short Circuit Current Response with Scaled Velocity Input [39] Copyright 2002 SAGE Publications

Bonomo et al. **[19]** presented experimental results of a cantilevered IPT under several harmonic excitations and it was observed that the output voltage signal trend was influenced by input loading type. Also, cantilevered transducers were tested also for ramp displacement inputs having different rates where the maximum tip deflection is 10mm [23]. It was seen that output voltage is linear as response to ramp displacement input, Figure 2.11. However, noise increases as input rate decreases.

Water solvated transducers and ionic liquid (IL) infused transducers were tested for dynamic input loading **[20]**. Experiments showed that transducers with IL have improved stability when operated in air as compared to those with water, while sensitivity decreases at high frequencies, Figure 2.12.

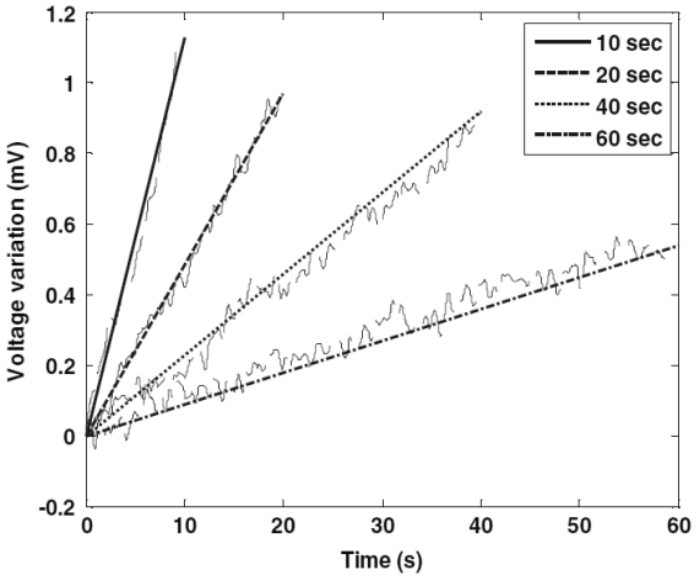

Figure 2.11. Sensor Response at Different Curvature Rates of 10 mm bending Deflection (500 mm radius of curvature) [23]

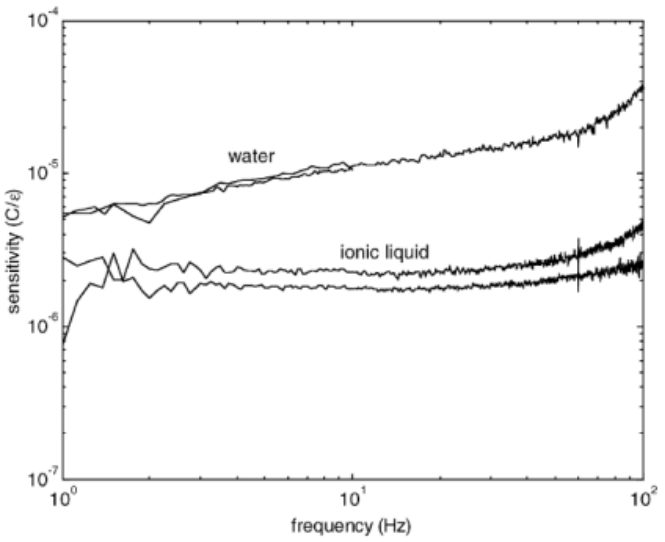

Figure 2.12. Sensitivity of IPTs in water and ionic liquid (EMI-TF) forms [20] Copyright 2004 Elsevier

In general, most IPT sensing experiments to date have imposed dynamic stimulation to observe some parameters` (*i.e.* hydration level, diluent type, counter-ion type, temperature and/or electrode material) effects over a frequency band **[4]**, **[19]**-**[23]** while some have studied periodic waves of step, ramp and impulse functions **[19]**, **[23]**. The outcome has been numerous postulates of the fundamental mechanism(s) responsible for the observed responses, and a general lack of consensus. In contrast, relatively few reports have studied step displacement stimulation **[24]**, **[25]** in the determination of some IPT parameters and characterization in sensing.

Furthermore, while most of the reports on sensing investigated the bending case, only a few studied shear deformation. For instance, in a shear sensing investigation, Farinholt et al. imposed a dynamic displacement input through the thickness of the sensor, where shear sensitivity was reported to be 0.0242 μC/ε on average. Subsequently, Tiwari et al. [40] deformed IPTs with a sine wave at different frequencies to observe energy harvesting capability in a shear

type mode applying force over the surfaces of the transducer which is clamped on both ends unlike the simple shear studied in this report where deformation is applied throughout the sensor thickness. Moreover, none of the foregoing reports have offered a hypothesis for the observed sensing response that could be argued for all modes of IPT mechanical deformation.

Recently, Weiland and Akle **[41**] imposed a constant frequency sine wave tip displacement to IPTs with varied electrode surface areas, where a correlation was found to exist between electrode surface area and peak sensitivity; the intent of that work was to establish a proof of principle for the streaming potential hypothesis as the fundamental mechanism responsible for sensing.

2.2 NAFION MORPHOLOGY AND IONIC POLYMER TRANSDUCER STRUCTURE

A basic understanding of ionomer morphology is prerequisite to discussion of the streaming potential hypothesis. Chemically, ionomers are composed of repeating moieties of electrically neutral units and a fraction of ionized units, which generally consist of carboxylic acid groups covalently bonded to the polymer backbone as pendant chains. The backbone is hydrophobic while the pendant ionic group is hydrophilic, resulting in a material system that displays phase separation. These polymers show a good chemical and thermal stability. The general formula for some of these membranes is given in Figure 2.13, Table 2.1.

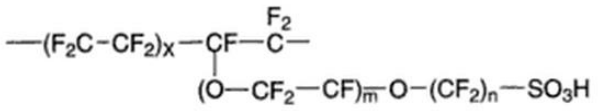

Figure 2.13. General Chemical Formula of Ionomers

Table 2.1. General Chemical Formula Constants of Ionomers

Membrane Type	m	N	x
Nafion	1	2	6-10
Flemion	0.1	1-5	3-10
Aciplex-S	0.3	2-5	1.5-14

Nafion®, a sulfonated tetrafluoroethylene based fluoropolymer-copolymer, is the first of a group of synthetic polymers having ionic properties, Figure 2.14. It is a commercial product of DuPont Company, was developed in the late 1960s, and is typically used in fabrication of IPTs as the base polymer. Ionomer ionic activity is often described by the metric equivalent weight (EW), which represents the amount (in grams) of dry Nafion per mole of sulfonic acid groups when the membrane is in acid form. Nafion 117 membranes are commonly used where the specification "117" refers to a film with an 1100 EW and a 0.007 inch nominal thickness **[42]**. Nafion has often been employed as a proton conducting membrane, and so draws attention also in fuel cell studies. As an actuator or sensor the material system is subject to an ion exchange process wherein a counter-ion other than H^+ is typically the mobile ionic species enabling electro-active response. Monovalent lithium and sodium ions are among the common counter-ions employed in IPTs.

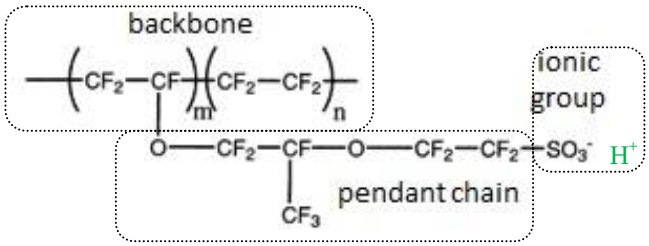

Figure 2.14. Chemical Structure of Nafion®. The counter-ion, illustrated here as a proton, H^+, is ionically attracted to the sulfonic group and the end of the pendant chain. Additionally, the pendant ionic pair is hydrophilic, resulting in the pendant groups residing in a fluid phase within the otherwise hydrophobic material system. The weak ionic attraction between the covalently attached sulfonic group and the counter-ion enables counter-ion mobility in the presence of a diluent.

As discussed in the previous sections, the ionomer becomes a transducer only after being sandwiched between conductive media. In particular, it is generally accepted that the ionomer region within the IPT is essentially a 'dead' region; rather it is the electrode-ionomer interface that enables transduction. This is sometimes referred to as simply the 'electrode' region, and is often likened to a capacitor on the basis that increased surface area tends to increase transduction, but therein draws attention to the importance of the electrode-ionomer interface.

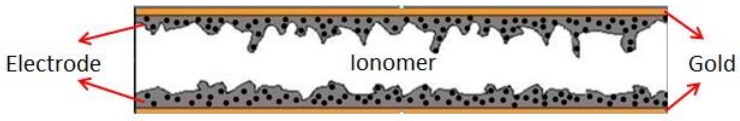

Figure 2.15. Schematic View of IPT Structure where a Dendritic, High Surface Area Electrode Tends to Enhance Transduction

It is generally accepted that the phase separated morphology that evolves in an ionomer enables charge and diluent transport through the material system in the presence of an external stimulus. A significant number of investigations have been carried out to understand Nafion's morphology, typically employing scattering methods. However, the exact phase separated morphology remains an open topic. In the absence of consensus on this point, modeling strategies have generally employed relatively simple morphological propositions involving particular structure assumptions **[42**]. The most widely used have been the 'cluster-network morphology' and the 'parallel channel morphology'. In this work, as a matter of modeling simplicity, the parallel channel morphology will be assumed.

2.2.1 Cluster-Network Morphology

In the cluster-network morphology proposition [43], [44], an elastic theory is employed to investigate ionic clustering evolution in perfluorinated ionomers assuming the required elastic energy for the hydrated cluster to form is balanced by the energy created by the favorable hydrophilic interactions at the surface and in the cluster interior. The ionic clusters exist as perfect spheres with a constant radius whose magnitude is influenced by cation type, equivalent weight, and hydration level.

A cluster forms as a hydrophilic phase consisting of polymeric charges and absorbed diluent that separates itself from the hydrophobic fluorocarbon backbone, Figure 2.16. The ions are presumably surrounded by liquid molecules closely positioned to the electrolyte-backbone interface which defines a spherical geometry. While the proposed cluster size can vary according to counter-ion type, and diluent type and uptake, a typical size for this theory is ~4nm. The clusters are assumed to be distributed in the Nafion matrix uniformly where the distance between

clusters, is also estimated (typical is ~5nm). Finally, per this theory, the clusters are connected to each other via nanochannels that enable ion transport between clusters and selective ion-exchange; the nanochannel size is not reported by Hsu & Gierke, though practitioners employing the theory have sometimes employed ~1 nm.

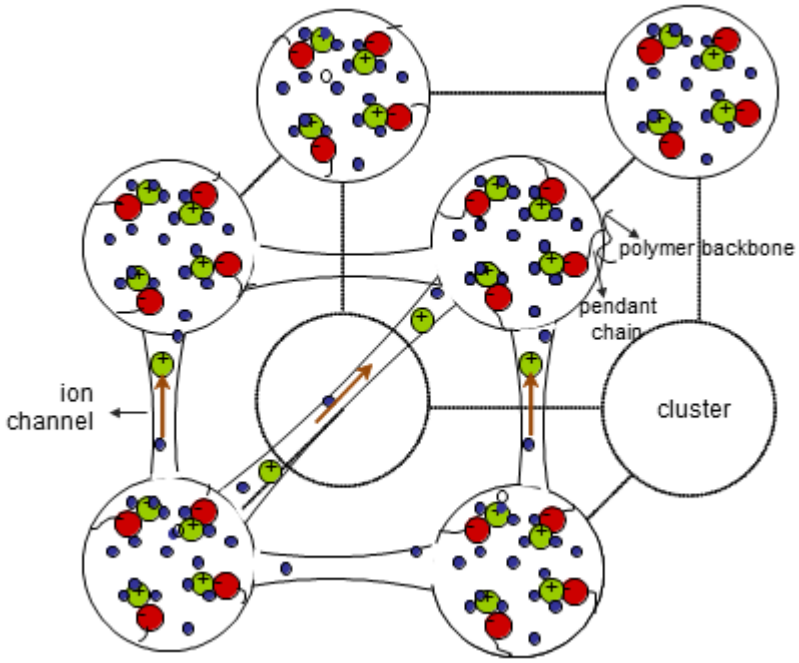

Figure 2.16. Cluster Network Morphology [41]

2.2.2 Parallel Channel Morphology

According to the parallel channel morphology proposition [45], the hydrophobic polymer backbone and hydrophilic ionic side groups in the hydrated Nafion reorganize themselves so as

to create elongated structures per arguments based on small angle x-ray scattering (SAXS) observations.

A schematic view of the parallel channel morphology is depicted in Figure 2.17. An inverted-micelle cylindrical structure forms since Teflon-like backbones take position on the outside while the hydrophilic ionic side groups define the water channel perimeter in the presence of electrolyte. It is proposed that the stiffness of the relatively straight helical polymer backbone sections balance the long cylindrical structures. The channels align locally parallel to each other and they all form as cylindrical inverted micelles. In the figure, the cross section of the polymer film displays the cylindrical water channels as white dots in the non-crystalline Nafion matrix shown with grey color, while black squares represent the crystallites in the polymer. Crystalline regions are physical crosslinks which influence the mechanical properties of the membrane, such as elastic modulus. They line up parallel to the water channels. With a hydration level of %20 by volume (%11 by weight), the diameter of the cylindrical water channel is proposed to be between 1.8 and 3.5 nm, with an average of 2.4 nm.

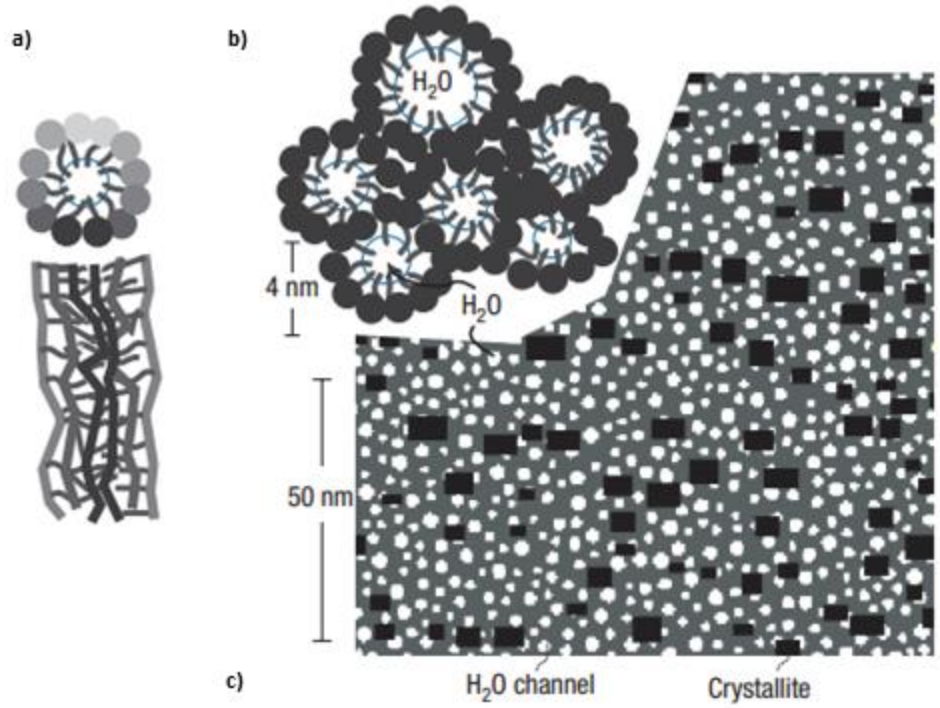

Figure 2.17. Parallel Channel Morphology: a) an Inverted-Micelle Cylinder b) approximately Hexagonal Packing of Several Inverted-Micelle Cylinders c) Cross-Sections of Nafion polymer [45] Copyright 2008 Nature Publishing Group

2.3 MODELING BACKGROUND IN SENSING TRANSDUCTION

To date, various models have been proposed to explain the behavior of IPTs. These can be characterized as black box empirical models; physics-based models, and grey box models that are hybrids of the first two. Among the first physics-based approaches was the hydraulic model **[46]**, which mostly focused on IPT actuation. Per this model, in the presence of an electric field, cations and diluent inside the membrane drift and pile up near the cathode leading to a local over pressure which tends to deform the membrane as in bending, Figure 2.18.

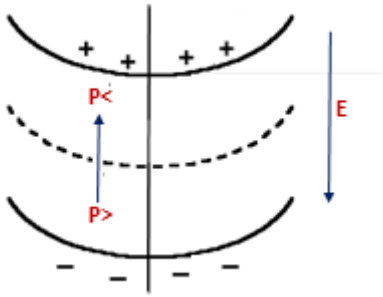

Figure 2.18. Principle of the "Inflation model": Under the field *E*, a water flux is entrained by the moving ions. This swells the bottom part of the strip, and deswells the top part and the strip bends. [46]

Nemat-Nasser et al. **[47]**, **[48]**, **[49]** subsequently presented a physics-based spherical cluster model, which again predominantly focused on actuation, but did explore sensing as well. Per this model, the application of the electric potential causes cations to migrate towards the cathode leading in an unbalanced overall cluster pressure which also drives water molecules through clusters, Figure 2.19. Therefore, the resulting volume changes of the boundary-layer clusters produce the macroscopic bending deformation of an IPT strip. When this model is adapted to sensing under imposed bending, it is suggested that electric potential is generated across the surfaces of the sensor because of the evolution of an effective dipole within the assumed spherical clusters. The cluster model was the first mechanistic sensing model to meet with some success. However, its predictive capability is strongly linked to the spherical cluster constraint (Section 2.2.1); while the exact morphology of ionic polymers remains an open question, it is generally accepted that a spherical morphology is incorrect **[50]**. As a matter of contrast, consider that Schmidt-Rohr and Chen **[45]** have recently argued that the hydrophilic regions may be more akin to long parallel water channels (Section 2.2.2) rather than interconnected spherical clusters for Nafion. Moreover, the IPT spherical cluster model for

sensing assumes perfectly paired anion-cation couples which are distorted under imposed bending deformation. This assumption for the sensing mechanism seems to be incompatible with the actuation portion of the same model where free counter-ions transfer between clusters. Finally, the spherical cluster model is developed regarding sensing in bending, but cannot explain the evolution of a sensing signal due to other types of deformation which have been previously reported [51], [52], [53].

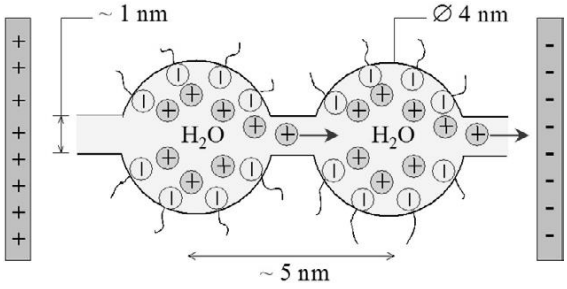

Figure 2.19. Cluster-Network Model: When subjected to an electric field, the unbound cations in the ion-exchange polymer membrane are free to move within the water that permeates the interconnected clusters [48]

Wallmersperger et al. **[8]**, **[54]** have introduced a chemoelectrical multifield formulation. The model predicts the evolution of a spatiotemporal volumetric charge density profile in the presence of an applied potential where Nernst-Planck equations address the effects of ion concentration gradient. The electric field is described by the one-dimensional Poisson equation. However, the electrodes are treated as ion blocking layers, Figure 2.20. The strength of this approach is that the chemo-electrical transport model is capable of computing the charge density profile in space and time and provides a base for other models. However, it is not clear that the

one dimensional treatment of transport phenomena is readily adapted to prediction of sensing in all modes of deformation. In addition, the treatment of the electrodes as ion blocking layers inhibits exploration of the role of electrode architecture in active response.

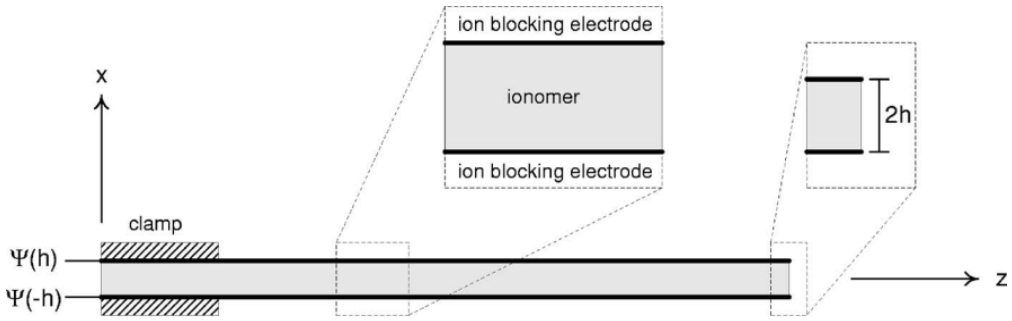

Figure 2.20. Transducer Geometry in Bending Analysis: Electrodes are treated as ion-blocking layers [8]

The models proposed so far contributed to the understanding of transduction mechanism of IPTs. However, they mostly ignored the electrode layer effect on the response. Among the few that mention the conducting part`s influence on the transducer response, a continuum approach exists.

2.3.1 Continuum Approach

Del Bufalo et al. **[55]** and Porfiri **[56]**, have implemented a mixture theory framework to develop an actuation model using continuum mechanics. The IPT capacitance is determined to evaluate sensing and actuation behavior calculating an effective thickness corresponding to the depth of

counter-ion boundary layers in the vicinity of the electrodes **[56]**. The influence of the electrode surface roughness is explored; it is argued that the average charge stored in the IPT increases as the electrode surface roughness increases due to the increased surface area [57], Figure 2.21. A multifield chemoelectrical framework initiated by Wallmersperger et al. **[8]**, is adopted employing the Poisson-Nernst-Planck model in the calculation of the transducer performance.

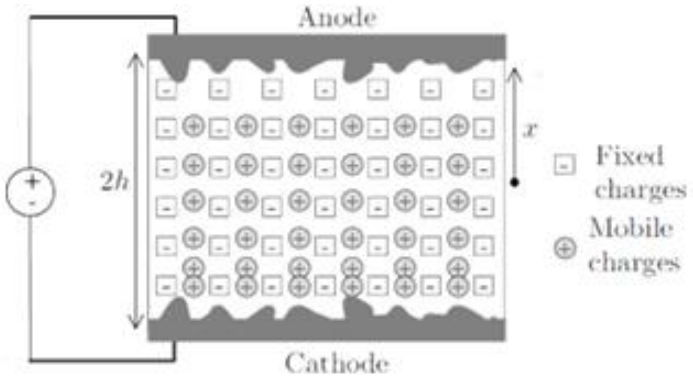

Figure 2.21. Sketch of the Transducer: Cation Enrichment in the Proximity of the Cathode and Cations Depletion in the Vicinity of the Anode Region [57]

In the definition of the polymer region *P* in Cartesian coordinates, the roughness of the interface between polymer and dendritic electrode is taken into account, Equation **(2.1**), supporting the idea that charge accumulating around the metallic layer plays an important role in transduction.

$$P = \{(x, y, z) : (y, z) \in S, \quad -h + \rho^{-}(y, z) \leq x \leq h - \rho^{+}(y, z) \qquad \textbf{(2.1)}$$

where *S* defines the membrane`s midsurface and metal protrusion into polymer surface is expressed by ρ^{-},ρ^{+}. The overall actuation response of the transducer is estimated using average

bending moment via Equation **(2.2**) while *m* states bending moment with respect to yz plane caused by electrostatic pressure, σ(x);

$$M = \frac{1}{|S|}\int_S m(y,z)dS = -\frac{1}{|S|}\int_P x\sigma(x,y,z)dP \quad \textbf{(2.2)}$$

In the calculation of the eloctrostatic pressure, the Poisson equation is utilized, Equation **(2.3**);

$$-\varepsilon_0\varepsilon_r\Delta\psi(x,y,z) = F(c(x,y,z)-c_0) \quad \textbf{(2.3)}$$

where ε_0 is the vacuum permittivity, ε_r is the dielectric constant of diluent infused membrane, ψ is electric potential, F is Faraday`s constant, $c$ is concentration, and $c_0$ is the fixed ions` concentration. Δ stands for the Laplace operator.

The strength of this model is that it investigates the role of the IPT capacitance in transducer performance regarding the influence of electrode surface roughness which is amenable to exploration of aspects of electrode architecture. However, the continuum nature of the electrode architecture effects may inhibit the ability to predict an in-practice saturation of improved sensitivity with increased electrode surface area, including through increased electrode volume.

2.3.2 Streaming Potential Hypothesis

A streaming potential hypothesis has also recently been suggested **[58**], **[59**], **[18**], **[60**], [53]. This hypothesis begins by viewing the diluent and counter-ions found within the

hydrophilic regions known to exist within ionic polymers as an electrolyte. Per classic streaming potential observations established over a century ago **[61**] that placing an electrode in an electrolyte results in the formation of an electric double layer of ions in the electrolyte, near the electrode surface, Figure 2.22. It is then argued that any relative motion of the IPT electrolyte with respect to, and in communication with, the electrode will disturb this double layer, resulting in the evolution of a streaming potential. Closing the circuit yields a streaming current. The physics attached to this theory are inherently multi-scale.

In particular, the magnitude of the predicted sensing signal per the streaming potential model can vary by orders of magnitude with assumed ionomer morphology, however, the trends for a given morphology are expected to be reasonable, and more importantly, the existence of a sensing signal is predicted for any assumed morphology **[59**]. This is especially noteworthy in the case of shear where there is no hydrostatic component of stress for inducing pressure driven diluent flow **[18**]. Finally, the streaming potential hypothesis is amenable to experimentally observed variations in sensing as a function of electrode morphology. The strength of this method is its ability to explain the existence of a sensing signal for any mode of deformation as well as its evolution as a function of electrode architecture. Its current weaknesses include limitation to inspection of predicted trends and lack of directly applicable experimental data for validation. It is however compelling due to its unique ability to directly explain the experimentally observed existence of a sensing signal for any mode of deformation.

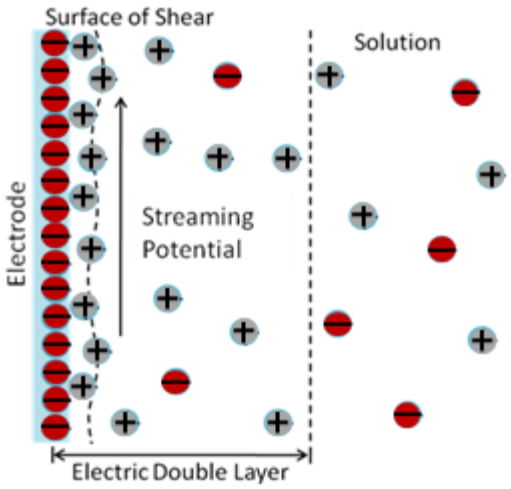

Figure 2.22. Electric Double Layer Formation **[62]**

2.3.2.1 Streaming Potential Hypothesis in Bending Mode

An introduction to the streaming potential hypothesis and relevant modeling in bending **[58]**, **[59]**, **[60]**, is offered in this section. According to the hypothesized mechanism of interest in this work, unpaired cations and diluent in the hydrophilic regions of the IPT essentially comprise an electrolyte. In the regions of the IPT where the metallic particulates in the electrode region comes into contact with this electrolyte, an electric double layer is expected to evolve as observed in the experiment, Figure 2.22, when an electrode is placed in an electrolyte. Thus, when the effective-electrolyte within the IPT moves with respect to the electrode, a streaming potential should result since the electric double layer formed at the electrode surface is disturbed. An important ramification of this hypothesis is that the sensing signal evolves exclusively in the electrode region. For the case of bending, a pressure driven flow of electrolyte will be the impetus for the relative motion of the electrolyte with respect to the electrode, as illustrated in Figure 2.23. While bending is arguably the simplest case to test, the fact that other IPT

deformation modes will necessarily result in relative motion of the electrolyte with respect to the electrode is intuitive.

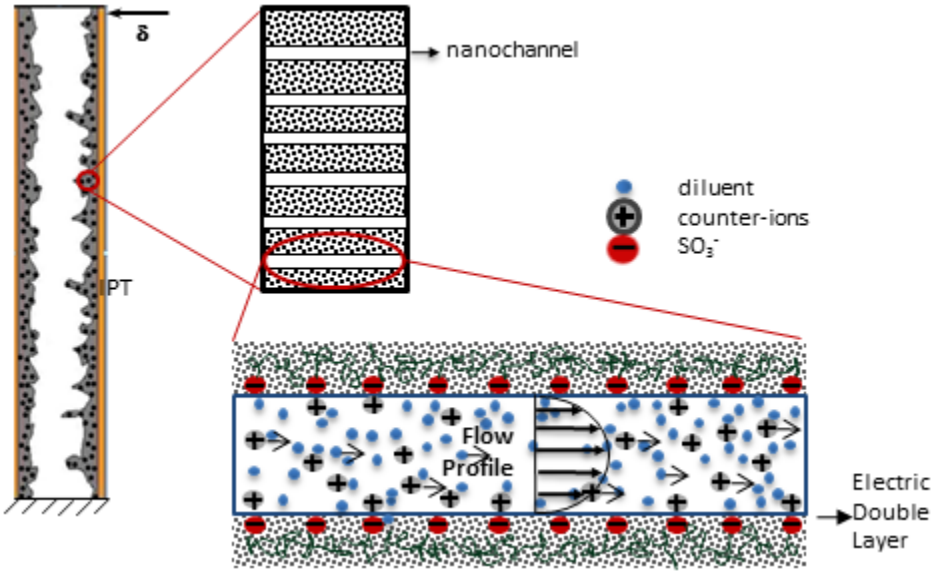

Figure 2.23. Schematic Illustration of the Evolution of Streaming Potential within the Electrode Region of an IPT: Assumption of a cylindrical morphology facilitates visualization as well as simplifies mathematical analysis of bending mode electrolyte flow, but is not required.

The total streaming current that can be obtained by an IPT is the summation of all the streaming currents developed in the electrode region of the transducer. While the existence of a streaming current can be argued for any assumed morphology **[59]**, for simplicity, parallel circular cylindrical channels in the electrodes are assumed in this assessment with dimensions consistent with the Schmidt-Rohr and Chen morphological proposition (Section 2.2.2) **[45]**. In general, streaming current generated in a single channel may be estimated via **(2.4)** **[63]**.

$$I_s = 2\pi \int_0^{r_{channel}} \rho(r) v(r) r \quad dr \tag{2.4}$$

where $r_{channel}$ is the channel radius, $\rho(r)$ is charge density of unpaired counter-ions, $v(r)$ is flow velocity and r is the distance from the channel center. An expression for the velocity profile for the case of a pressure driven flow within a channel, such as Poiseuille flow depicted in Figure 2.23, is expressed in Equation **(2.5**) as:

$$v(r) = \frac{\Delta P\left(r_{channel}{}^2 - r^2\right)}{4\mu l_{channel}} \tag{2.5}$$

where ΔP is the pressure difference between the two ends of the nanochannel caused by bending, μ is the viscosity of the fluid, and $l_{channel}$ is the length of the channel. For simplicity it is assumed that all hydrophilic channels are ideally aligned for pressure driven flow through the thickness of the IPT electrodes. Thus, for the cantilevered IPT which is exposed to tip deflection δ, classic beam theory may be imposed to estimate the pressure difference between the two ends of the channel, ΔP. The streaming current in one, ideally aligned channel can be expressed as:

$$I_s = \frac{3\pi\rho_e r_{channel}{}^4 E\left(l_{IPT} - x\right)}{8\mu l_{IPT}{}^3}\delta \tag{2.6}$$

where E is the elastic modulus, l_{IPT} is free length of the cantilevered sensor, x is the distance from the fixed end and ρ_e is the charge density of unbound counter-ions in the flow. The streaming current in a given channel depends on its distance from the cantilevered base, with the maximum case occurring at $x = 0$:

$$I_{s\max} = \frac{3\pi\rho_e r_{channel}^{\ 4} E}{8\mu l_{IPT}^{\ 2}}\delta \tag{2.7}$$

The total streaming current in the sensor can be estimated by summing the contributions from all channels. Because the channel dimensions are assumed *a priori* in this assessment, based the Schmidt-Rohr and Chen morphological model, the total number of ideal, parallel channels, $N_{channels}$, penetrating the thickness of the transducer with electrolyte volume fraction of f_l is estimated by relating the channel dimensions to the total volume fraction of diluent uptake via Equation **(2.8**) where w_{IPT} is the width of the IPT:

$$N_{channels} = \frac{f_l w_{IPT} l_{IPT}}{\pi r_{channel}^{\ 2}} \tag{2.8}$$

thus the total current (I_{IPT}) is calculated via:

$$I_{IPT} = \frac{3}{16}\frac{f_l w_{IPT} r_{channel}^{\ 2} \rho_e E}{\mu l_{IPT}}\delta \tag{2.9}$$

It is an interesting observation that the length of the channel drops out of this expression **[58**]. This is a ramification of the series of simplifying assumptions, which are considered reasonable for the goals of that study, but are not retained for more complex theoretical assessments. For instance, in a shear sensing model **[18**], multiple flow orientations have been assessed and predictions suggest that the nanochannel length and orientation with respect to the direction of the IPT loading plays a significant role in the evolution of a streaming current.

The foregoing equation is instructive for understanding the fundamental principle; however, it does not consider the volume fraction of metal particulate in the electrode region,

while it is the electrode region that is of primary concern. This is addressed via an adaptation of Darcy's Law, a constitutive equation that describes fluid flow through a porous medium. The electrode is taken to be composed of the metal particles and the voids between particles. The void is a mixture of the ionomer and the diluent for a DAP transducer. These voids can be represented as the porosity of the electrode, Φ. Implementing Darcy's Law to describe the flow, the corresponding total streaming current of a transducer in the porous interpenetrating electrode region may be expressed as **[58]**:

$$I_{IPT} = \frac{3}{2}\frac{Cf_l w_{IPT} r_{channel}^{\ 2} \rho_e E}{\Phi \mu l_{IPT}}\delta \qquad \textbf{(2.10)}$$

where C is a dimensionless constant that is related to the configuration of the flow-paths. The evolution of sensing with electrode particulate volume fraction for DAP based IPTs with different electrode architecture is investigated and it is noted that the channel size in the electrode will necessarily be influenced by the evolution of the elastic energy with particulate volume fraction, which is then captured via evolution of a ratio β. β parameter physically shows how the nanochannel cross-section size is influenced by metallic phase in the electrode region. It has previously been estimated as evolution of spherical cluster size with the expression developed by Li and Nemat-Nasser **[49]**, and employed on channel cross-sectional size evolution by Weiland and Akle **[41]**. In this respect, the channel radius is multiplied with β. The corresponding total IPT current is then estimated via Equation **(2.11)**:

$$I_{IPT} = \frac{3}{2}\frac{Cf_l w_{IPT} f_p \beta^2 r_{channel}^{\ 2} \rho_e E}{\Phi \mu l_{IPT}}\delta = B\frac{f_p \beta^2}{\Phi} \qquad \textbf{(2.11)}$$

where f_p is volume fraction of metal particles. For IPTs exposed to the same tip displacement, dividing Equation **(2.11)** by the constant B enables inspection of the remaining terms' effects, collectively described as the streaming current factor **[58]**.

The bending model estimations were improved further by Zangrilli [64] employing the *local* elastic modulus in the calculation of total current, Equation **(2.11)**, instead of *global* elastic modulus. By this way, the predicted current value is noticeably reduced which provides a better match with the experiments. For example, Gao and Weiland [62] estimate the current as 0.9 mA in bending for a cantilevered transducer when exposed to 2 mm tip deflection (IPT with the dimensions of 5mmx15mm) while an experimental study ([39]) is cited in the same work such that the current output is measured as 0.1 mA. In the work of Zangrilli, corresponding current is estimated as 0.4 mA for the same case when a local stiffness value estimated for the cylindrical morphology is used in the calculation. Therefore, local stiffness application rather than macroscale one eliminates a possible source of error.

Moreover, Zangrilli [64] revised the streaming potential modeling to estimate the sensor response for a given bending deflection which also incorporates the time domain in the model, Figure 2.24.

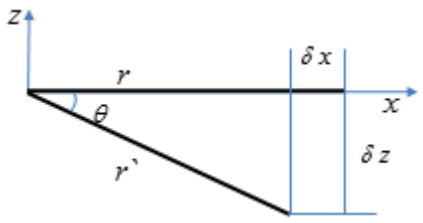

Figure 2.24. Coordinate System for 2D Bending Deflection Model

The electrolyte flow (v) driven by a pressure gradient, where P stands for pressure, is calculated via Equation **(2.12)** utilizing the conservation of the momentum to be used in the calculation of streaming current as in Equation **(2.1)**;

$$\rho\left(\frac{\partial v}{\partial t}\right)=\mu\left(\frac{\partial^2 v}{\partial y^2}\right)-\frac{\partial P(x,t)}{\partial x}+\rho_e\nabla_y\Psi(x,y) \qquad \textbf{(2.12)}$$

where Ψ is distribution of the electrical potential field in the channel.

2.4 CHAPTER SUMMARY

The foregoing chapter has offered a review of the fundamental material structure of IPTs, fabrication methods, and the current state of understanding with emphasis on sensing. The chapter has also provided prior studies intended to motivate continued testing of the streaming potential hypothesis. It must however be noted that a full theoretical assessment of the multiscale phenomena inherent to this approach is well beyond the scope of this effort. Rather a straight forward adaptation of the key aspects of the streaming potential hypothesis is sought to preliminarily assess and refine the correlation between the hypothesis and the experimental results. Notably missing from assessment of the streaming potential hypothesis are (*i*) fabrication of transducers with controllable properties amenable to testing the streaming potential hypothesis; (*ii*) step-displacement bending mode experiments designed specifically for testing this hypothesis, (*iii*) step-displacement shear mode experiments designed for and in parallel with models specifically designed to test this hypothesis, and (*iv*) step-displacement compression

experiments and model development designed specifically for testing this hypothesis. Each of these aims is addressed, respectively, by each of the following chapters.

3.0 FABRICATION OF TRANSDUCERS

The DAP was selected for IPT fabrication because it enables the usage of any type of ionomer, diluent, and conducting powder. It also allows direct control over the electrode thickness and composition **[13**] and thereby offers a pathway to ultimately systematically explore hypotheses for the physical mechanisms responsible for the observed sensing response. EMI-TF, a type of nonvolatile ionic liquid, was chosen as the diluent because it is stable in air **[20**] when compared to water and therefore eliminates dehydration effects from the study. Lithium was selected as the counter ion because previous reports suggest that sensitivity is typically enhanced for this ion exchange. The electro active polymer Nafion-117 was selected because it aligned with a significant number of previous reports to enable comparison. The specific procedure employed in the fabrication of the ionic polymer sensors was the DAP for building solvated transducers, such as the one illustrated in Figure 2.4 follows a progression;

1. The Nafion membrane is boiled in sulfuric acid (H_2SO_4) solution for half an hour (Essentially cleaning).
2. The cleaned membrane is boiled in metal salt (for example; LiCl) solution for two hours to exchange protons (H^+) with metal cations (for example; Li^+), and then rinsed with deionized (DI) water to remove excess metal salt precipitates.

3. The ion exchanged membrane is boiled in DI water for two hours to be cleaned, and then dried in a 150 °C oven for 12 hours to remove unbound water in the ionomer to the extent practicable.
4. The dried Nafion is soaked in the ionic liquid, EMI-TF, in a 150 °C oven for two hours for diluent uptake. (This step is conducted before application of the electrodes to avoid swelling-induced cracking, especially in the thin gold layer.)
5. The electrode solution mainly consists of high surface area ruthenium dioxide (RuO_2) conductive metallic powder and 5% Nafion polymer solution. In preparation of the electrode mixture, first, RuO_2 and Nafion solution are mixed, as desired portions by volume. Second, ionic liquid is added to the metallic powder-polymer solution mixture so as to weigh 58% of polymer in Nafion solution as the EMI-TF absorption capacity of Nafion. Furthermore, DI water and isopropyl alcohol are added to increase the dispersion to ease spraying which will evaporate during the following steps of fabrication. To assure uniformity of the electrode solution, the mixture is stirred with a magnetic stirring bar for 20 minutes, then sonicated for 100 minutes, and then stirred again for 20 minutes. Then, the electrode mixture is painted as several layers on each surface of the Nafion making use of air spray equipment while the sample is dried in the oven over 100 °C as needed during spraying to eliminate wrinkling, Figure 3.1.

6. Finally, the electrode painted membrane is sandwiched between gold sheets to melt press two layers of gold (50nm thick) on the outer surfaces of the sample to increase conductivity on the surfaces of the transducer. Pressure (2MPa - 4MPa) is applied on the

gold-painted membrane-gold structure at 160 °C - 180 °C making use of a load frame-heat chamber system.

A representative transducer is depicted in Figure 3.2.

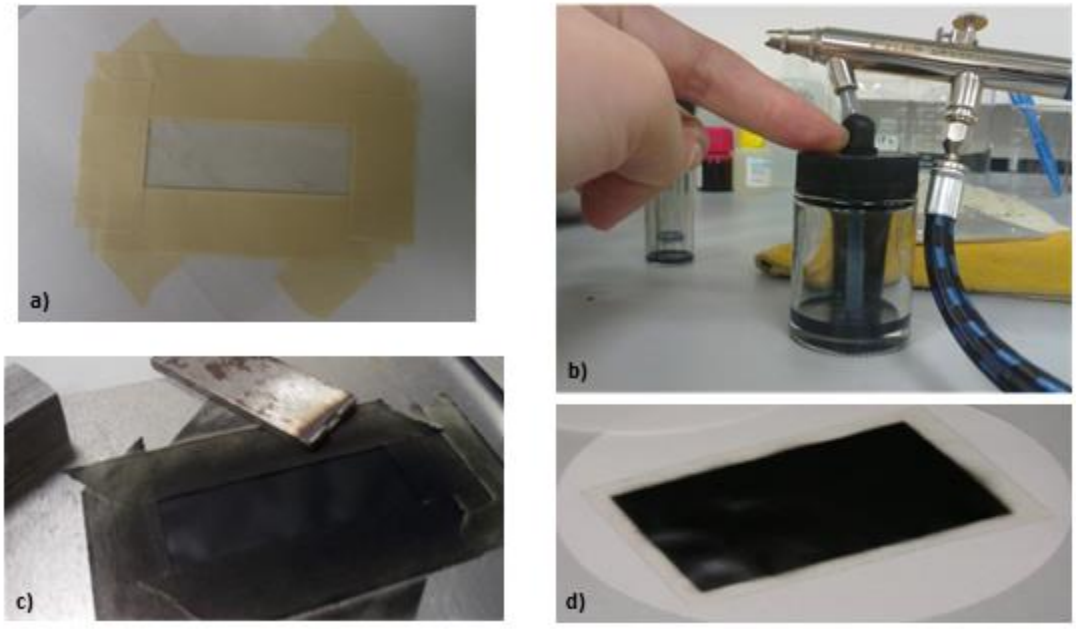

Figure 3.1. Electrode Painting: a) Nafion membrane is taped to eliminate wrinkling b) Air brush is used to spray the electrode mixture to enhance the uniformity of the electrode solution dispersion c) Painted membrane is dried in the oven as needed to eliminate wrinkling d) Electrode painted membrane.

Figure 3.2. Transducer Produced by adopting the Direct Assembly Process

4.0 EXPERIMENTAL CHARACTERIZATION OF IONIC POLYMER TRANSDUCERS IN BENDING

IPT bending is the most often considered sensing mode, which might be attributed to the relative simplicity in design and implementation of these experiments, as well as to the comparatively large signal generated in this mode. In this research, bending mode is studied because: (*i*) preliminary bending tests could be used to validate the test fixture with respect to past reports, (*ii*) a frame of reference exists when exploring the transient tests presented here; and (*iii*) the existing streaming potential models for bending lacked access to appropriate experimental validation data. The presented experiment was designed, constructed, and implemented accordingly.

4.1 METHODOLOGY

4.1.1 Bending Test Setup and Experiments

The experiment is designed to measure the output current response of the IPTs when a step displacement input is applied at the free end of the cantilevered transducer. The test setup is composed of a clamping tool, a solenoid motor, an amplifier, an amplifying electric circuit,

batteries, and data acquisition hardware including data acquisition card and computer; the assembly of test equipment is depicted in Figure 4.1.

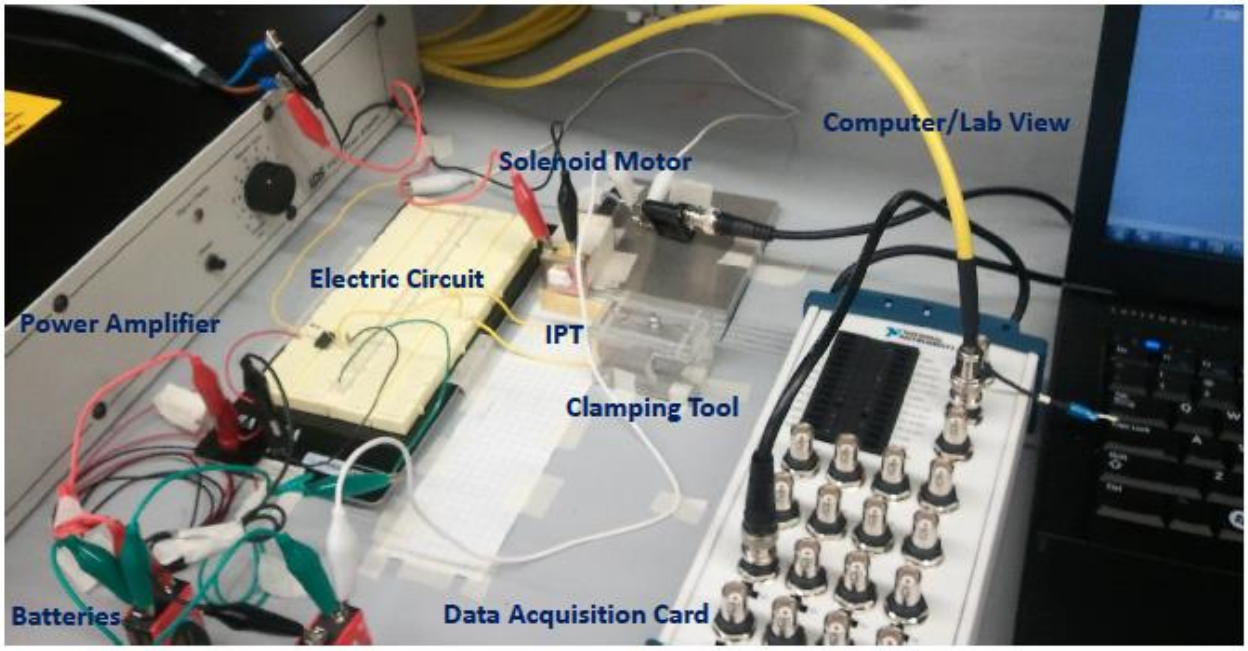

Figure 4.1. Bending Experimental Rig

The schematic representation of the test setup and the flow of the data are presented in Figure 4.2. In application, a voltage signal, created via a LabVIEW code through the data acquisition card, is first amplified via a power amplifier and then sent to the solenoid motor to apply a step displacement input to the free end of the cantilevered transducer. The current produced by the IPT is amplified via a signal conditioning circuit. Finally, the transducer output data is gathered via the data acquisition card and sent to the computer for post processing. All data acquisition processes are completed via LabVIEW and NI USB-6216 BNC type data acquisition card.

The electric circuit (similar to the one offered by Farinholt et al. **[51]**), whose schematic illustration is shown in Figure 4.3 is a signal conditioning circuit which enables short circuit current measurement. The output resistance, 100kΩ, leads in a 10μA/V sensitivity. The operational amplifier (OP177) is fed by 9V batteries.

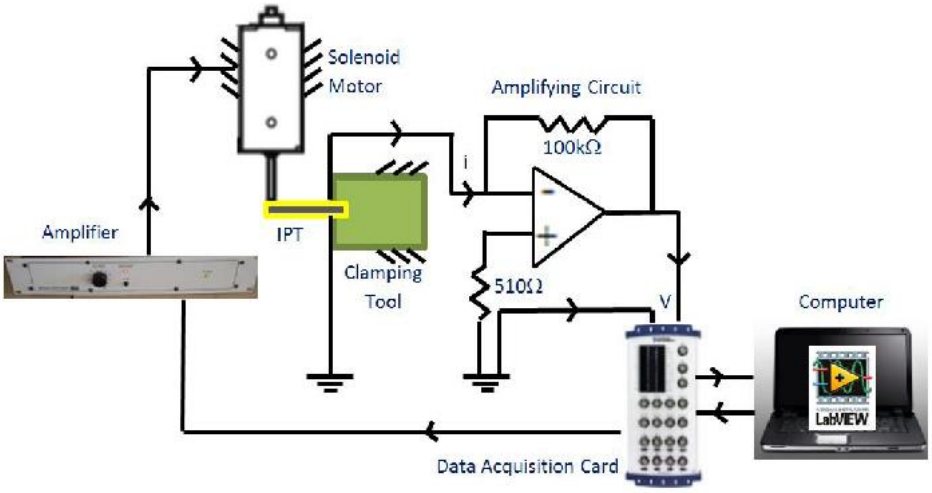

Figure 4.2. Schematic Representation of the Bending Experimental Rig

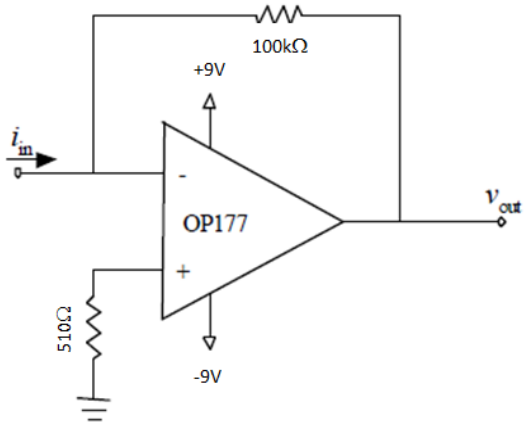

Figure 4.3. Signal Conditioning Circuit (Sensing)

4.1.2 Results and Discussion

Two batches of five transducers with 42 vol% RuO_2 and five transducers with 21 vol% RuO_2 in the electrode by volume were tested for different bending displacement stimuli. The IPTs under investigation were 15 mm x 47 mm surface dimensions and the electrode mixture was prepared to create ~14 μm thick layers on both sides of the IPT. Each sample is clamped from 40 mm. The tests were repeated reversing the opposite sides of the transducers in order to determine possible face sensitivity. The output current for IPTs, which have different RuO_2 concentration in the electrode, with respect to time are illustrated for representative ones in Figure 4.4. It is seen that the generated current decreases as input tip deflection decreases, as expected. A signal reversal is also observed, which is consistent with previous reports; **[25**], showing that current evolves as a peak followed by a reverse peak when a step displacement input caused by impulse velocity stimulation is applied to the cantilevered beam at the tip. It is hypothesized that the vorticities in the fluid through the nanochannels can be the reason creating a backflow in the velocity which may trigger the reverse current **[52**]. Another plausible explanation for the reverse current evolution is related with the situation that a new electrical balance forms between free counter-ions and the fixed ionic groups which may induce a backflow after the pressure difference in the nanochannels in response to deformation is dissipated. Furthermore, the small oscillations following the reverse current can be caused by the input step deflection itself due to high strain rate, **[52**], **[53]**.

Furthermore, generated current caused by a tip deflection and the one after the sensor is inverted show similarity. These results indicate face insensitivity for the cantilevered transducers exposed to bending, unlike the outcomes of the study on IPT response for static tip deflections **[24**] which states that a different trend occurs when the transducer is bent in the opposite

direction. The reason for the earlier observation can be related with a situation that the reverse sides of the transducers may have been tested before the open circuit voltage vanishes. It was previously experienced that it takes a while for signal to diminish before applying displacement excitation to eliminate unwanted signal and noise which can develop during actions affecting the capacitive behavior of the IPT and the circuit [65].

It was also observed that the current signal caused by step input dies out in a shorter time for 21vol% RuO_2 IPT than for 42vol% RuO_2 IPT. One plausible explanation may be related to the evolution of channel dimensions in the presence of varied volume fractions of the comparatively stiff metal particulate. For 21vol% transducers, the lower elastic energy of the electrode region as compared to the 42vol% case is expected to include wider cross section nanochannels, enabling streaming current evolution in a shorter time since resistance to cation-diluent passage is lower.

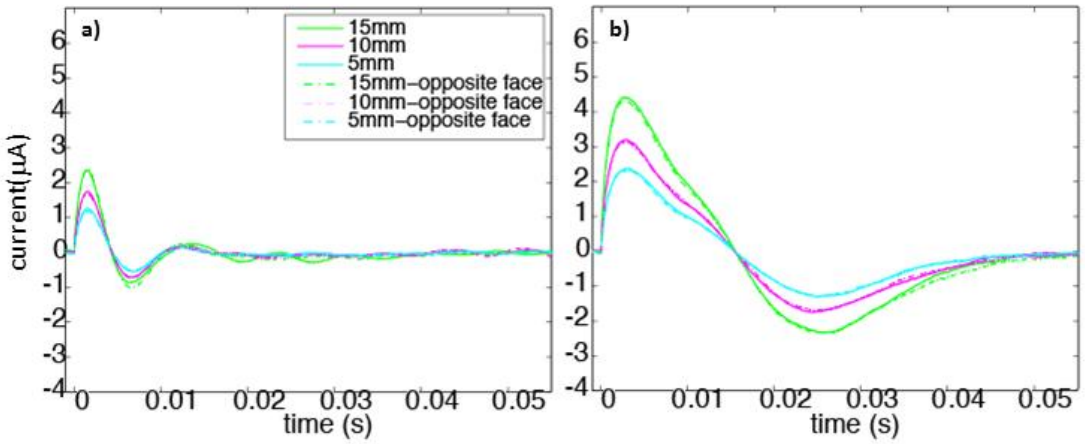

Figure 4.4. Current Output of a Representative IPT Under Step Bending a) 21vol% RuO_2 case b) 42vol% RuO_2 case

The maximum current obtained from each transducer is compared in Figure 4.5 for different tip displacements for different electrode structure cases. It is observed that the difference seen among the maximum current output of the samples is small and can be caused by minor experimental errors. Also, in Figure 4.5, the maximum current and the maximum current for reversed sensor exhibit similarity but a slight difference occurs when different transducers are compared. This is a natural outcome of small differences in fabrication of IPTs. Besides, the difference increases as the deflection increases which can be attributed to instability occurring for bigger deflections. However, the trend and the magnitudes of the maximum voltages show a reliable correspondence when all samples are considered. Therefore, results of the experiments show consistency assuming minor discrepancies are not significant.

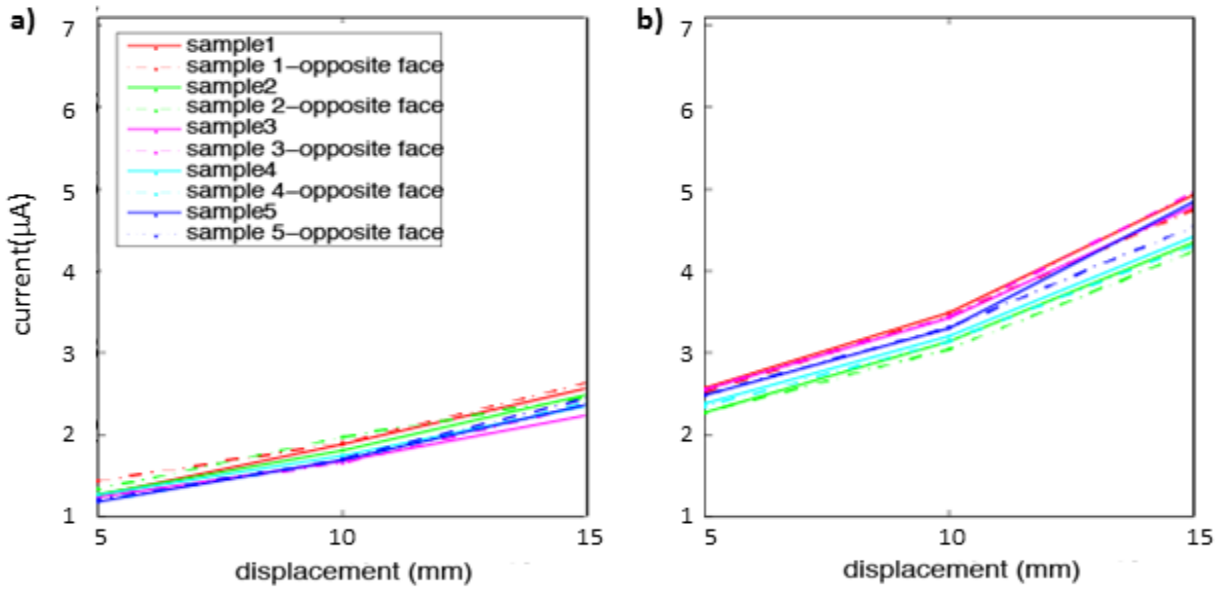

Figure 4.5. Maximum Current Outputs in Bending: a) 21vol% RuO_2 case b) 42vol% RuO_2 case

Furthermore, the mean value of all maximum currents of five transducers for each deflection is presented in Figure 4.6. The error bars represent the range of measurements where the limits show maximum and minimum current measured during experiments on different samples. It is seen that the experimental variation among the tests conducted with all samples as well as their reverse sides is minimal. The strong repeatability derives from the use of an ionic liquid diluent as well as from batch processing of the IPTs. Similar consistent behavior is accomplished in frequency domain experiments; however, it is more difficult to achieve consistency in step input experiments. Compared to Bonomo et al. **[4]**, observed errors in our study are noticeably smaller.

Figure 4.6 also establishes that the results for the cases considered are meaningfully different. When the current outputs of the 21vol% RuO_2 IPTs and the 42vol% RuO_2 IPTs are compared, it is observed that the generated current increases as the metal loading in the electrode solution is increased. This shows that the mechanism responsible for IPT sensing is influenced by the electrode architecture such that an increase in metal particulate volume fraction in the electrode mixture leads to higher sensitivity. This is believed to be the natural outcome of an increase in total surface area of the metal particulates in the porous electrode structure which enables electric double layer (EDL) formation and capacitive behavior. When the EDL is disturbed throughout the channels within the electrode, current is generated. However, as the metal particulate concentration increases, the cross section of the nanochannels that enable electrolyte passage decreases, which interferes with the formation of streaming current at some point as similarly presented by Weiland and Akle **[41]**. Thus some optimum particulate loading must exist. For instance, a sensitivity peak at about 50vol% RuO_2 was predicted; after this peak value, sensitivity decreases as the metal particulate volume fraction increases **[58]**.

To enable inspection of comparative trends, the average values of the maximum responses produced by each sensor are calculated for different tip deflections in bending tests for IPTs with 42vol% RuO_2 and compared to the 21vol% RuO_2 samples` outputs. It is observed that the relationship between current and displacement shows linearity within the error bars exhibiting compatibility with streaming potential theory that predicts a linear relationship between the input displacement and output current.

These results may also be used to assess the prediction of the streaming potential theory. Namely, peak response of the 42vol% RuO_2 IPT is predicted to be 2.2 times that of the 21vol% RuO_2 IPT via streaming potential hypothesis **[58**] while the streaming current factor in Equation **(2.11)** is estimated as 0.27 and 0.60 for the IPTs with 21vol% RuO2 and 42vol% RuO2, respectively. When comparing the experiment results of 21vol% case with true step loading with the 42vol% case, the relative variation in peak response is found to be 1.95 which is close to the streaming potential theory prediction, 2.2. In the estimation of streaming potential in bending employed here, the pressure difference between the surfaces of the transducer is accepted as the source of streaming fluid flow.

The experimental results were also assessed to evaluate streaming potential modeling estimations developed recently by Zangrilli [64] which also incorporates time dependency into the bending modeling. The model, which is described in 2.3.2.1, estimates the current output of Li exchanged, EMI-TF infused, 15 mm x 40 mm Nafion based IPT with electrode thickness of ~14 micrometer for 5 mm step tip deflection as in Figure 4.7;

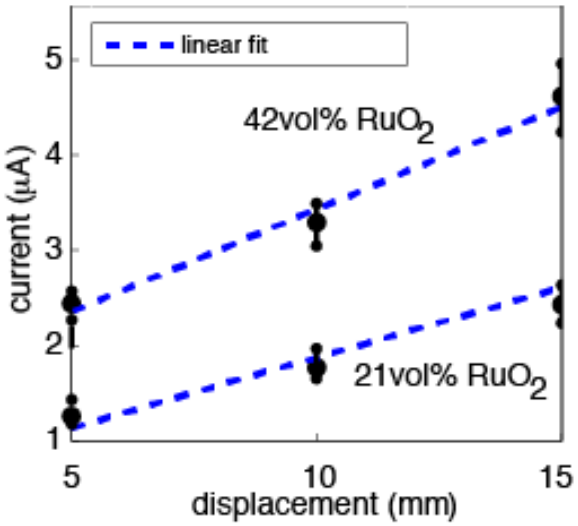

Figure 4.6. Average of Maximum Current Outputs for IPTs with 21vol% RuO2 and with 42vol% RuO_2 for Step Bending and Linear Fit

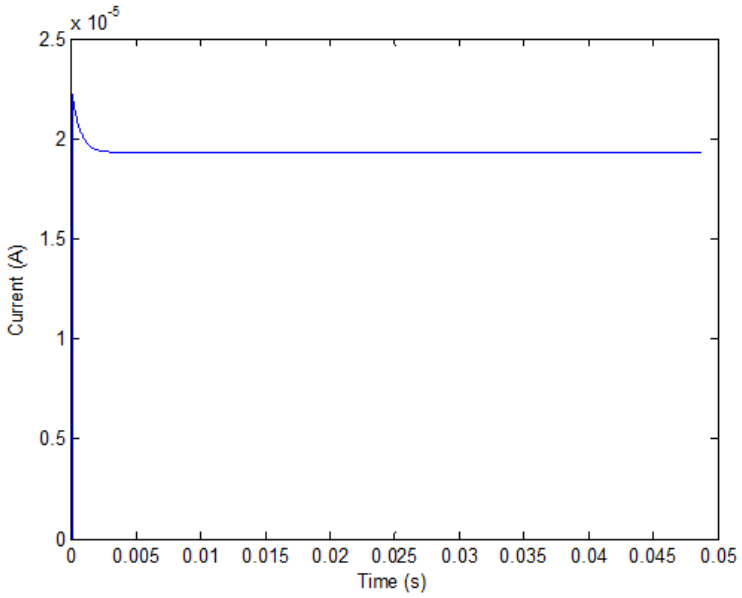

Figure 4.7. Streaming Potential Model Current Estimation in Bending [64]

The model estimates maximum current and steady state current as 22.2 μA and 19.3 μA, respectively, while the experimental peak current is measured as 2.2 μA, Figure 4.4. Compared to Gao`s model [66], the order of magnitude of prediction gets closer to the measured current through *local* modulus usage in the calculations as also explained in Section 2.3.2.1. However, the weakness of the model, as also expressed by Zangrilli [64], is that for the current state of development, the model cannot predict the expected decay in the current signal but instead predicts a steady state value. Incorporation of time dependent local effects has been proposed by Zangrilli for future model development.

It is pertinent to offer discussion of how the other IPT electromechanical coupling hypotheses might accommodate the experimental observations offered in this report. To begin, consider that a classic hydraulic model **[46**], which attributes electromechanical behavior to pressure difference caused by cation drift along with diluent, clearly states that electrode effects are ignored; it is further acknowledged in **[46**] that it is an especially weak assumption for a system which contains finely divided conducting particles as obviously illustrated in our experiments. Similarly, according to the cluster/dipole sensing model **[47**], in the determination of the electric field of a dipole, which is produced by the difference in displacement of anion and cation charge centers in a cluster due to imposed deformation on IPT, the electrode mixture effect is not considered. However, it is stated that nano-structure of the membrane and the electrode morphology determine diluent and cation transport and electric conductivity of a transducer where metal plating influence is included in the stiffness calculation of the IPT in actuation **[48**]. Thus neither the hydraulic nor the cluster-dipole hypotheses are currently able to directly explain the physical implications of electrode morphology.

A recent continuum type study has specifically considered electrode morphology in terms of contour roughness **[57**]. The method of that report is able to describe the distribution of the electric potential and the concentration of mobile counter-ions in response to a static voltage difference applied across the electrodes implementing Poisson-Nernst-Planck model and to investigate the formation of thin boundary layers in the proximity of the polymer-electrode. It is stated that the stored charge linearly increases with the polymer-electrode interface area. However, it is not clear that if it can accommodate the influences of varied electrode composition on sensing, observation of optimal loading as well as predicting response in modes other than bending.

In contrast, in the streaming potential theory, the EDL forms on the electrode which is shaped primarily by the metallic powder mixture. Thus, only the part of streaming signal produced in the electrode portion is taken into account where the generated current can be collected over conducting metal particles. Therefore, as total surface area of the metallic phase increases, capacitance of the transducer is enhanced as observed in the experiments in our study.

4.1.3 Electrode Optimization

In order to specifically explore the streaming potential prediction that some optimum electrode particulate volume fraction exists at around 50vol% RuO_2 (**[58**]), the methodology validated for reliability per the above was imposed for IPTs with more broadly varying electrode compositions **[69**]. Two IPTs (15mm x 47mm with ~14μm electrode thickness) were produced for each kind of transducer with different metallic powder volumetric concentration in the electrodes, namely; 30vol% RuO_2, 40vol% RuO_2, 50vol% RuO_2, 60vol% RuO_2. In this study, forty eight tests were conducted using eight samples which are clamped from 40mm utilizing the

bending test rig shown in Figure 4.1. The IPTs were tested for two different tip step displacement inputs in bending; 20mm, 15mm and current responses were measured and each test was repeated three times to ensure reliability of the experiments as well as test setup **[69**], Figure 4.8.

Mean values of the maximum currents produced for transducers of each electrode composition were calculated for each tip excitation and depicted in Figure 4.9 where the measured current interval is presented via an error bar displaying consistency. It is observed that the sensitivity enhances as the RuO_2 volume percent in the electrode solution increases up to the value 40%. However, further increase of metallic powder content leads to a reduction in the produced current, as predicted. Thus, the experimentally determined optimum value for metal loading of 40vol% is similar to the 50vol% predicted by theory; the similarity is in fact quite good when it is recalled that the streaming potential theory is inherently multi-scale. In addition to supporting theory, physically this result indicates that the role of electrode communication both with itself and the ionomer-diluent channels represents an important parameter. A similar trend was also observed for the cases of 15mm and 20mm tip deflection. That shows the magnitude of deflection influences the peak current but not the optimum sensitivity which depends on electrode structure as indicated via streaming potential hypothesis.

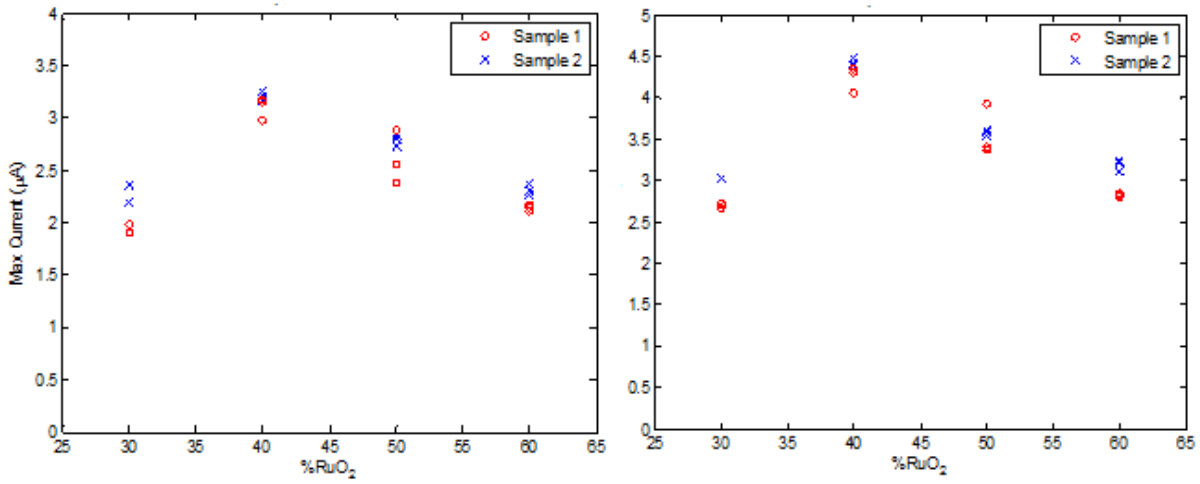

Figure 4.8. Maximum Current Outputs for IPTs with Several Electrode Architectures for 15mm (left) and 20mm (right) Step Displacement in Bending

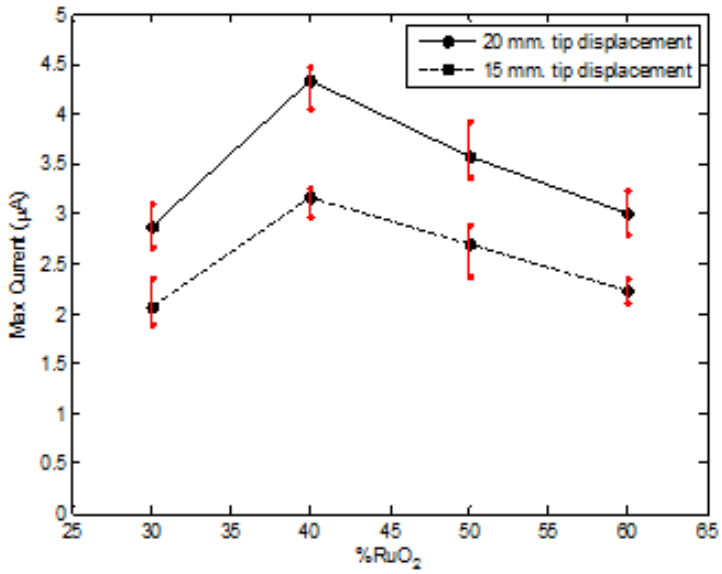

Figure 4.9. Average of Maximum Current Outputs vs. Metal Loading for Bending Step Tests

4.1.4 Annealing Experiments

The performance of IPTs depends on many variables including the stiffness of the polymer which evolves with the level of semicrystallinity within the base polymer. As noted in the literature review chapter, a significant claim of Zangrilli's studies was the need to impose accurate *local* stiffness in the projection of streaming current [64], **[70**]. Because this in turn is related to the validity of the streaming potential theory, an experiment was developed as part of this work to test Zangrilli's argument. Zangrilli simultaneously inserted transient predictions into bending model assessments. Thus this set of experiments also enabled, inspection of the strengths and weaknesses of the streaming potential theory's ability to project transient response.

In this study it is argued that the extent of semicrystallinity within the material system is expected to significantly affect local stiffness, and subsequently IPT sensing. Thus, transducers fabricated with polymers having different semicrystallinity percentages were tested in bending. Specifically in this case, annealing effects, which influence the semicrystallinity and stiffness of the polymer, on IPT sensing were explored in bending. Furthermore, experimental results were compared to streaming potential hypothesis estimations on current outputs generated by IPTs having base polymers with different stiffness.

The Nafion 117 samples (annealed and as-received) were first tested in tensile tests utilizing MTI-1K tensile machine according to the standard offered in ASTM D882 in order to observe the annealing effect on polymer stiffness. First, polymer samples were cut in dog bone shape according to the standard ASTM D638, and then annealed overnight. Annealing temperature was chosen as 195 ℃ according to two criteria: *(i)* it should be higher than the glass transition temperature of Nafion to change the semicrystallinity properties of the membrane which is in the range of 140-150℃ [67] (ii) it should not be so high to prevent membrane liquefying or

degradation which was estimated as 250°C-300°C [68]. Then, IPT test samples were fabricated with annealed and as-received membranes while the diluent, cation and electrode metal employed in the process are EMI-TF, Na^+ and RuO_2, respectively.

It was observed that the elastic modulus of the membrane was increased up to approximately 300 MPa from approximately 190 MPa via annealing. However, Nafion`s maximum diluent uptake capacity (for EMI-TF) was calculated measuring the weight before and after diluent uptake procedure and it was observed that diluent absorbed by membrane decreased to 16% by weight from 59% by weight upon annealing. This outcome also validates the implications proposed by Zangrilli [64] that the semicrystallinity level and the backbone polymer stiffness of Nafion increase upon annealing.

The current generated by IPT samples based on as-received and annealed Nafions were measured in response to step bending to investigate IPT sensing performance and shown in Figure 4.10 while tests were repeated two times to ensure reliability. The decrease in maximum currents for annealed IPT can be identified with the smaller amount of the diluent uptake. It was also seen that reverse current did not evolve for IPTs which were fabricated with annealed IPTs. One plausible explanation may be the very small amount of diluent absorbed and resulting in better damping properties.

When reviewed through the lens of the companion modeling performed by Zangrilli [64], **[70]**, the streaming potential model, with the current estimations shown in Figure 4.11, performed well in projecting the results of the foregoing experiment as summarized in Table 4.1, which also appears in [64]:

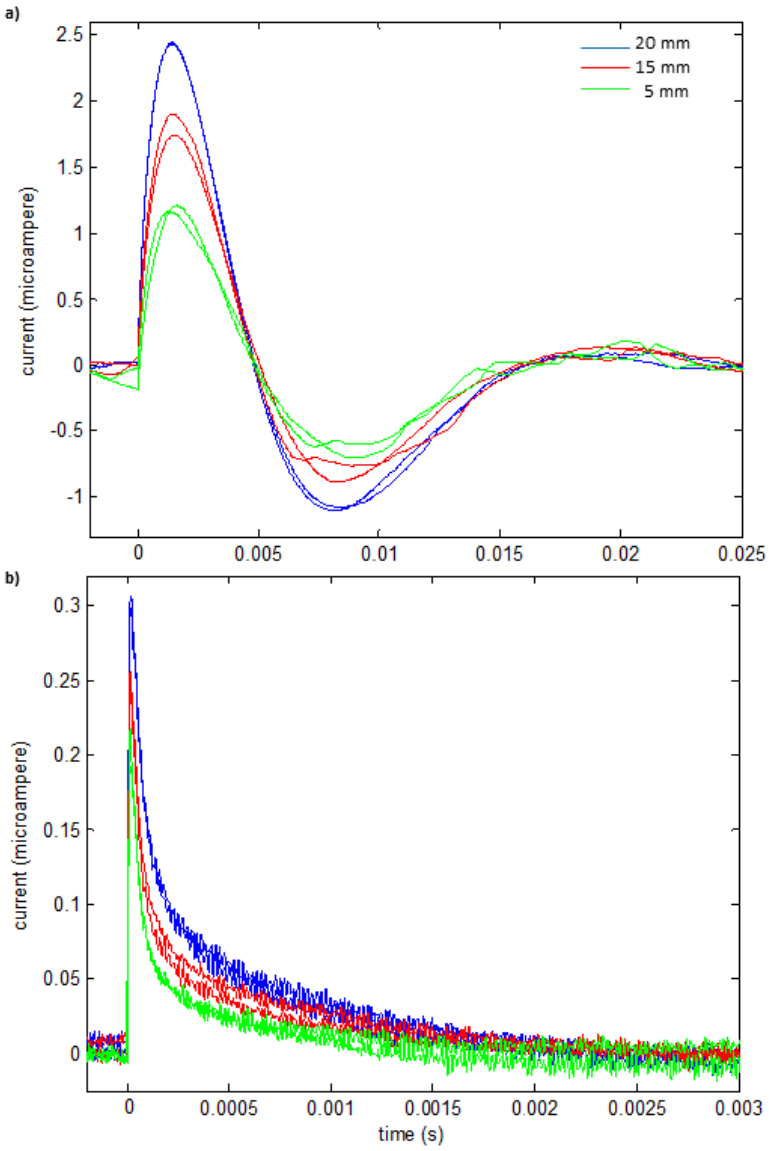

Figure 4.10. Step Bending Current Measurements of IPTs based on Nafion in Conditions: a) As-received b) Annealed

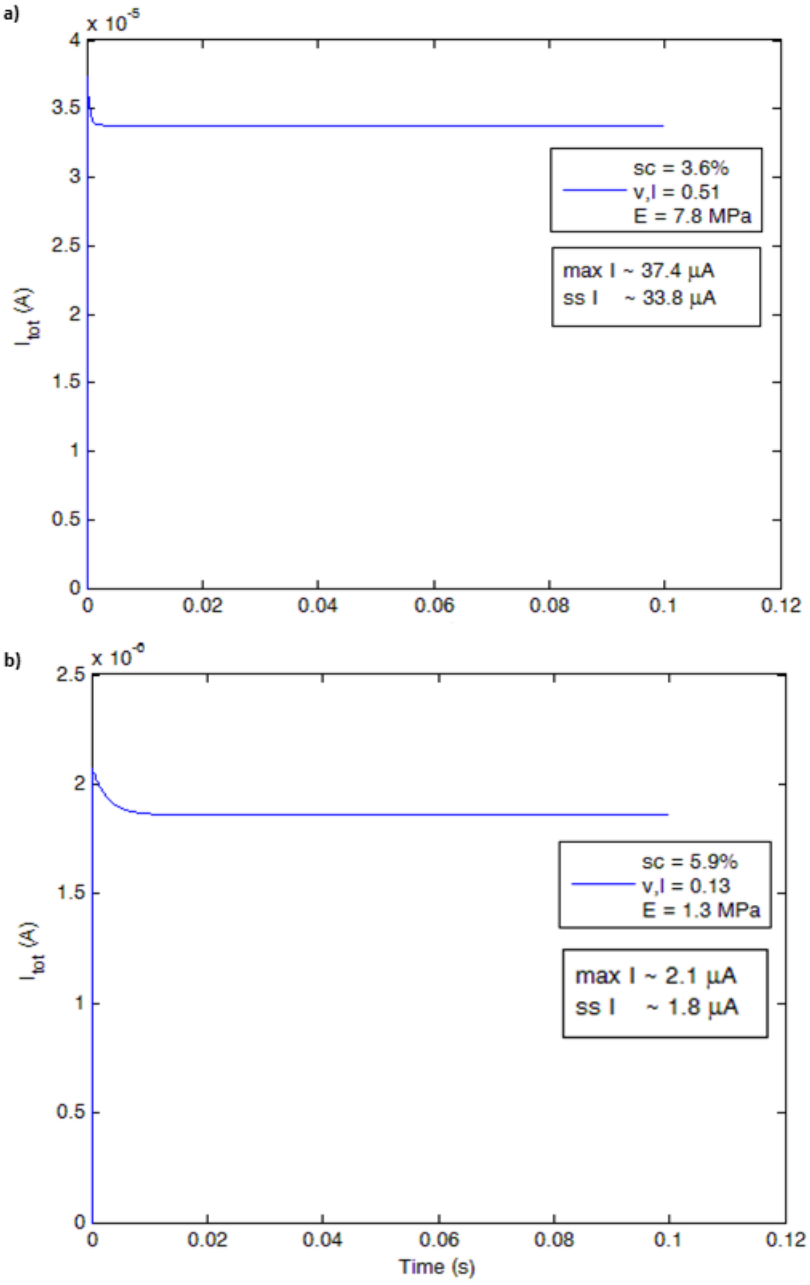

Figure 4.11. Step Bending (15 mm tip deflection) Current Estimations of Streaming Potential Model for IPTs Based on Nafion in Conditions: a) As-received b) Annealed

Table 4.1. Complete Summary of Modeling and Experiment Results between the As-received and Annealed Polymer based IPTs in Bending

Bending Tip Deflection= 15 mm	As-Received		Annealed	
Variable	Hypothesis	Experiment	Hypothesis	Experiment
Semicrystallinity of Polymer (%)	3.7		5.9	
Electrolyte Volume Fraction (%)	0.52		0.13	
Backbone Modulus (MPa)	7.8		1.3	
Current Output (μA)	33.7	~1.75	2.7	~0.25

The most important result is the last line of Table 4.1. Namely, the relative performance ratios of the model versus experiment are consistent and within the same order of magnitude, showing that model can assess the changes in properties of engineered polymers which is considered a compelling result for a multiscale methodology.

Akin to the current state of development of the time dependent bending model and as also expressed by Zangrilli [64], the weakness of the model presented here is that, , the model cannot assess the expected decay in the current signal in its current form. It is argued that inclusion of the time-dependent, local effects is important and represents an area of on-going research.

4.2 CHAPTER SUMMARY

The preceding chapter has offered a method for experimental characterization of IPTs in bending sensing that is especially suited to exploration of the streaming potential hypothesis. Notable outcomes of the presented experimental investigations are as follows;

i. A testing methodology was proposed, developed, and implemented which enables unprecedented reliability and repeatability in assessing step displacement IPT sensing in bending;

ii. The strength of the testing methodology resides in interfacing carefully planned DAP sample preparation with appropriate signal conditioning during testing;

iii. The evolution of streaming current was shown to be linear with imposed step displacement, which is consistent with stream potential theory;

iv. The existence of an optimum conductive particulate loading in the electrode as predicted by streaming potential modeling was shown to exist and with magnitude similar to that of earlier predictions.

v. The influence of polymer stiffness on the evolution of the sensing signal was assessed via a series of annealing experiments and found to display the trends consistent with those projected by streaming potential theory; and

vi. As part of the annealing tests, predicted transient sensing response was compared to observed transient response, enabling inspection of the strengths and weaknesses of the current state of modeling.

5.0 CHARACTERIZATION OF IONIC POLYMER TRANSDUCERS IN SHEAR SENSING MODE

While bending is arguably the simplest case to test, the fact that other IPT deformation modes will necessarily result in relative motion of the electrolyte with respect to the electrode is intuitive. For instance, IPTs also display a signal under shear deformation while the reports to date have mostly focused on bending. Of the modes of IPT deformation, shear mode is arguably the most difficult to isolate, both theoretically and experimentally **[18**] which may likely explain why it has not been researched widely so far. As similarly stated in bending sensing, it is hypothesized that streaming potential dominates the sensing mechanism in shear. Diluent and free counter-ions in the hydrophilic regions of the IPT act as electrolyte that flows in response to deformation. A streaming potential is expected to evolve since this flow disturbs the electric double layer formed on the metallic phase of the electrode, Figure 5.1. Furthermore, the sensing signal evolves exclusively in the electrode region where the EDL forms and metal particulates communicate with each other.

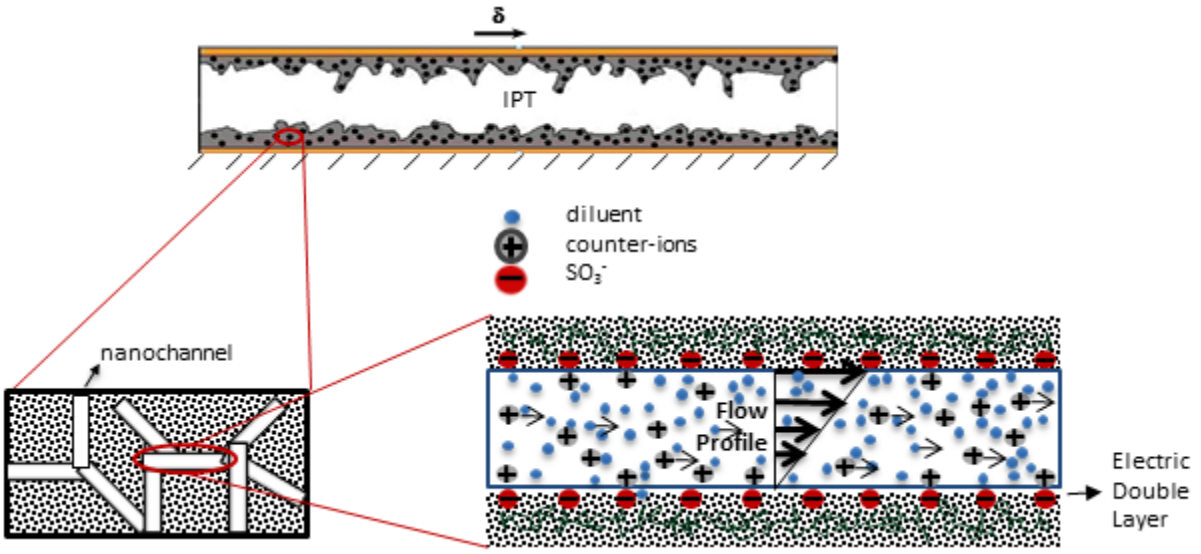

Figure 5.1. Streaming Current Evolution in IPT in Shear Sensing

Development of the shear mode model per the streaming potential hypothesis was developed in collaboration with the experiments of this work. The companion model development was led by Zangrilli [64], with a summary of that collaborative effort offered in Section 5.1.

5.1 SHEAR MODE MODELING

In shear sensing modeling, similar to the bending case, the starting point is estimating the nature of the diluent flow through the channels formed in the electrode layers since it is the impetus for the EDL disruption and corresponding streaming potential observation. However, the absence of a hydrostatic component of shear loading makes the determination of the flow through the channels more complicated. Therefore, unlike the bending case, a finite element approach has

been utilized to ascertain the diluent flow profile. Furthermore, in the streaming potential hypothesis evaluation for the shear case, imperfect flow path alignments were also taken into account; varied path orientations as in Figure 5.2 were considered, **[18**], [53].

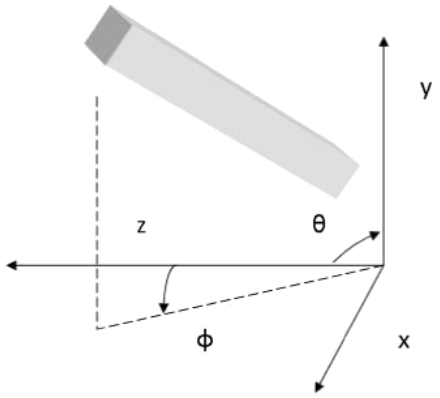

Figure 5.2. Orientaion of a Channel in The Electrode Region [18]

A small value of wall shear stress is estimated and imposed to generate a flow in the channel where the channel walls are assumed to be solid without pores. A proportional approach was used in order to relate the shear load applied on the sensor to the shear load observed by the channel wall, Equation **(5.1)**;

$$\tau(E,\gamma) = \frac{E}{2(1+\nu)} \quad \frac{\gamma \quad l_{channel}}{l_{IPT}} \tag{5.1}$$

where τ is shear stress in one channel, E is local modulus, ν is Poisson's ratio, γ stands for the global strain seen by the entire IPT, $l_{channel}$ and l_{IPT} are the length of nanochannel and IPT, respectively. Then, shear stress is applied to the walls of a single channel with different

orientations shown in Figure 5.2 and the corresponding fluid flow velocity is resolved. The streaming current generated in single channel having a square cross section, $I_{channel}$, is estimated via Equation **(5.2)** where diluent is treated as unipolar solution;

$$I_{channel} = \rho_e w \int_0^h \vec{v} \quad \vec{dy} \tag{5.2}$$

where ρ_e is charge density, w is channel width, h is channel height and v is diluent velocity profile obtained via finite element analysis. It was found that parallel channel alignment to the load leads in a transient extreme followed by a steady state response and transient part vanishes as the alignment degrades and total magnitude decreases. Curves were fit to the diminishing steady state streaming current estimated via increasing rotations in axis where the maximum streaming current is the steady state value for the perfectly aligned case. The streaming current developed in a nanochannel for a given orientation is defined as in Equation **(5.3)** for a specific case of global strain.

$$I_{channel}(\theta,\phi) = I_{\max} f(\theta,\phi) \tag{5.3}$$

Then a volume averaging is introduced to create a projection of the streaming current over a small volume to define an average current, $I_{ave\_channel}$, that is the range $(0,\pi/2)$, :

$$I_{ave\_channel} = \frac{\int_0^{\pi/2}\int_0^{\pi/2} I_{channel}(\theta,\phi) \quad d\theta \quad d\phi}{\int_0^{\pi/2}\int_0^{\pi/2} d\theta \quad d\phi} \tag{5.4}$$

Finally, total IPT current is calculated through the multiplication of the number of channels by the average channel current calculated in Equation **(5.4)**, as suggested in Equation **(5.5)**;

$$I_{IPT} = I_{ave\_channel} \frac{f_p f_c l_{IPT} w_{IPT} t_{electrode}}{V_{channel}} \quad \textbf{(5.5)}$$

where f_p anf f_c are the conductive particulate volume in electrode region and cluster volume fraction, respectively. V_{channel} stands for the volume of a single channel. Also, w_{IPT}, l_{IPT}, $t_{electrode}$ are width of the IPT, length of the IPT and thickness of the electrode, respectively. The resulting steady state current prediction is about two order of magnitude lower than the one estimated for a system of perfectly aligned channels. Therefore, taking flow path orientation into consideration significantly affects the estimation.

Furthermore, a viscoleastic 2N+1 analogical model was employed to represent the microstructure of the polymer where 'N' stands for the number of parallel elements that have a spring and dashpot in series and '1' is an additional single spring element in parallel [64], [53]. This approach enables a relatively straight forward approach to projection of transient effects. Each successive spring and damper represents a single polymer chain within the polymer region. The behavior of the polymer chain in response to the external deformation is simulated via a damper where the viscous nature depends on the diluent infused in the IPT. Moreover, the spring element in series models the local stiffness of the polymer chain and is estimated via Rotational Isomeric State (RIS) theory to quantify how polymer stiffness evolves at the local level.

Moreover, the effect of the metal particulates` volume fraction in the electrode layers on expected current is investigated since it is a key parameter at microscale level [64],

[53]. To this end, a 'β' parameter is incorporated to include the effects of change in radius of the nanochannels in electrode region which caused by the change in metal particulate volume concentration, as in bending case. The total streaming current is estimated as in Equation **(5.6)**:

$$I_{IPT} = I_{ave\_channel} \frac{\beta^2 \quad f_p \quad f_l \quad l_{IPT} \quad t_{electrode} \quad w_{IPT}}{w_{channel}^{\ 2} \quad l_{channel} \quad \Phi} \tag{5.6}$$

where $w_{channel}$ stands for the width of the channel and $l_{channel}$ is channel length. Also, Φ takes the porosity of the electrode region into account.

5.2 SHEAR MODE EXPERIMENTS

The goal of the experiments is to examine IPT characteristics in shear response and to evaluate the streaming potential hypothesis for shear mode. For this purpose, an experimental rig was designed to apply step displacement and measure transient current response in shear mode.

5.2.1 Shear Test Setup and Experiments

The function of the test setup is to exert step shear displacement stimuli of several magnitudes to the upper face of the IPT while the bottom side is fixed and to enable *in situ* measurement of current developed across the faces of the sensor. This test rig is composed of mainly three parts: IPT fixture unit, laser vibrometer unit, and data acquisition unit and auxiliary equipment, Figure 5.3.

The IPT fixture unit is the main part where the sensing tests are performed and it is bolted on a vibration isolation table. It includes a piezoelectric ("piezo") actuator, glued to a fixed support on the fixture, to achieve displacement excitation at micrometer levels. The transducer is placed between thin, self-stick copper tapes enabling adhesion of the IPT surfaces to the conducting media without additional usage of liquid adhesives. Data is gathered through these copper bands through measurement wires. One end of the measurement wire is directly connected to the sticky copper band while the other end is attached to the electric circuit. The conductive band-IPT sandwich is adhered between two Plexiglas plates by means of thin, insulating, double-sided bonding tapes while the lower Plexiglas plate is fixed. The bands used to fix the IPT to the Plexiglas plates absorb some of the shear energy. Therefore, the actual values of produced currents are expected to be higher than the experimental outcomes. However, shear deflection of the intermediate layer is expected to be much lower than that of IPT considering its smaller thickness and higher stiffness. Thus, the minor variation in output data is assumed to be negligible. The IPT fixture unit is then bolted on the vibration isolation table to eliminate noise. The laser vibrometer unit consists of the laser head that is directed to a point on the Plexiglas plate at top and a fixture enabling the attachment of laser head to vibration isolation plate. The data acquisition unit utilizes a computer with LabVIEW data acquisition software and a data acquisition card.

During a test period, similar to a bending test, a step voltage signal is sent to the piezo actuator to create a step deflection on the upper face of the transducer that is fixed at the bottom. The response signal caused by the deformation of the IPT is then collected and amplified by means of the signal conditioning circuit, Figure 5.3.c.

Displacement inputs applied via *initial* impact of excitations caused by the piezo actuator were estimated through integration of the velocity signal collected from the plate at the top. The experiments were repeated several times to examine repeatability of the test and evaluate the reliability of the test setup.

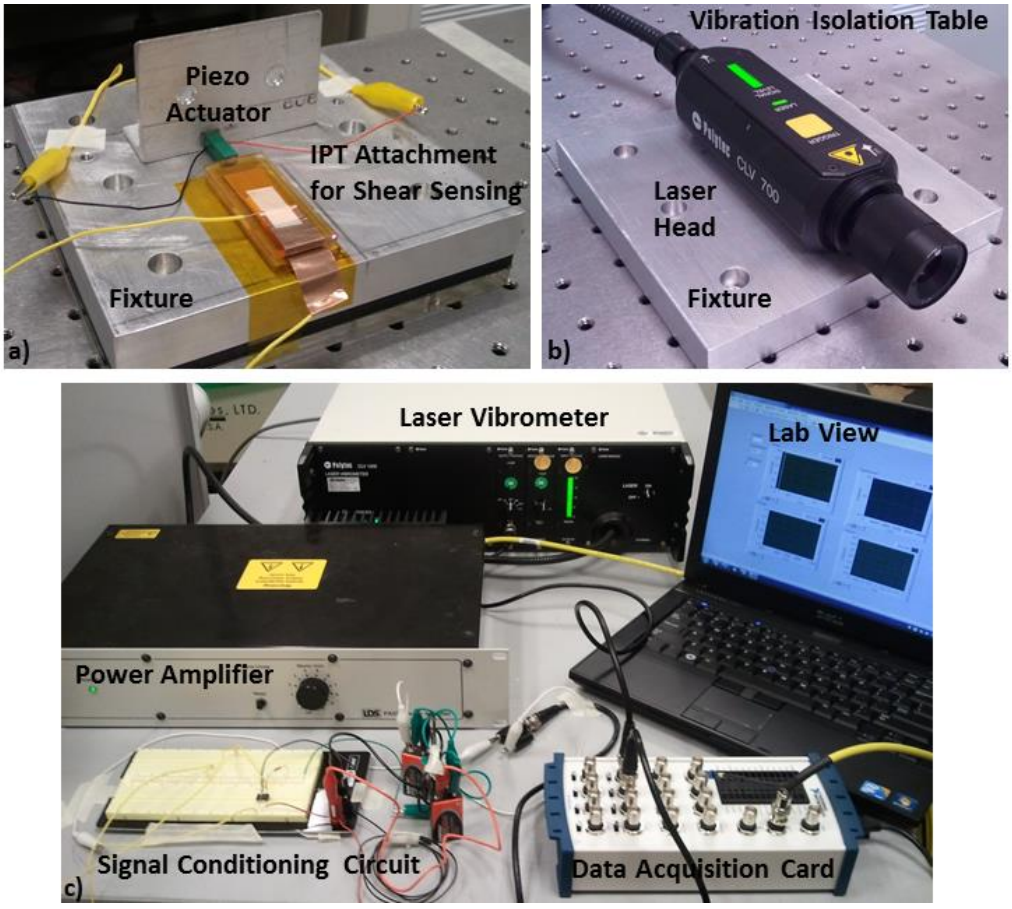

Figure 5.3. Shear Test Rig: a) IPT Fixture Unit b) Laser Vibrometer Unit c) Data Acquisition Unit and Auxiliary Equipment

5.2.2 Results and Discussion

A batch having three transducers with 42 vol% RuO_2 in the electrode by volume was tested for different shear displacement stimuli. The IPTs under investigation were 15 mm x 47 mm in dimensions and the electrode mixture was prepared to create ~14 μm thick layers on both sides of the IPT.

The current signal evolving in time under each shear stimulus is shown in Figure 5.4 for a representative transducer. The current generated by an IPT increases as input shear deflection increases, as expected. In this study, the original intent was application of a step shear deflection over the upper surface of the IPT. Therefore, a step voltage signal was sent to the piezo actuator to create shear deformation pushing the Plexiglas plate at top. However, additional oscillations were observed in current output measurements before dying out. Subsequent investigation into causes for these oscillations revealed that they can be attributed to the oscillatory behavior of the input itself, which was confirmed via velocity measurement taken from the tip of the actuator by the laser vibrometer, as in Figure 5.8. It was seen that the velocity input exerted on the upper plate by the piezo actuator, in addition to a single impulse, oscillated for a while before dying out. This situation ultimately caused additional oscillations superimposed over the step displacement rather than a perfect step, indicating that piezo stack actuator dynamics affect its actuation. Ultimately an alternate strategy was proposed to enable inspection of the effects of a true step input; however it was deemed that inspection of the oscillatory input:output was also meritorious and therefore offered here.

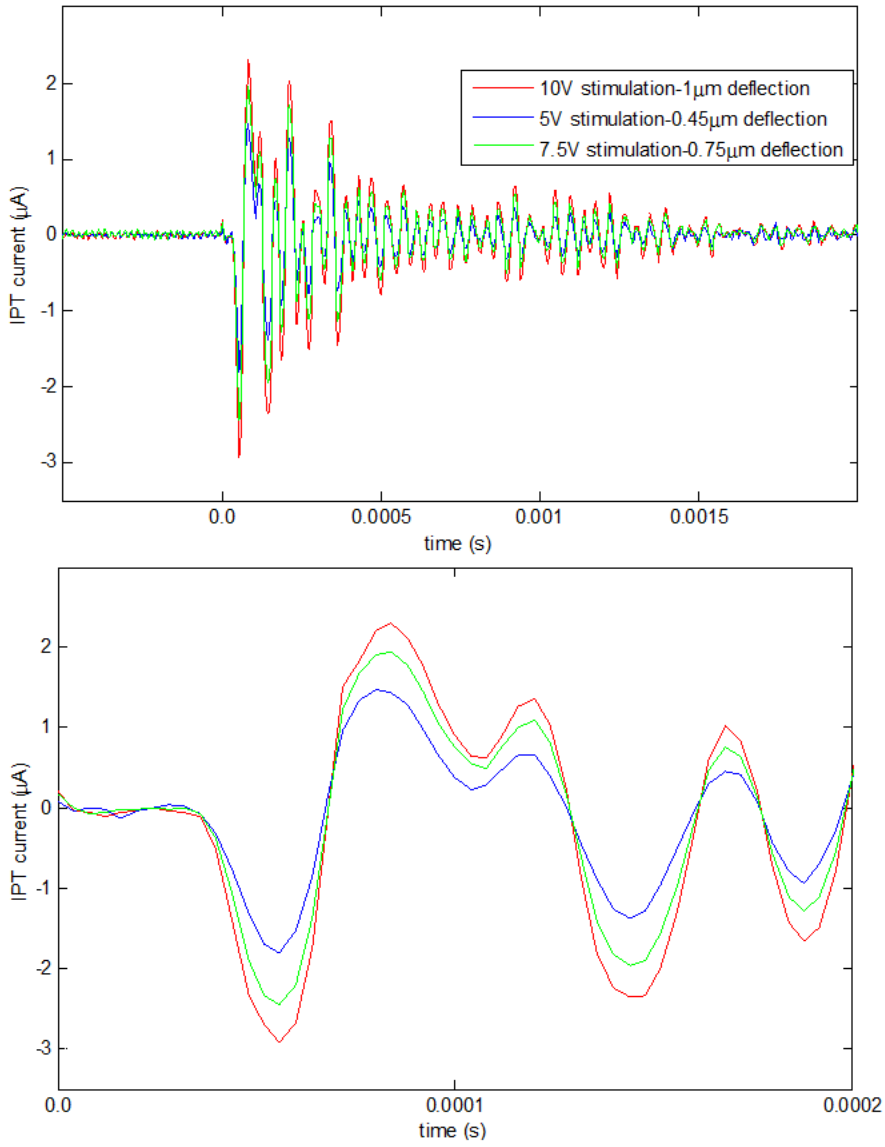

Figure 5.4. Current-Time Signal of a Representative IPT for Shear Testing in the Presence of Superimposed Input Oscillations with Close Up Figure, at the bottom

The absolute maximum value of the current occurs shortly after imposing shear deflection via piezo actuation. The corresponding movement of the upper Plexiglas for each stimulus was estimated via integrating the velocity signal collected. The maximum currents generated by corresponding *initial* displacement inputs for three IPTs under investigation are

depicted in Figure 5.5. It is observed that the difference among the maximum current outputs of the samples is very small while sample 3 differs somewhat which is still reasonable. This outcome can be identified with minor experimental errors and small differences in fabrication of the IPTs. Furthermore, when the results of sample 1 for which the experiments were repeated three times, and the results of sample 2 for which the experiments were repeated two times, are examined, the consistency is noticeably seen. This shows the repeatability of the tests and reliability of the shear test setup.

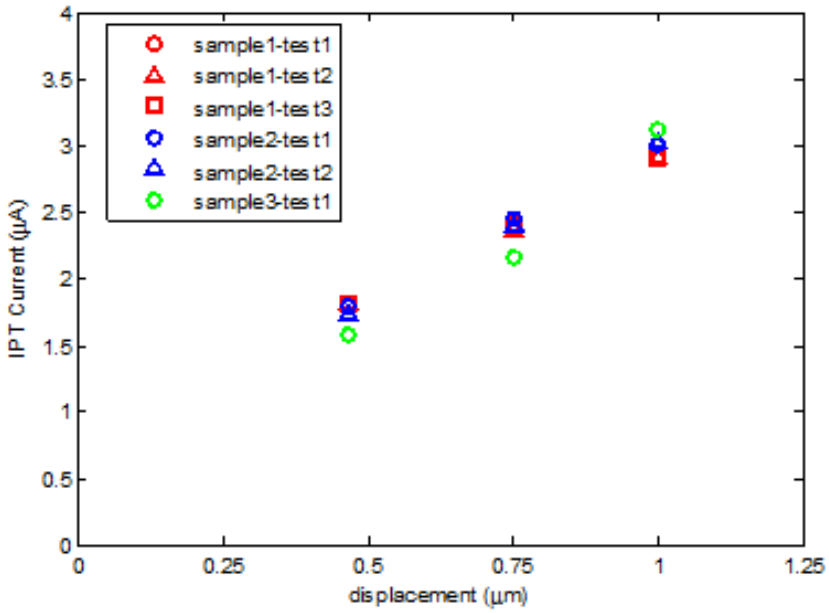

Figure 5.5. Shear Test Maximum Currents of All Samples

Moreover, the average of the absolute maximum currents produced at each test for different deflection inputs is depicted in Figure 5.6 where error bars represent the range of measurements with the limits showing maximum and minimum current observed during

experiments. A linear polynomial is fitted to the data in the range of measurements which is compatible with the streaming potential estimations that predicts a linear relationship between displacement and current output.

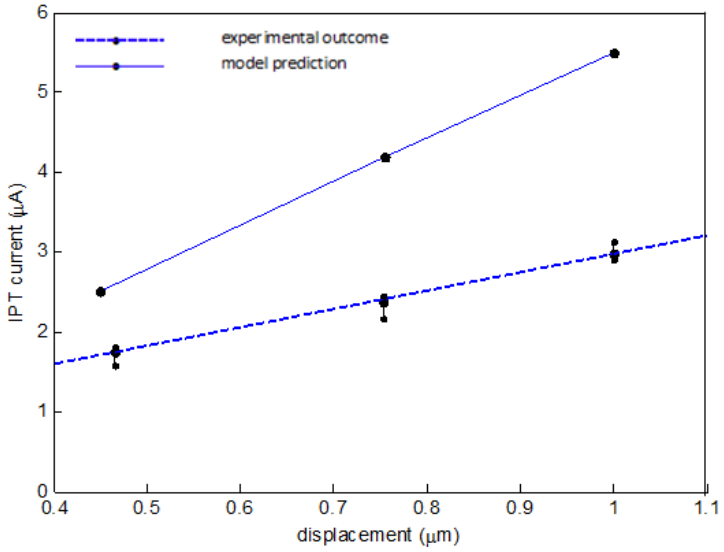

Figure 5.6. Average Value of Shear Test Maximum Currents with Linear Fit and Streaming Potential Hypothesis Estimations

The average values of the maximum currents measured were compared to the ones estimated via the streaming potential theory for an IPT with dimensions very close to those tested as illustrated in, Figure 5.6 [52], [53]. It is observed that both predicted and measured current increase as imposed deflection increase displaying linearity between current and displacement, in the range of imposed deflection. The predicted steady state value of current and test current output are in the same order; because the model is purely physics-based, and was at no point calibrated to the experiments, the similarity offers strong support for the streaming

potential hypothesis. That the results are this similar between a series of device length-scale experiments and a physics-based, un-calibrated model operating at the nano-length scale and then volume averaged to the mm length scale, is compelling and promising. The current measurements are expected to be approximately 85%-90% of the values presented in the Figure 5.6 if the true step displacement application method (Section 5.2.3) is employed, comparing the current measurements in response to step and smooth step displacements in Figure 5.10.d. Even in this case, the modeling estimations and the experimental results are in the same order and related discussion is still valid in this case. Furthermore, the peak current increases linearly as the initial excitation velocity peak increases, Figure 5.7.

Next, an alternate strategy is proposed to enable inspection of the effects of a true step input. To this end, application of shear step displacement was amended by making use of a sigmoid function to operate the piezoelectric actuator; this largely eliminates the input oscillations. Furthermore, shear studies have been expanded in order to explore the optimum metallic powder content in the electrode structure for a sensor with maximum sensitivity.

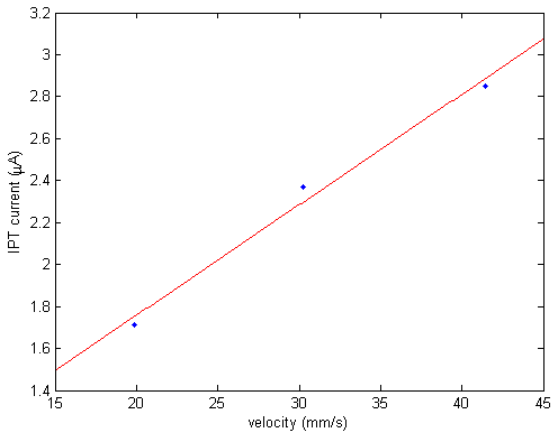

Figure 5.7. Shear Test Maximum Currents in Response to Velocity Excitations

5.2.3 Application of True Step

The piezoelectric actuator dynamics were investigated under step voltage excitation as well as sigmoid voltage input with different speeds. A laser vibrometer was used to measure the velocity and displacement rate of the actuator tip. It was seen that as the step function smoothness changes, *i.e*. the speed of transition to constant voltage from zero value, the amplitude and the width of the velocity spike changes, as shown in Figure 5.8. As the step voltage input to the piezoelectric actuator gets smoother (in the direction of arrows), the amplitude of the resulting velocity output spike decreases while its width increases, and the following oscillations diminish. By this means, additional oscillations superimposed to step displacement vanish. However, as the transition speed decreases, displacement output deviates from a sharp step. In this respect, to obtain a step displacement output without additional oscillations, the optimum profile to power the piezoelectric actuator seems to be a sigmoid function, the case of s = 10k. The optimum speed was regulated per this method when the tests were performed completely taking also the IPT damping characteristics into account.

Lastly, transient model response shown in Figure 5.9, lately offered by Zangrilli [64], [53], was evaluated with the experimental results in Figure 5.10.c, d for the case s=5k which was proposed as the true step application. It was seen that although the peak current values shows a very good similarity in magnitude but the decay rate is so slow that it cannot capture the experimentally observed behavior.

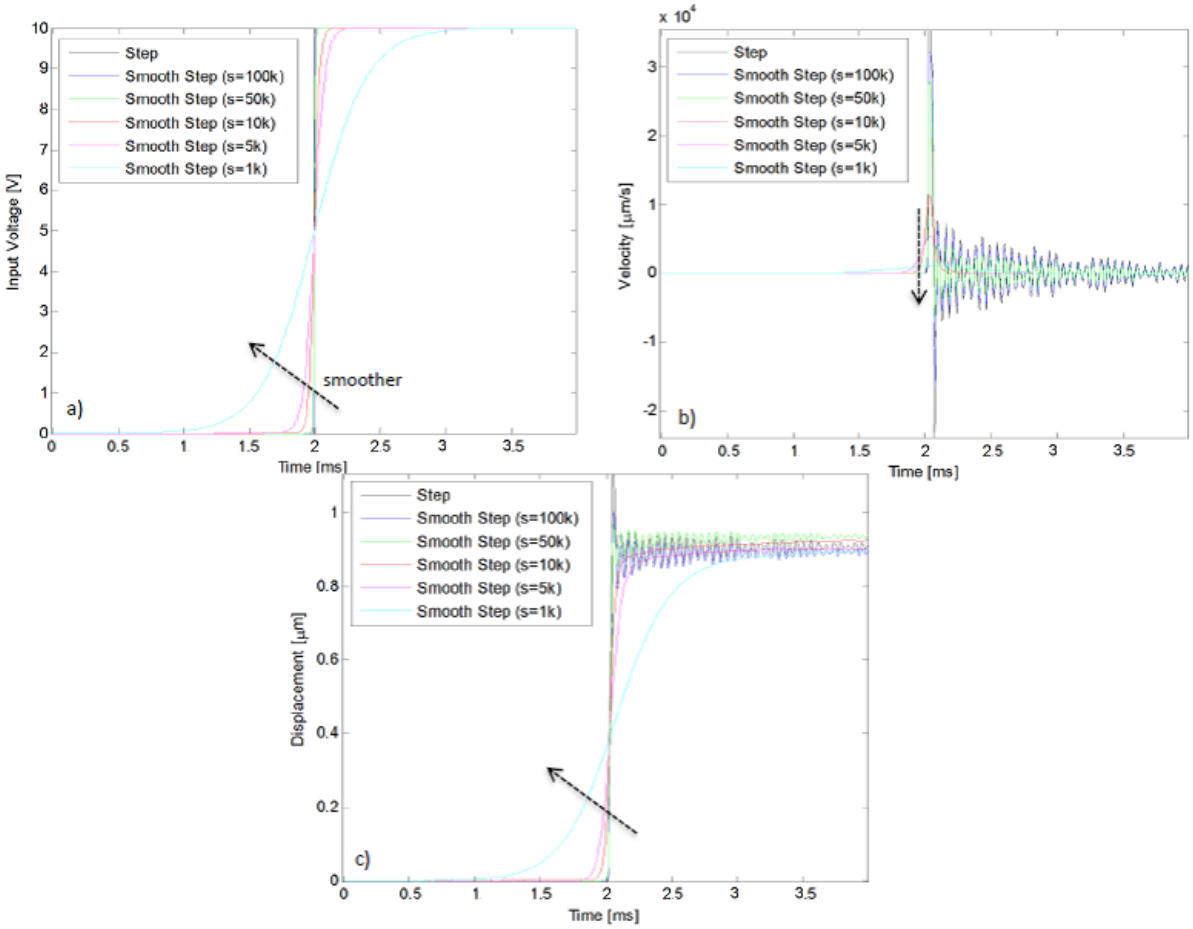

Figure 5.8. Piezo Actuator a) Input Voltage b) Tip Velocity c) Tip Displacement

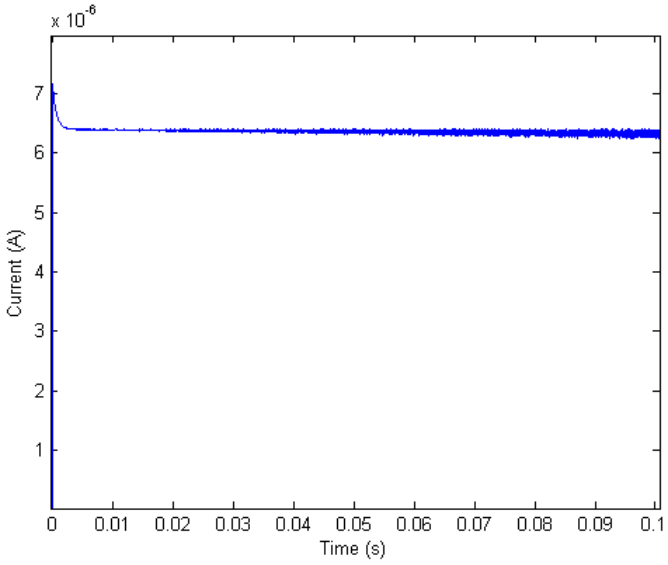

Figure 5.9. Transient Model Estimations for Current Output [64]

5.2.4 Electrode Optimization

A sample that is 18 mm x 51 mm in dimensions and with ~14 mm thick electrodes having 30% RuO_2 by volume was tested with step and sigmoid voltages, as suggested in Section 5.2.3, and current outputs were measured via the shear test rig, Figure 5.10. It was observed that, as the voltage applied to power the piezo gets smoother, the additional oscillations in the output current diminish while maximum current decreases. In this respect, optimum input function was chosen as the sigmoid function with 5k speed to simulate shear step input.

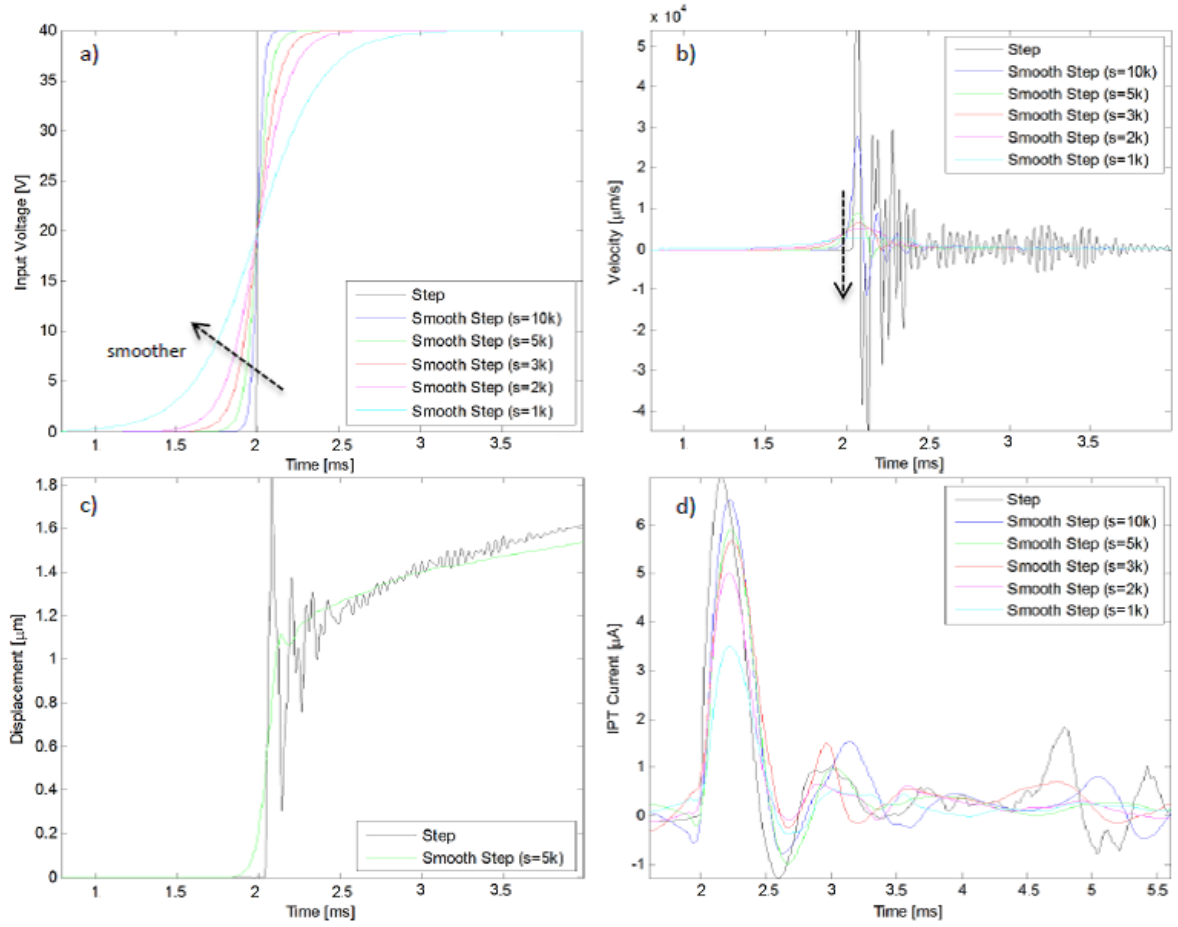

Figure 5.10. Step Shear Testing of an IPT with 30vol% RuO_2 a) Input Voltage to Piezo Actuator b) Upper Plate Velocity c) Upper Plate Displacement d) Current Output of IPT

Furthermore, electrode structure effects on shear sensing were explored testing IPTs fabricated per the DAP with different electrode compositions, namely; 30vol% RuO_2, 40vol% RuO_2, 50vol% RuO_2, 60vol% RuO_2. Similar to the findings of bending tests, an optimum value for metal loading in the electrode comes out in the vicinity of 40vol% RuO_2 for the highest sensitivity, Figure 5.11.a. Moreover, this outcome was utilized to evaluate the streaming potential hypothesis estimations. Modeling results indicate a peak at some point in the vicinity of

35 vol % metal particulate loading, but then show diminished returns in the expected current as the particulate loading increases, Figure 5.11.b. Therefore, the magnitude of the expected current output from the model at various metal particulate loadings and the optimum electrode structure are in good agreement with the experiments.

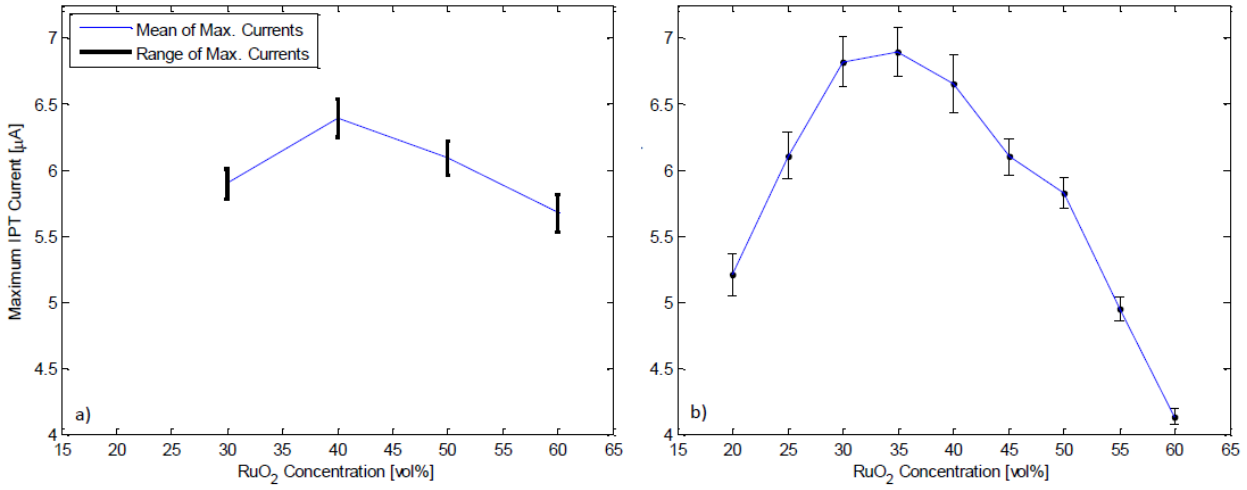

Figure 5.11. Average of Peak Current Outputs for Varied Electrode Metal Loading in Shear Sensing: a) Experiments b) Model

5.3 CHAPTER SUMMARY

The preceding chapter has offered a method for experimental characterization of IPTs in shear sensing that was collaboratively developed in parallel with a companion modeling method. Notable outcomes of the presented investigations are as follows;

i. Drawing in part from lessons learned in the development of the bending test rig discussed in the previous chapter, a testing methodology was proposed, developed,

and implemented which enables unprecedented reliability and repeatability in assessing step displacement IPT sensing in shear;

ii. The strength of the testing methodology resides in minimizing losses within the shear composite and imposing a sigmoid function to control input instabilities;

iii. The evolution of streaming current was shown to be linear with imposed step displacement, which is consistent with streaming potential theory;

iv. The model projected sensing signals were of the same magnitude as those observed experimentally despite the absence of empirical fitting; comparison of model and experiment enables insight into the strengths/weaknesses of the model, where the model displays a very small decay rate.

v. The existence of an optimum conductive particulate loading in the electrode as predicted by streaming potential modeling was shown to exist, with magnitude similar to that of earlier predictions, and with magnitude similar to that of the bending case.

6.0 CHARACTERIZATION OF IONIC POLYMER TRANSDUCERS IN COMPRESSION SENSING

In this chapter, a computational model is proposed to estimate the sensing current output of IPTs in response to compression deformation employing streaming potential modeling, and then compared to the results of the step displacement experiments designed specifically for hypothesis validation. It is argued that modeling of IPT sensing in a third mode consistent with experimental findings will be sufficient to argue the validation of the theory since experimental research conducted in bending and shear modes showed the legitimacy of the streaming potential hypothesis. Validation of the hypothesis opens the opportunity to optimize IPT sensors for specific applications via a generalized tool which may ultimately lead to widespread usage of these transducers.

6.1 COMPRESSION MODE MODELING

In this study, it is hypothesized that streaming potential dominates the physical mechanisms responsible for compression sensing similar to the bending sensing and shear sensing cases. According to streaming potential hypothesis implications, any kind of flow of the electrolyte in nanochannels formed throughout the electrode region results in a streaming current where the

analytical formulation for sensing in response to compression deflection is discussed in this section.

For the hydrated IPT, Figure 6.1, the ionic groups located at the tip of the pendant chains, and the diluent embedded by the polymer establish the hydrophilic regions which form as nanochannels. In contrast, the amorphous backbone of the polymer is the hydrophobic part which is assumed to constitute the walls of the channels. In this study, channel walls are assumed to be solid without pores. Moreover, an electric double layer is expected to develop in the electrode region of the IPT, since metallic particulates contact the electrolyte, as detected in previous observations established over a century ago [61], Figure 2.22.

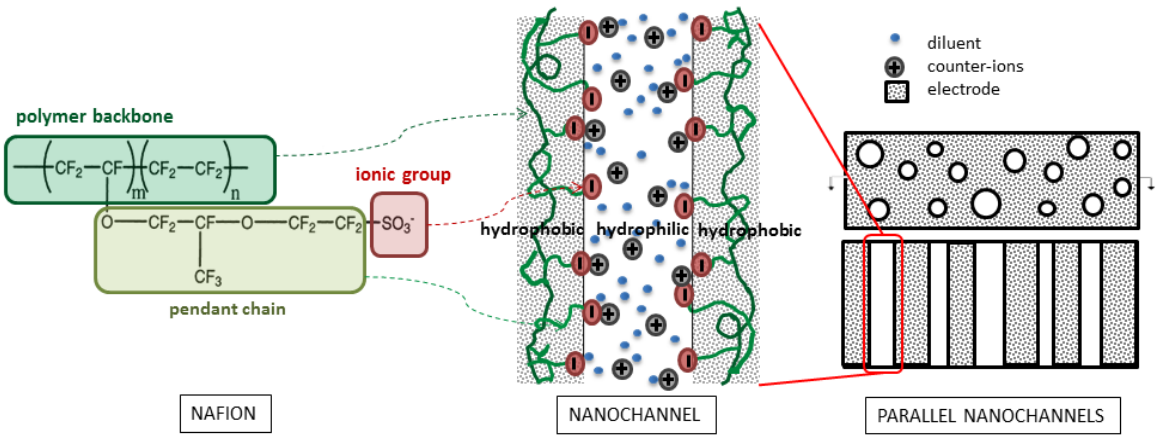

Figure 6.1. Illustration of a Hydrated Nafion Morphology and the Nanochannels Morphology Adaptation

When a deflection is imposed in the direction of the IPT thickness, diluent infused in the hydrophilic regions tends to move as previously proposed by Weiland and Akle [41], carrying the free ions as well, Figure 6.2.

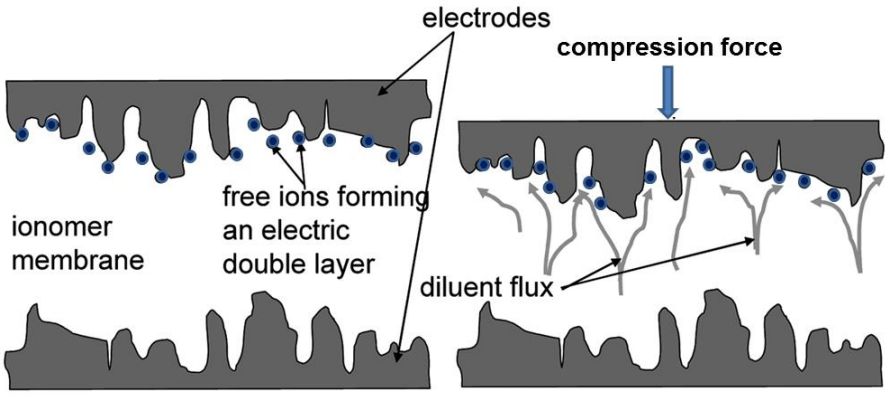

Figure 6.2. Illustration of IPT Streaming Potential: The schematic shows the hypothesized relative motion of diluent because of sensor compression [22]

As the electrolyte flows in the channels oriented in different directions, the electric double layer formed on the metallic phase of the electrode is disturbed, Figure 6.3. Therefore, similar to bending and shear sensing, a streaming potential is expected to evolve while a streaming current occurs when the electrodes are shorted. Moreover, the sensing signal evolves exclusively in the electrode region where the EDL forms and metal particulates communicate with each other.

Similar to the bending and shear cases, Equation (2.4), the short circuit streaming current is calculated in the same way for a nanochannel having a circular cross-section as follows [72];

$$I_s(t) = 2\pi \int_0^{r_{channel}} \rho(r) v(r,t) r \quad dr \tag{6.1}$$

where ρ, and v stand for charge distribution and velocity profile across the cross-section of a channel, respectively. Also, t is time, r is radius and $r_{channel}$ is the radius of the circular nanochannels.

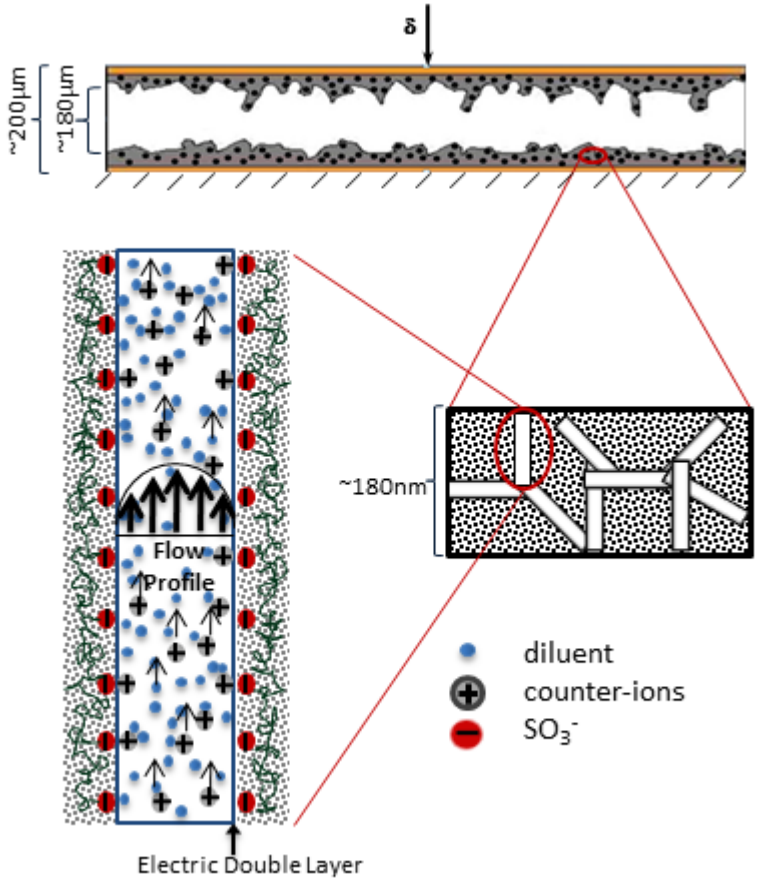

Figure 6.3. Streaming Channel Current Evolution in IPT for Compression Mode

6.1.1 Flow Formation

Electrolyte flow is the driving force that is observed for each type of deformation since it disturbs the EDL. Therefore, flow formation must be investigated first. It is assumed that, given

the pressure difference between each end of a nanochannel in, ΔP, the diluent flow profile is described by Poiseuille flow where hydrophilic pendant chains assure no-slip boundary conditions at the wall, Figure 6.4.

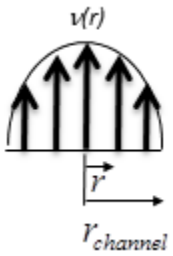

Figure 6.4. Poisouille Flow

The Poisouille flow profile throughout the cross-section in time ($v(r,t)$) is calculated with the Equation **(6.2)**;

$$v(r,t) = \frac{\Delta P(t)\left(r_{channel}{}^{2} - r^{2}\right)}{4\mu l_{channel}} \qquad \textbf{(6.2)}$$

where $\Delta P(t)$ is time dependent pressure difference, r is radius, μ is diluent viscosity, and l is length. Stress caused by the applied deformation is the impetus for the flow. To define the inelastic behavior of the IPT, the Maxwell model [73] is utilized which consists of a damper and an elastic spring in series, Figure 6.5. This viscoplastic approach is an adaptation of the ideology of the shear model, where the intent is to minimize model complexity while projecting the response of step compression sensing in the absence of sigmoid smoothing. The absence of the in-parallel spring will result in an elevated predicted signal magnitude, but should otherwise

offer clear insight into the implications of an oscillatory load superimposed on a step function per the streaming potential hypothesis.

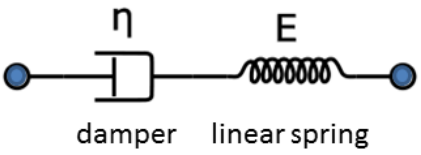

Figure 6.5. Maxwell Model [73]

In order to calculate the stress seen by the global IPT, $\sigma(t)$, is estimated solving the governing equation of the Maxwell model element [73], Equation **(6.3)**, numerically.

$$\frac{1}{E}\frac{d\sigma(t)}{dt}+\frac{\sigma(t)}{\eta}=\frac{d\varepsilon(t)}{dt} \qquad \textbf{(6.3)}$$

For elastic modulus (E), a local value which has previously been calculated taking the hydration level, and the metallic region in the electrode into account, [18], is used. Strain in time, $\varepsilon(t)$, is calculated dividing the displacement stimuli by IPT thickness where displacement is estimated via integrating the velocity signal measured with a laser vibrometer when experimental data is available. η stands for the damping and has previously been calculated by Zangrilli [18]. While a spring element accounts for the local stiffness of the media in modeling, a dashpot represents the viscous nature of the polymer. The solution of the governing equation, Equation

(6.3), for $\sigma(t)$ defines the stress relaxation behavior in response to a strain input where E, ε and η are known parameters representing some IPT characteristics.

After calculating stress on the IPT caused by deformation, the portion of the stress seen by a single channel is estimated to determine the pressure difference between the ends of a channel by applying the Voigt approach, where the strain is the same in all elements of the model. The pressure difference leading to electrolyte flow is then determined via Equation **(6.4)**;

$$\Delta P(t) = \sigma(t) \frac{l_{channel}}{t_{IPT}} \qquad \textbf{(6.4)}$$

where $l_{channel}$ is channel length and t_{IPT} is IPT thickness. Knowing the pressure difference, the velocity profile throughout the cross-section of the nano-channel is calculated using Equation **(6.2)**.

6.1.2 Channel Streaming Current

The streaming current generated in a single channel is calculated via Equation **(6.1)** taking charge density throughout the cross-section, electrolyte velocity profile and channel dimensions into account. The flow profile is determined in 6.1.1. It has previously been argued by Gao that the charge density of the electrolyte is a constant value for a nanochannel existing in the IPT, [66]. The charge density is zero beyond the electric double layer effective zone which is defined by Debye length. In an IPT, the EDLs of the adjacent walls of a channel overlap since the channel radius is smaller than the Debye length. Therefore, charge density of the electrolyte in nanochannels becomes a unipolar solution of counter-ions at a concentration that neutralizes the surface charge of

the channel. In the calculation of the streaming channel current, $I_{channel}(t)$, unipolar solution charge density (ρ_e) is used and the equation turns into the following formula;

$$I_{channel}(t) = \frac{1}{8} \times \frac{\Delta P(t) \pi \rho_e r_{channel}^{\ 4}}{\mu l_{channel}} \qquad \textbf{(6.5)}$$

In order to estimate the total current generated by the IPT, channel current is multiplied by number of active channels in an IPT. The total number of channels ($N_{channels}$) is estimated by dividing the total volume of polymer which is available for channel formation in the electrode layers by single channel volume, Equation **(6.6)**:

$$N_{channels} = \frac{V_{polymer}}{V_{channel}} = \frac{\left(2t_{electrode} w_{IPT} l_{IPT}\right) \times \left[\left(1 - f_p\right) f_c\right]}{\left(\pi r_{channel}^{\ 2}\right) \times l_{channel}} \qquad \textbf{(6.6)}$$

where $t_{electrode}$ stands for electrode thickness, w_{IPT} is IPT width, l_{IPT} is IPT length, f_p and f_c stand for particulate volume fraction in the electrode region and channel volume fraction in the polymer phase, respectively.

6.1.3 Channel Orientations

Equation **(6.5)** gives the streaming current for a perfectly aligned channel, which is in the direction of the applied displacement. However, the channels in the electrode region are randomly oriented (Figure 6.6), and where the shear model studies presented in the previous chapter have shown that consideration of this parameter has significant impact on predictions (shear predictions that considered random orientation were 2 orders of magnitude lower than

those that did not). To take this effect into account, stress transformation is employed to determine stress for channels deviated from perfect alignment, Equation **(6.7)**. Then the stress element in the direction of rotated channel is used in the calculation of velocity profile.

$$\sigma_{transform}(t,\theta,\phi) = A_{z\_rot}(\phi)\left[A_{x\_rot}(\theta)\sigma(t){A_{x\_rot}}^{T}(\theta)\right]{A_{z\_rot}}^{T}(\phi) \tag{6.7}$$

$$A_{x\_rot}(\theta) = \begin{bmatrix} 1 & 0 & 0 \\ 0 & \cos(\theta) & -\sin(\theta) \\ 0 & \sin(\theta) & \cos(\theta) \end{bmatrix} \qquad A_{z\_rot}(\phi) = \begin{bmatrix} \cos(\phi) & -\sin(\phi) & 0 \\ \sin(\phi) & \cos(\phi) & 0 \\ 0 & 0 & 1 \end{bmatrix} \tag{6.8}$$

A is transformation matrix which is used in the calculation of new stress state, $\sigma_{transform}(t,\theta,\phi)$, caused by rotations of *x* and *z* axis, Equation **(6.8)**.

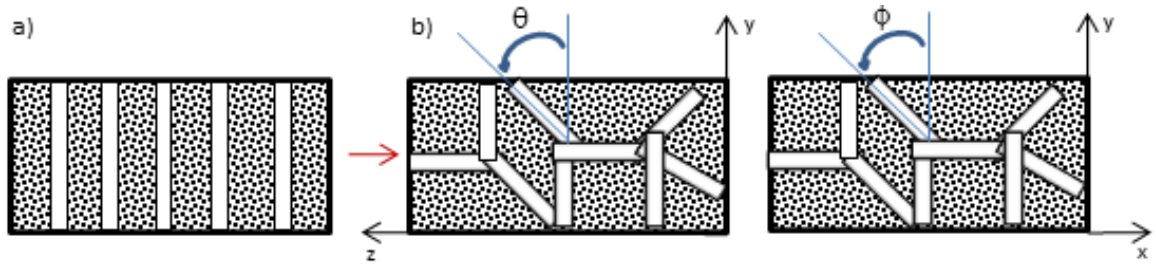

Figure 6.6. Channel Orientations: a) Perfectly Aligned Channels b) Randomly Oriented Channels

After considering random channel orientations in the calculations, Equation **(6.5)** turns into Equation **(6.9)**, which actually defines a surface with respect to the rotation angles (θ, and ϕ);

$$I_{channel}(t,\theta,\phi) = \frac{1}{8}\left[\Delta P(t)\left(\frac{1}{2}+\frac{\cos(2\theta)}{2}\right)\left(\frac{1}{2}+\frac{\cos(2\phi)}{2}\right)\right]\frac{\pi \times \rho_e \times {r_{channel}}^4}{\mu \times l_{channel}} \tag{6.9}$$

6.1.4 Average Channel Streaming Current

Assuming that all the channel orientations have the same possibility to exist, average current obtained by a single channel, $I_{ave\_channel}(t)$, is calculated through a volume averaging technique which is widely used in multiscale models, Equation **(6.10)**. Observation is made in a quadrant over the range of angle (0, π/2). Therefore, streaming current over a small volume is integrated over this range and normalized.

$$I_{ave\_channel}(t) = \frac{\int_0^{\pi/2}\int_0^{\pi/2} I_{channel}(t,\theta,\phi)\ d\theta\ d\phi}{\int_0^{\pi/2}\int_0^{\pi/2} d\theta\ d\phi} \qquad \textbf{(6.10)}$$

6.1.5 IPT current

The total current that can be obtained from an IPT in compression is then calculated by multiplying total number of channels, Equation **(6.6)**, and average channel streaming current, Equation **(6.10)**, as in Equation **(6.11)**:

$$I_{IPT}(t) = N_{channels} I_{ave\_channel}(t) \qquad \textbf{(6.11)}$$

Substituting the variables into Equation **(6.11)** and combining all the terms into one equation, the total IPT current can be estimated by the given formula for a given velocity input in time:

$$I_{IPT}(t) = \frac{1}{16}\sigma(t)\left[\frac{\rho_e {r_{channel}}^2 (1 - f_p) f_c t_e w_{IPT} l_{IPT}}{\mu l_{channel} t_{IPT}}\right] \quad \textbf{(6.12)}$$

where stress, σ(t), is solved for a given velocity input, as also mentioned in Section 6.1.1.

6.2 COMPRESSION MODE EXPERIMENT

A compression test rig was designed to explore IPT characteristics in compression sensing. For this purpose, transient current response of the IPT was measured in response to step compression displacement input. Furthermore, experimental outcomes will be compared to the streaming potential hypothesis implications proposed in Section 6.1 in order to evaluate the effectiveness of the compression model.

6.2.1 Compression Test Setup and Experiments

The function of the compression test rig, Figure 6.7 is to apply a step displacement input to one face of the IPT in the thickness direction while the other face is fixed. Also, the generated current signal is gathered simultaneously to evaluate sensing characteristics of IPTs in compression.

The compression test rig (Figure 6.7), similar to the shear test setup (Figure 5.3), comprises three main parts: IPT fixture unit, laser vibrometer unit, data acquisition unit and auxiliary equipment. The IPT fixture unit, bolted on a vibration isolation table, is composed of

two metal supports on which the IPT compression apparatus and piezo stack actuator are attached, Figure 6.8.

The piezo actuator provides a step displacement excitation at micrometer levels. The IPT which is exposed to compression is placed between two pieces of conductive band that enable collection of the current generated due to compression deformation over the gold surfaces of the sensor. The conductive band-IPT sandwich is placed between two thin Plexiglas plates via double-sided, insulative kapton tapes, one of which is adhered on one of the metal supports. These tapes absorb some of the compression energy so actual generated currents are expected to be higher than the experiment results. However, the deflection of the intermediate layer is expected to be much lower than that of IPT considering its smaller thickness and higher stiffness. Therefore, small discrepancies in experimental findings are assumed to be negligible.

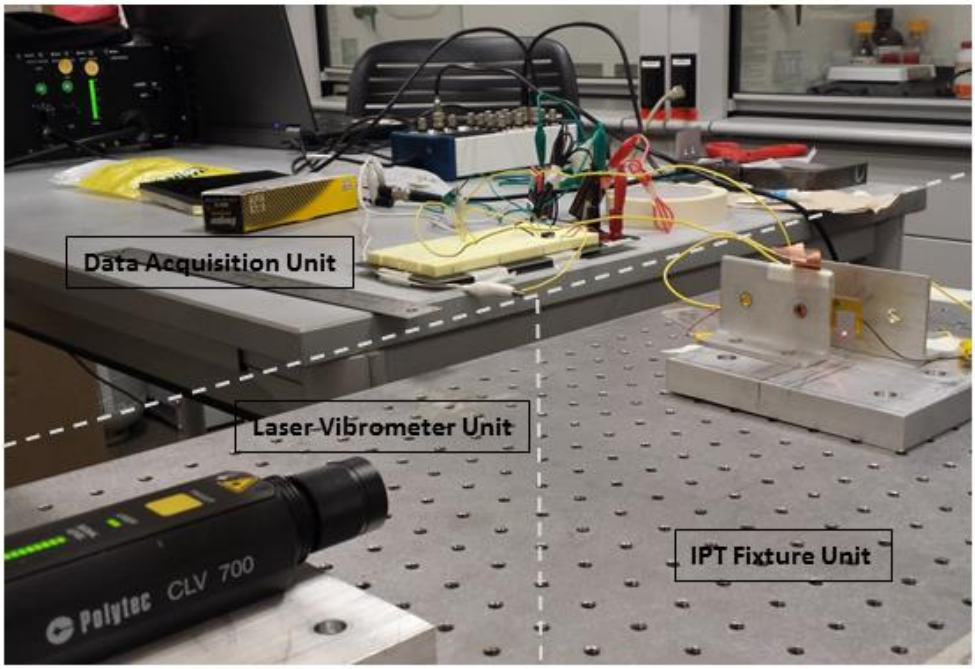

Figure 6.7. Photographic View of Compression Test Setup

The laser head is bolted on a vibration isolation plate through a metal fixture. The laser is pointed to the free Plexiglas plate through which compression displacement is exerted, Figure 6.8. The data acquisition unit is composed of a current amplifying electric circuit, a computer with LabVIEW data acquisition software and a NI USB-6216 BNC type data acquisition card.

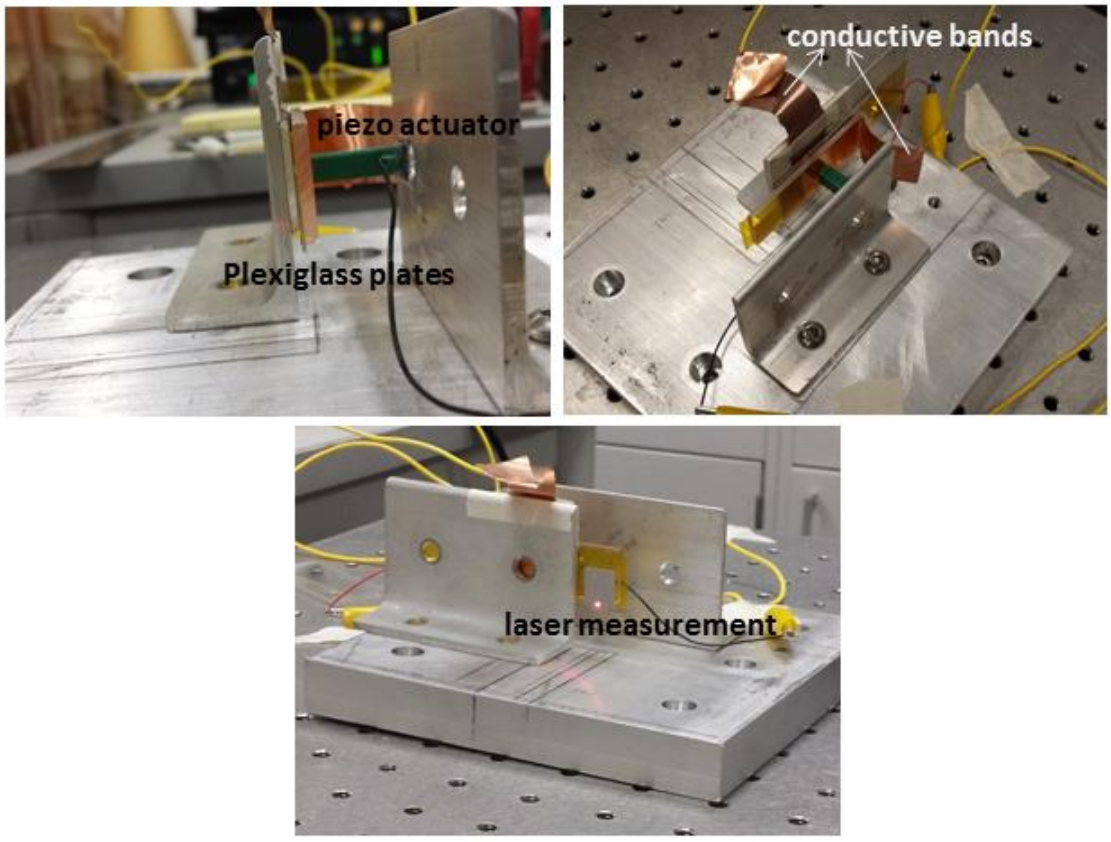

Figure 6.8. IPT Fixture Unit of Compression Test Setup

Throughout a compression test, similar to the bending and shear tests, the flow of the data is depicted in a schema in Figure 6.9. First, the piezo actuator is operated via a step voltage with

different magnitudes to exert several step deflections on the free plate to compress the IPT between the two Plexiglas plates. Meanwhile, current generated due to compressive deformation is collected and amplified by means of the signal conditioning circuit, a part of data acquisition unit. Finally, data is sent to the computer through data acquisition card for post processing. Similarly, a LabVIEWcode specifically designed for the compression tests are utilized.

In situ measurement of stimulation velocity was measured by means of laser vibrometer. Displacement inputs applied via initial excitations caused by the excitation was determined by integrating this velocity signal. The experiments were repeated two times to examine repeatability of the test and evaluate the reliability of the test setup.

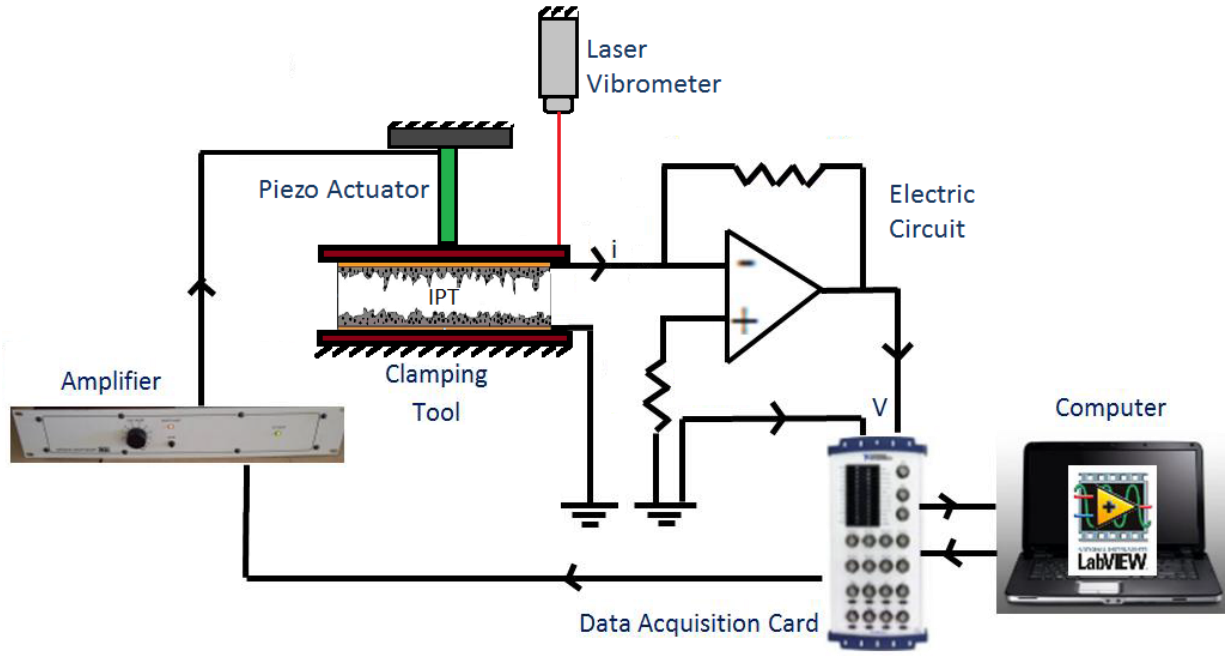

Figure 6.9. Schematic View of Compression Test Setup

6.2.2 Results and Discussion

An EMI-TF infused, Li^+ exchanged, Nafion based transducer sample that is 19 mm x 19 mm in dimensions and with ~14 mm thick electrodes having 30% RuO_2 by volume was tested with several step voltages to apply different step displacement inputs and current outputs were measured via the compression test rig, Figure 6.7. The generated current in response to each compression stimulus is depicted in Figure 6.10 for each excitation where excitation velocity and the resulting displacement are shown in Figure 6.11 and, Figure 6.12, respectively. A step voltage signal was sent to the piezo actuator to create compressive deformation on the transducer between two Plexiglas plates. Additional oscillations were observed in current output measurements before dying out that can be attributed to the oscillatory behavior of the excitation itself where a perfect impulse is required an impulse to create a perfect step displacement. However, the compression modeling, Section 6.1 , was already constituted to run with all types of input velocity. Therefore, although the input deflection is a step displacement superimposed with oscillations, current output will be estimated via streaming potential model accordingly.

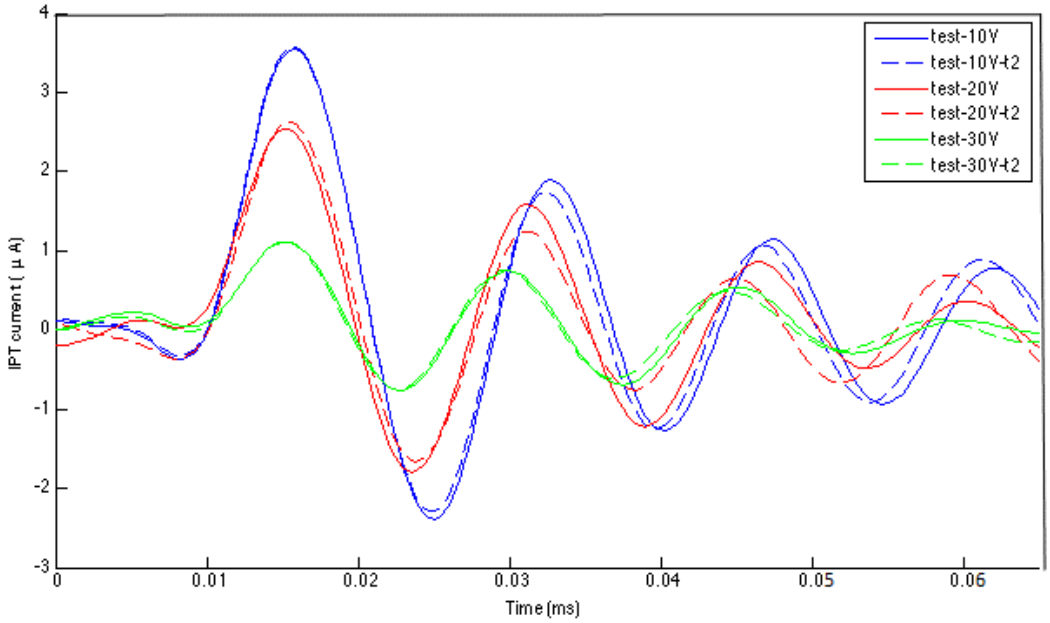

Figure 6.10. Current-Time Signal of the IPT in Compression

The absolute maximum value of the current occurs shortly after compression stimulation applied by means of the piezo actuator, Figure 6.10. The corresponding compression deflection for each stimulus is estimated via integrating the velocity signal collected from the free Plaxiglass plate. It is seen that the peak current increases with the displacement linearly exhibiting compatibility with the streaming potential estimations that predicts a linear relationship between displacement input and current output. Furthermore, when the results of the test sample for which the experiments are repeated two times are considered, the consistency is noticeably seen where the dashed and solid lines of the same color represent the repeated tests for each excitation. This certifies the repeatability of the tests and the reliability of the

compression test rig. Furthermore, peak current increases linearly as the initial excitation velocity peak increases, Figure 6.13.

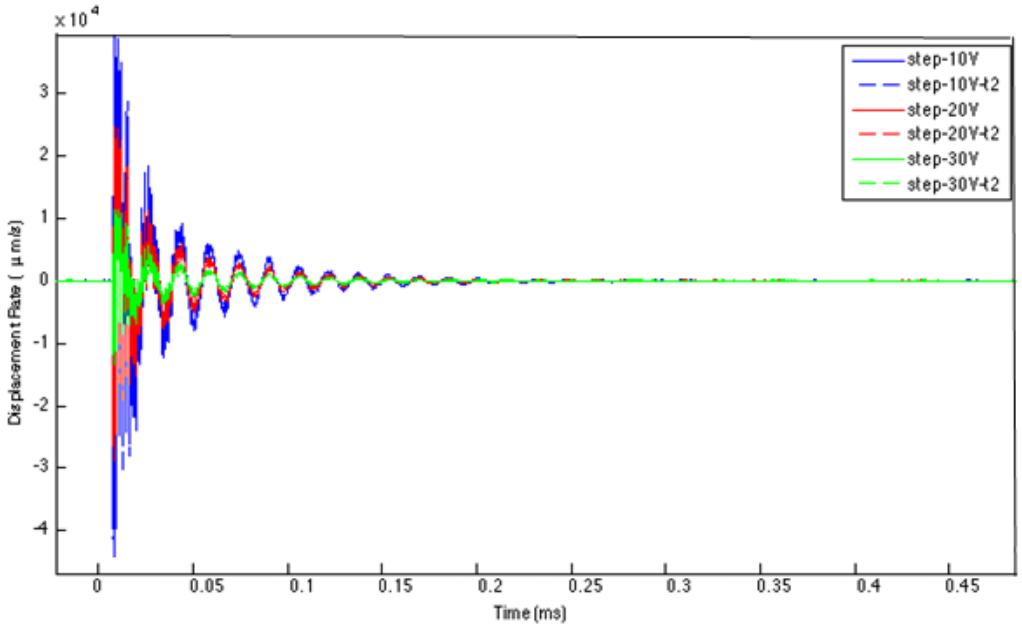

Figure 6.11. Compression Velocity Input

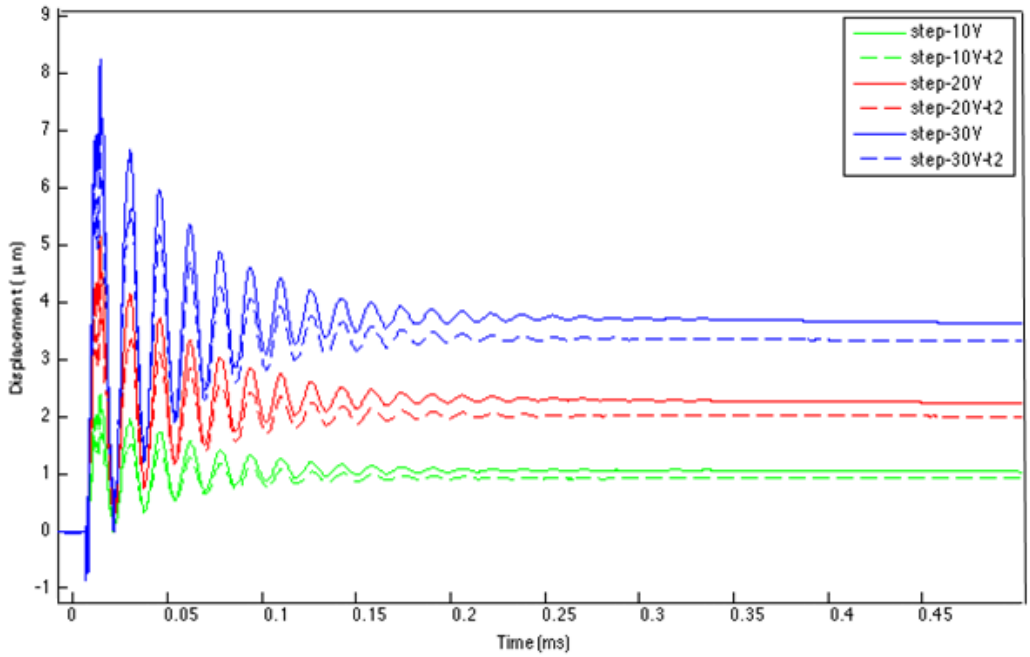

Figure 6.12. Compression Deflection Input

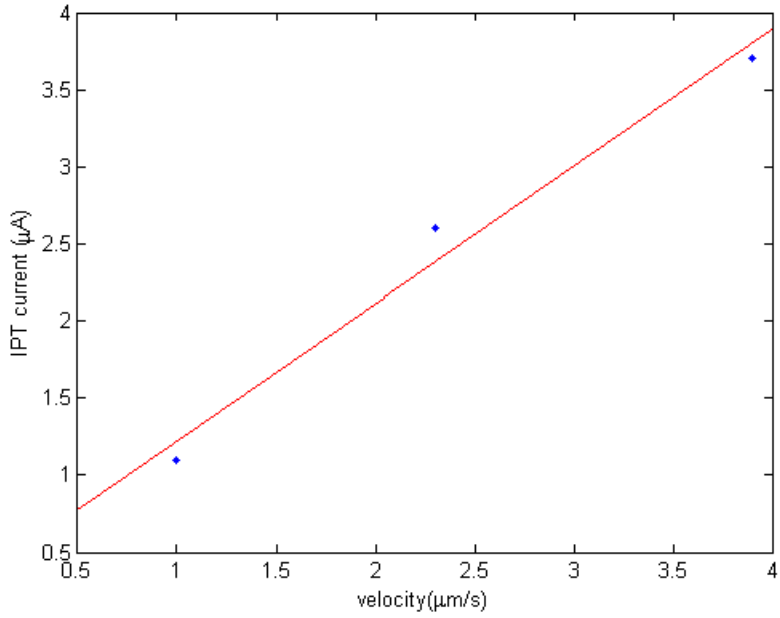

Figure 6.13. Compression Test Maximum Currents in Response to Velocity Excitations

Furthermore, the delay between input displacement and corresponding IPT current measurement is not significant as shown in Figure 6.14.

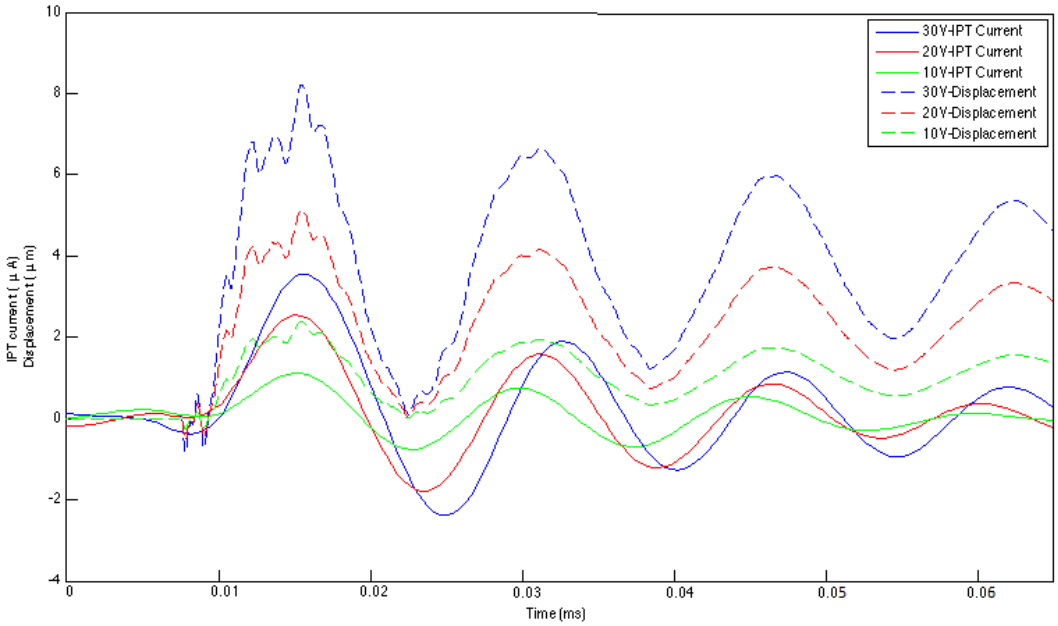

Figure 6.14. Compression Test Current Outputs In Response to Displacement Inputs

Besides the characterization of IPTs in compression sensing, the results of these experiments are also used to assess the streaming potential modeling in compression which was proposed in Section 6.1. The parameter values to run the model for the specific IPT tested are given in Table 6.1.

Table 6.1. Streaming potentail modeling parameters for EMI-TF infused, Li^+ exchanged, Nafion based IPT

Parameters	Value	Unit
$r_{channel}$ [45]	1.2e-9	m
μ [66], [64]	0.045	Pa*s
$l_{channel}$	90e-9	m
E [64]	5.5e6	Pa
η [64]	3577	kg/(m*s)
t_{IPT}	2.06e-4	m
ρ_e [64]	2164723	C/ m^3
$t_{electrode}$	14e-6	m
w_{IPT}	19e-3	m
l_{IPT}	19e-3	m
f_p	30%	unitless
f_c [66], [64]	30%	unitless

The model uses velocity data that is recorded during tests. The current estimations for the IPT with the parameters in Table 6.1 were calculated and presented in Figure 6.15 for the three excitations shown in Figure 6.11.

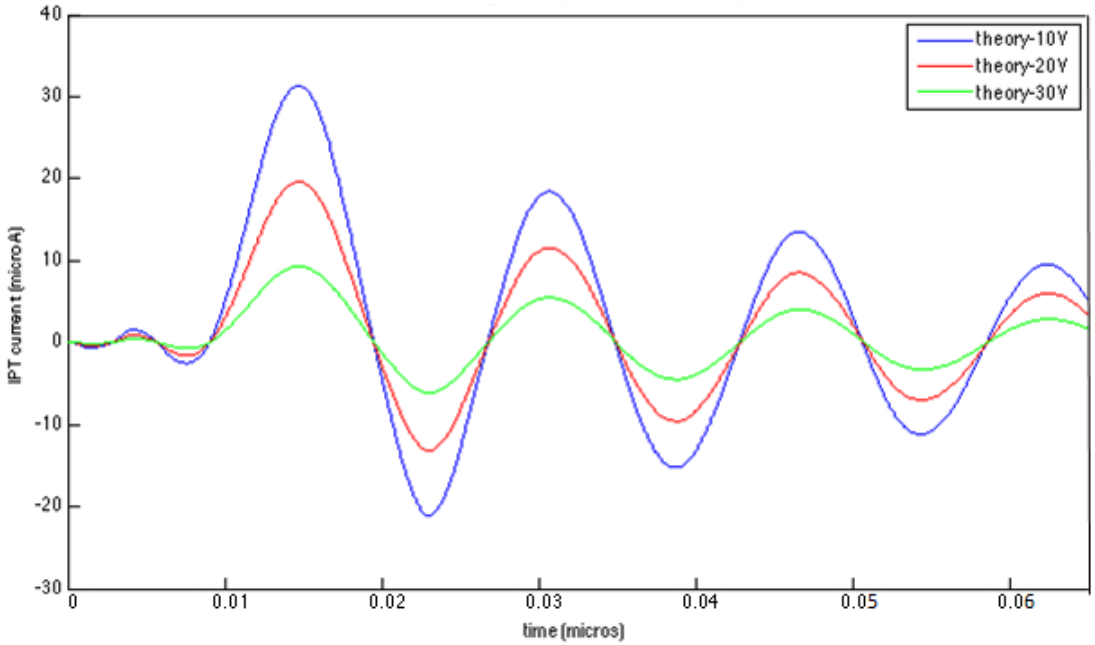

Figure 6.15. Streaming Potential Model Current Estimation for Compression Sensing

It is seen that the streaming potential model current estimation (Figure 6.15) is approximately an order higher than the ones measured in experiments (Figure 6.10). However, for such a physics based multiscale model, the predicted order of magnitude is reasonable. To evaluate the compression model, normalization will be appropriate in the assessment of model-experiment comparison. Therefore, normalized current predictions and normalized test results are given in the same plot, Figure 6.16, to assess the compatibility in trends at the current state of modeling where no calibration is made. Rather than magnitude, the trend estimation is more important in multiscale studies **[71]**.

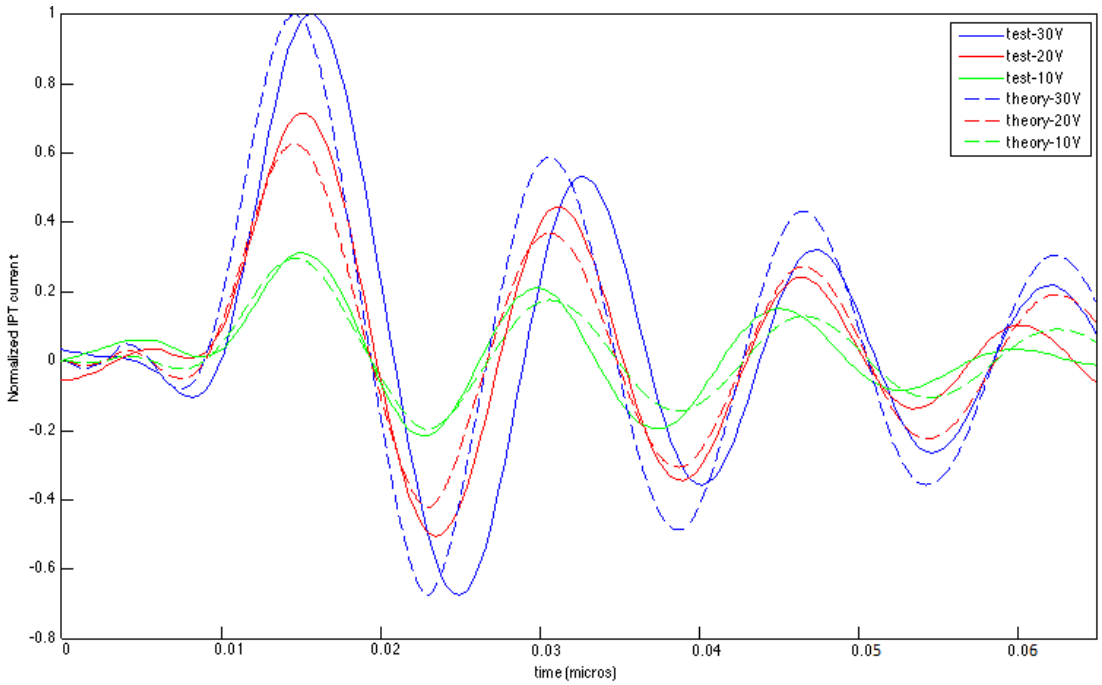

Figure 6.16. Streaming Potential Model-Experiment Comparison in Compression Sensing

The similarity in trends between the estimated current through modeling and the experimental results for each excitation, Figure 6.16, shows that model estimations are valid for any input deformation when it is normalized using the outcomes of an experiment corresponding to just one excitation. This offers a very strong support for the streaming potential hypothesis in compression sensing. Small offset seen in the real measurement, compared to model prediction, can be attributed to the time delays caused by test equipment or IPT itself. That the results are this compatible between a series of device length-scale experiments and the model operating at nano-length scale and then volume averaged to the mm length scale is compelling and promising.

6.2.3 Electrode Optimization

As in shear and bending modes, to explore the existence of optimum electrode architecture which maximizes the sensitivity of an IPT. IPTs with different electrode structures were fabricated and tested in compression employing the testing method offered in Section 6.2.1. The transducers tested had the volumetric concentrations of metallic phase; 30vol% RuO_2, 40vol% RuO_2, 50vol% RuO_2, 60vol% RuO_2. Compression stimulation was applied on the transducers and first peak observed in the step displacement input was recorded as approximately 4.7μm while the peak current corresponding to this displacement was measured for each transducer. This test was repeated 2 times for each sample having different metal particulate volumetric concentration in the electrode region.

Mean values of the peak currents generated by each kind of sensor are shown in Figure 6.17. (Because of the reuse of input parameters and modeling ideology, the modeling analog will necessarily mirror that of the previous chapter.) The error bars combine the minimum and maximum value observed as the peak current. Consistency in repeated experiments is detected by the narrow error bars. Furthermore, it is observed that generated current increases as the RuO_2 percentage in the electrode region of the IPT increases. However, further increase of metallic powder volumetric concentration, beyond 40% leads to a reduction in the produced current, as similarly observed in bending and shear observations. This shows that when RuO_2 content in the electrode solution is the variable, the optimum IPT electrode architecture comes out in the vicinity of 40%vol RuO_2 case regardless of deformation mode for an EMI-TF infused, Li^+ exchanged IPT. Furthermore, the streaming potential modeling implication is supported one more time by compression tests that the metallic particulate communication both with itself and

the ionomer-diluent channels in the electrode layers of the transducer plays an important role in sensing mechanism.

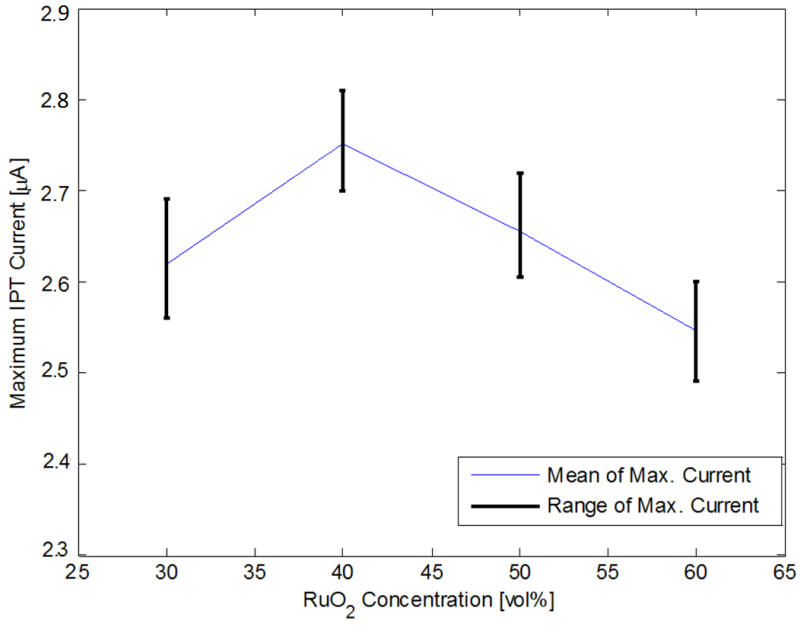

Figure 6.17. Average of Maximum Current Outputs vs. Metal Loading for Compression Tests

6.3 CHAPTER SUMMARY

The preceding chapter has introduced a novel experiment design where a sudden impulsive velocity is intended to apply in order to create a step displacement through the thickness of the IPT while generated current is measured via an electric circuit to characterize IPT behavior in compression. This chapter serves as a new research direction in the IPT sensing field showing that IPT sensing is not limited to bending. Furthermore a new compression model

was proposed projecting the key aspects of the streaming potential hypothesis. The modeling estimations exhibited a successful correlation to the experiments. Therefore, it is stated that streaming potential modeling consistent with a third mode is enough to affirm its validation. The significant outcomes of the investigations in compression sensing and experiment-model comparison are as follows;

i. IPT response increases as compression deflection increases.

ii. Experimental findings showed the influence of the electrode structure effect on IPT response. Optimum volumetric content of the metal phase in the electrode mixture which maximizes the sensor output was found out to be in the vicinity of 40 vol% RuO_2 case, showing a consistency with the bending and shear modes. This indicates that optimum electrode structure is independent from the mode of deformation for an EMI-TF infused, Li^+ exchanged IPT.

iii. A compression sensing modeling is proposed adopting streaming potential hypothesis which is able to estimate the output current in response to any simulation, given any displacement rate.

7.0 CONCLUSIONS

The presented research has had the objective of accomplishing experimental design and implementation for transient response characterization of Ionic Polymer Transducers in different sensing modes; bending, shear and compression. The experimental research conducted significantly expands the performance database for bending, shear and compression transduction in a general sense, furthermore and specifically facilitates testing of the streaming potential hypothesis.

Fabrication procedure steps of an IPT were explained in detail which are mainly *(i)* ion-exchanging, *(ii)* diluent uptake, *(iii)* electrode painting, and, *(iv)* gold hot-melt press. Different electrode metal loadings were employed in order to explore electrode architecture effect on sensing to optimize the electrode structure to obtain peak sensitivity which was possible with the fabrication technique called Direct Assembly Process. This method was chosen since it can offer a pathway to ultimately systematically explore hypotheses for the physical mechanisms responsible for the observed IPT sensing response. In this research, EMI-TF, a type of ionic liquid known as nonvolatile, was used as the diluent because it is stable in air when compared to water and therefore eliminates dehydration effects from the study. Lithium was selected as the counter ion because previous reports suggest that sensitivity is typically enhanced for this ion exchange. The electro active polymer Nafion-117 was selected as the base polymer because it aligned with a significant number of previous reports to enable comparison.

A novel test setup and experimental procedure was proposed for each sensing mode. The objective of the experimental study was to unveil the transient physical mechanisms responsible for sensing. Research to date has focused predominantly on actuation, while identification of the fundamental physical mechanism responsible for IPT sensing is different from actuation and remains an open topic. Tests were designed to apply step displacement stimulation to IPT to characterize transient response of the sensors in all IPT sensing modes. Measurement of current output was performed by means of a signal conditioning circuit and a laser vibrometer was used to evaluate input deflection in micromemeters. Tests were repeated several times with several excitations. The reliability of the experimental setup and the repeatability of the tests were clearly demonstrated which may especially be challenging for step input tests. Furthermore, the optimum metal particulate concentration was found out to be in the vicinity of 40%vol RuO_2 case regardless of deformation mode for an EMI-TF infused, Li^+ exchanged IPTs.

Particularly, streaming potential hypothesis implications were evaluated through step input experiments. The outcomes of the experimental investigations supported the streaming potential estimations in all three modes: *(i)* it can explain the existence of a sensing signal in any deformation, *(ii)* it can address the changes in current output in response to variations in input, (ii) it can assess the heat treatment effect on sensing response, and, *(iii)* it can address the electrode architecture`s influence on sensing transduction and optimization of the electrode structure.

Another significant objective was to complete the modeling framework for the streaming potential hypothesis for compression. The hypothesis argues that the presence of unbound counter-ions within the hydrophilic phase of an ionic polymer behaves as an electrolyte in the presence of the electrode. Thus, as per classic streaming potential analyses, relative motion of the

electrolyte with respect to the electrode will result in the evolution of a streaming current since the electric double layer which forms on the electrode region is disturbed by the electrolyte flow due to transducer deformation. Furthermore, the compression model is able to estimate the output current in response to any simulation, given any displacement rate. The modeling estimations exhibited a successful correlation to the experiments. Therefore, it is stated that streaming potential modeling consistent with a third mode is enough to affirm its validation and proves its strengths and robustness over its counterparts.

8.0 FUTURE WORK

Based on the work presented in this research, the recommendations as future work are;

i) Experimental investigation on the effects of other parameters (such as type of conductive media in electrode, diluent, cation) on optimized IPT structure to maximize sensitivity.

ii) Observation of electrode thickness effects on sensing.

iii) Enhancement of compression modeling especially improving how model takes different electrode compositions into account incorporating `porosity` studies.

iv) Improvement of the model to capture the viscoelastic behavior thoroughly with an additional spring in parallel which also includes semicrystallinity influences.

BIBLIOGRAPHY

[1] Sadeghipour K, Salomon R, Neogi S 1999 Development of a novel electrochemically active membrane and 'smart' material based vibration sensor/damper Smart Mater. Struct. 1(2) 172

[2] Shahinpoor M, Kim KJ 2005 Ionic polymer-metal composites: IV. Industrial and medical applications Smart Mater. Struct. 14 197

[3] Aureli M, Prince C, Porfiri M, Peterson SD, 2010 Energy harvesting from base excitation of ionic polymer metal composites in fluid environments Smart Materials and Structures 19(1) 015003

[4] Bonomo C, Brunetto P, Fortuna L, Giannone P, Graziani S, Strazzeri S 2008 A tactile sensor for biomedical applications based on IPMCs Sensors Journal, IEEE 8(8) 1486-9

[5] Yeom SW, Oh IK 2009 A biomimetic jellyfish robot based on ionic polymer metal composite actuators Smart Mater. Struct. 18 085002

[6] Najem J, Sarles SA, Akle B, Leo DJ, 2012 Biomimetic jellyfish-inspired underwater vehicle actuated by ionic polymer metal composite actuators Smart Materials and Structures 21(9) 094026

[7] Chen Z, Um TI, Bart-Smith H 2011 A novel fabrication of ionic polymer-metal composite membrane actuator capable of 3-dimensional kinematic motions Sensors Actuators A: Phys. 168(1) 131-9

[8] Wallmersperger T, Leo DJ, Kothera CS 2007 Transport modeling in ionomeric polymer transducers and its relationship to electromechanical coupling Journal of Applied Physics 101(2) 024912

[9] Akle BJ, Habchi W, Wallmersperger T, Akle EJ, Leo DJ 2011 High surface area electrodes in ionic polymer transducers: Numerical and experimental investigations of the electro-chemical behavior Journal of Applied Physics 109 074509

[10] Pugal D, Jung K, Aabloo A, and Kim KJ 2010 Ionic polymer--metal composite mechanoelectrical transduction: review and perspectives Polymer international 59(3) 279-89

[11] Newbury KM, and Leo DJ 2002 Electromechanical Modeling and Characterization of Ionic Polymer Benders J. Intell. Mater. Syst. Struct.13(1) 51-60

[12] Akle BJ, Bennett MD, Leo DJ 2006 High-strain ionomeric--ionic liquid electroactive actuators Sensors Actuators A: Phys. 126(1) 173-81

[13] Akle BJ, Bennett MD, Leo DJ, Wiles KB, McGrath JE 2007 Direct assembly process: a novel fabrication technique for large strain ionic polymer transducers J. Mater. Sci. 42 7031-41

[14] Akle BJ, Leo DJ 2012 Experimental demonstration of the active area model in extensional ionic polymer transducers Smart Mater. Struct. 21(10) 105034

[15] Akle BJ, Leo DJ 2013 Softening and heating effects in ionic polymer transducers: An experimental investigation Journal of Intelligent Material System and Structures

[16] Kim B, Kim D, Jung J, Park J 2005 A biomimetic undulatory tadpole robot using ionic polymer--metal composite actuators Smart Mater. Struct. 14(6) 1579

[17] Bandopadhya D, 2008 Quasi-static tip positioning of multi-segmented IPMC for micro-manipulation following Euler-Bernoulli and pseudo-rigid body model Journal of Reinforced Plastics and Composites

[18] Zangrilli U and Weiland LM 2011 Prediction of the ionic polymer transducer sensing of shear loading Smart Mater. Struct. 20 094013

[19] Bonomo C, Fortuna L, Giannone P, Graziani S, Strazzeri S 2006 A model for ionic polymer metal composites as sensors Smart Mater. Struct. 15 749

[20] Bennett MD, Leo DJ 2004 Ionic liquids as stable solvents for ionic polymer transducers Sensors Actuators A: Phys. 115 79–90

[21] Newbury KM, Leo DJ 2003 Linear electromechanical model of ionic polymer transducers-part II: experimental validation J. Intell. Mater. Syst. Struct. 14 343–57

[22] Buechler MA, Leo DJ 2007 Characterization and variational modeling of ionic polymer transducers J. Vib. Acoustics 129 113

[23] Bahramzadeh Y, Shahinpoor M 2011 Dynamic curvature sensing employing ionic-polymer–metal composite sensors Smart Mater. Struct. 20 094011

[24] Shahinpoor M, Bar-Cohen Y, Simpson JO, Smith J 1998 Ionic polymer–metal composites (IPMC's) as biomimetic sensors, actuators and artificial muscles-a review Smart Mater. Struct. 7(6) R15-30

[25] Farinholt K and Leo DJ 2004 Modeling of electromechanical charge sensing in ionic polymer transducers Mech. Mater. 36 421–33

[26] Nemat-Nasser S 2002 Micromechanics of actuation of ionic polymer-metal composites Journal of Applied Physics 92(5) 2899-2915

[27] Asaka A, Oguro K, Nishimura Y, Mizuhata M and Takenaka H 1995 Bending of polyelectrolyte membrane–platinum composites by electric stimuli: I. Response characteristics to various wave forms Polym. J. 27 436–40

[28] Shahinpoor M and Kim K J 2002 Novel ionic polymer–metal composites equipped with physically loaded particulate electrodes as biomimetic sensors, actuators and artificial muscles Sensors Actuators A: Phys. 96 125–32

[29] Kim K and Shahinpoor M 2003 Ionic polymer–metal composites: II. Manufacturing techniques Smart Mater. Struct. 12 65–79

[30] Akle B, Leo D, Bennett M, Wiles K and McGrath JE 2006 Direct assembly process for fabrication of ionomeric polymer devices US Patent App. 20,060/266,642

[31] Akle B J and Leo D J 2007 Characterization and modeling of extensional and bending actuation in ionomeric polymer transducers Smart Mater. Struct. 16 1348

[32] Najem J, Sarles SA, Akle B, and Leo, DJ 2012 Biomimetic jellyfish-inspired underwater vehicle actuated by ionic polymer metal composite actuators Smart Materials and Structures 21(9) 094026

[33] Nemat-Nasser S, Zamani S, and Tor Y, 2006 Effect of solvents on the chemical and physical properties of ionic polymer-metal composites Journal of Applied Physics 99(10) 104902

[34] Oguro K, Kawami Y, and Takenaka H 1992 “An actuator element of polyelectrolyte gel membrane-electrode composite,” *Osaka Kogyo Gijutsu Shikensho Kiho*. **43**(1) 21-24

[35] Shahinpoor M 1992 Conceptual design, kinematics and dynamics of swimming robotic structures using ionic polymeric gel muscles Smart Materials and Structures 1(1) 91

[36] Shahinpoor M, 1995 Micro-electro-mechanics of ionic polymeric gels as electrically controllable artificial muscles Journal of Intelligent Material Systems and Structures 6(3) 307-14

[37] Akle B, Nawshin S, Leo D 2007 Reliability of high strain ionomeric polymer transducers fabricated using the direct assembly process Smart Materials and Structures 16(2) S256

[38] Sadeghipour K, Salomon R and Neogi S 1992 Development of a novel electrochemically active membrane and 'smart' material based vibration sensor/damper Smart Mater. Struct. 1 172

[39] Newbury KM and Leo DJ 2002 Electromechanical modeling and characterization of ionic polymer benders J. Intell. Mater. Syst. Struct. 13 51–60

[40] Tiwari R, Kim KJ, and Kim S, 2008 Ionic polymer-metal composite as energy harvesters Smart Structures and Systems 4(5) 549-63

[41] Weiland LM and Akle BJ 2010 Ionic polymer transducers in sensing: the streaming potential hypothesis Smart Structures and Systems 6 211-223

[42] Mauritz KA and Moore RB 2004 State of Understanding of Nafion Chemical reviews 104(10) 4535-86

[43] Hsu W Y and Gierke TD 1982 Elastic theory for ionic clustering in perfluorinated ionomers Macromolecules 15 101–5

[44] Hsu WY, Gierke TD 1983 Ion transport and clustering in Nafion perfluorinated membranes Journal of Membrane Science 13(3) 307-326

[45] Schmidt-Rohr K and Chen Q 2007 Parallel cylindrical water nanochannels in Nafion fuel-cell membranes Nature Mater. 7 75–83

[46] de Gennes PG, Okumura K, Shahinpoor M, Kim KJ 2000 Mechanoelectric effects in ionic gels Europhysics Letters 50 513

[47] Nemat-Nasser S, Li JY 2000 Electromechanical response of ionic polymer-metal composites J. Appl. Phys. 87 3321

[48] Nemat-Nasser S, Wu Y 2006 Tailoring the actuation of ionic polymer-metal composites Smart Mater. Struct. 15 909

[49] Li JY and Nemat-Nasser S 2000 Micromechanical analysis of ionic clustering in Nafion perfluorinated membrane Mech. Mater. 32 303–14

[50] Paddison SJ 2003 Proton conduction mechanisms at low degrees of hydration in sulfonic acid-based polymer electrolyte membranes Annu. Rev. Mater. Sci. 33 289–319

[51] Farinholt K, Newbury K, Bennet M and Leo D 2002 An investigation into the relationship between charge and strain in ionic polymer sensors First World Congress on Biomimetics and Artificial Muscles (Albuquerque, NM)

[52] Kocer B, Zangrilli U and Weiland L M 2012 Experimental and theoretical characterization of non-bending ionic polymer transducer sensing Proc. SPIE 8345 83454X

[53] Kocer B, Zangrilli UT, Akle B, Weiland LM, 2014 Experimental and Theoretical Investigation of Ionic Polymer Transducers in Shear Sensing Journal of Intelligent Material Systems and Structures [in press].

[54] Wallmersperger T, Horstmann A, Kroplin B and Leo D J 2009 Thermodynamical modeling of the electromechanical behavior of ionic polymer metal composites J. Intell. Mater. Syst. Struct. 20 741–50

[55] Bufalo G D, Placidi L and Porfiri M 2008 A mixture theory framework for modeling the mechanical actuation of ionic polymer metal composites Smart Mater. Struct. 17 045010

[56] Porfiri M 2009 An electromechanical model for sensing and actuation of ionic polymer metal composites Smart Mater. Struct. 18 015016

[57] Porfiri M 2009 Influence of electrode surface roughness and steric effects on the nonlinear electromechanical behavior of ionic polymer metal composites Phys. Rev. E 79 041503

[58] Gao F and Weiland LM 2010 Ionic polymer transducers in sensing: implications of the streaming potential hypothesis for varied electrode architecture and loading rate J. Appl. Phys. 108 034910

[59] Gao F and Weiland LM 2011 Streaming potential hypothesis for ionic polymer transducers in sensing: roles of ionomer state and morphology J. Intell. Mater. Syst. Struct. 22 1623–30

[60] Kocer B, Weiland LM 2013 Experimental investigation of the streaming potential hypothesis for ionic polymer transducers in sensing Smart Mater. Struct. 22(3) 035020

[61] Helmholtz H 1853 Pogg.Ann. LXXXIX 211\

[62] Gao F, Weiland LM 2009 The streaming potential method for modeling the electromechanical responses of ionic polymer transducers SPIE Smart Structures and Materials Nondestructive Evaluation and Health Monitoring 72924H

[63] van der Heyden, F. H. J., Stein, D. & Dekker, C. Streaming Currents in a Single Nanofluidic Channel. Physical Review Letters 95,(11) 116104 (2005).

[64] Zangrilli UT, 2013, Multiscale Implications of Stress Induced Ionic Polymer Transducer Sensing, PhD Dissertation, University of Pittsburgh.

[65] Kocer B, Weiland LM 2011 Experimental Characterization of Direct Assembly Process Based Ionic Polymer Transducers in Sensing Proceedings of the ASME-SMASIS

[66] Gao F, 2010, Computational Study of Ionic Polymers: Multiscale Stiffness Predictions and Modeling of the Electromechanical Transduction, PhD Dissertation, University of Pittsburgh.

[67] Li, Q., He, R., Jensen, J. O. & Bjerrum, N. J. 2003 Approaches and recent development of polymer electrolyte membranes for fuel cells operating above 100 C. *Chemistry of Materials* **15**,(26) 4896-4915

[68] DuPont. *Fuel Cells: Literature*, 2014, <http://www2.dupont.com/FuelCells/en_US/products/nafion.html>

[69] Kocer B, Weiland LM 2012 Experimental Optimization of Electrode Composition for Ionic Polymer Transducers in Sensing Proceedings of the ASME-SMASIS

[70] Zangrilli UT, Kocer B, Weiland LM 2013 Investigation of Annealed Ionic Polymer Transducers in Sensing Proceedings of the SPIE

[71] Oden JT, Prudhomme S, Romkes A and Bauman PT 2006 Multiscale modeling of physical phenomena: adaptive control of models SIAM J. Scient. Comput. 28 2359

[72] van der Heyden FHJ, Stein D, and Dekker C, 2005 Streaming currents in a single nanofluidic channel *Phys. Rev. Lett.* **95** 116104

[73] Lemaitre J, and Chaboche J 1990 Mechanics of solid materials Cambridge University press